Faculdade de Engenharia da Universidade do Porto

Study of the regulatory effect of neuronal electrical activity on mitochondria axonal transport dynamics

Catarina Eduarda Fernandes Ricardo

DISSERTATION

Mestrado Integrado em Bioengenharia

Orientador: Cátia Lopes
Co-orientador: Paulo Aguiar

27th of september of 2021

Study of the regulatory effect of neuronal electrical activity on mitochondria axonal transport dynamics

Catarina Eduarda Fernandes Ricardo

Mestrado Integrado em Bioengenharia

Resumo

Os neurónios são a unidade funcional do sistema nervoso e são responsáveis pelo processamento, geração e propagação de sinais eletroquímicos. A correta condução e propagação destes impulsos elétricos é assegurada pelo axónio. No corpo humano, os axónios podem ter até um metro de comprimento, o que impõe um desafio substancial para a manutenção adequada de tal comunicação. Qualquer perturbação no funcionamento deste mecanismo pode desencadear eventos precoces de neurodegeneração promovendo falhas no transporte de organelos necessários nos terminais pré-sinápticos e degradação de outros no soma. Por essa razão, torna-se imperativo compreender os mecanismos neurobiológicos que controlam a dinâmica do transporte axonal e a sua relação com a atividade elétrica axonal e a transmissão de sinais através da rede neuronal. Embora alguns estudos recentes estabeleçam a relação entre alguns componentes intracelulares do transporte axonal com a atividade neuronal, o nosso conhecimento sobre este mecanismo regulador subjacente permanece pouco claro. Por conseguinte, esta dissertação explora com maior detalhe de que forma a atividade neuronal regula a dinâmica do transporte axonal, em particular de mitocôndrias, organelos fundamentais responsáveis pelo fornecimento de energia às células. Para atingir este objetivo, é utilizada uma abordagem combinatória em tempo real, em que a aquisição de imagem das cargas transportadas ao longo dos axónios será simultaneamente combinada com a análise eletrofisiológica da atividade elétrica dos axónios. A atividade neuronal será modulada para diferentes níveis de atividade e o seu impacto na dinâmica do transporte axonal será avaliado. Isto será explorado utilizando a plataforma μEF estabelecida, no laboratório de acolhimento, que combina matrizes de microEléctrodos e câmaras microFluídicas de forma a permitir a compartimentalização axonal num ambiente mais adequado para a avaliação simultânea da atividade elétrica e da dinâmica do transporte axonal.

Abstract

Neurons are the functional unit of the nervous system and are responsible for the processing, generation and propagation of electrochemical signals. The correct conduction and propagation of these electrical impulses is ensured by the axon. Axons can be several meters long, which imposes a substantial challenge for the proper maintenance of such electrochemical communication between the somatodendritic and axonal compartments. Any disturbance in the functioning of this mechanism can trigger early neurodegeneration events by promoting failures in the transport of necessary organelles in the presynaptic terminals and degradation of others in the soma. For that reason, it becomes imperative to understand the neurobiological mechanisms controlling the axonal transport dynamics and its relationship with the axonal electrical activity and signal carriage through the neuronal network. Besides some recent studies suggest an activity-dependent axonal transport dynamic for particular cargoes, our knowledge regarding this underlying regulatory mechanism remain unclear. Therefore, this dissertation aims to investigate if and how neuronal activity regulates axonal transport dynamics of neuronal cargoes. To achieve this goal, it will be used a combinatory approach where the live-imaging of cargoes transport along the axons will be simultaneously combined with the real-time electrophysiological acquisition of the axon electrical activity. Neuronal activity will be modulated to different ranges of activity and its impact on axonal transport dynamics will be assessed. This will be explored using the μEF platform established in the host lab, which combines microelectrode arrays and microfluidics devices in a way that enable the concurrent assessment electrical activity and trafficking dynamics.

Acknowledgements

This dissertation would not be possible without the NCN group at i3S who I would like first to indulge my gratitude. To my supervisor Dr. Cátia Lopes that besides all the teaching and mentoring has guided me and helped me grow academically, critically thinking and embrace new opportunities, to Dr. Paulo Aguiar for the opportunity to work, widen my knowledge and overcome challenges in a welcoming environment. A special thanks to Domingos and Andreia for teaching me that there's more to it than just being in the lab, to Palma for the good nights closing i3S, to Mateus for teaching me always something new, to Ana for the availability to always help and Miguel for putting up with me with my doubts.

The closure of 5 years ends with a 6 month internship, however I would not have come this far without a hand full of people. I would like to thank my friends to where I started, together we held our head up high and were ambitious to where we wanted to be. For helping me achieve this goal, I am thanking you Esquivel, Kika … To Tânia for growing up with me in the funniest way possible, for the comradeship that we both know. Maia, for joining me in this journey (we finally did it!) and walk through the same door always helping each other out (intellectually and in a sleep deprived way). And additionally, I have to add the metal header that is Afonso, who might always show up late but always cares.

To the people that started out as strangers but became a family after gatherings, lots of anniversaries, a quarantine, disputes and loads of travelling. Those times were hard… but we sticked together and got over the fact that a pandemic was taking its shape. Instead, we bounded and stayed... To complaining about the fact the working from home in our field does not work, to gather strengths to continue our Erasmus and finish our reports.

To my family, you have has always encouraged me to pursue my dreams even if that took me away from home, to giving me strength to continue and not quit, for believing that I could do it, to my mum for biggest supporter, to my dad to lend me his vision and kindness, to my brother for the times when I needed a break. And at last, to the person that knows me more than myself, for the stupid moments, for the support without asking, for the call unexpected, for the kindness you have. You are person that I ask for help and the one that tells me you can do it even when I don't believe it. By being a Caccun in a nutshell you nurture by ambitions and it's a good thing that I came to FEUP.

“No matter where you are, great rewards await those who are willing to put in the time and look a little closer for things that others might miss”

Anonymous

Index

List of Figures

List of Tables

Abbreviations

ADP	Adenosine Diphosphate
AIS	Axonal Initial Segment
ALS	Amyotrophic Lateral Sclerosis
ALS2	Alsin Rho guanine nucleotide exchange factor
ANS	Autonomic Nervous System
APP	Amyloid Precursor Protein
ATP	Adenosine Triphosphate
BCC	Bicuculline
BMP	Bone morphogenetic protein
CKA	Choline Kinase
CMT1	Charcot-Marie-Tooth 1
CNS	Central Nervous System
DCTN1	Dynactin subunit 1
DRG	Dorsal Root Ganglion
DYNCH	Dynein Heavy Chain
DYNCI	Dynein Intermediary Chain
DYNCL	Dynein Light Chain
EpoD	Epothilone Polyketide synthase D
ESCRT	Endosomal Sorting Complex Required for Transport
GABAA	γ-amino butyric acid type A
GFAP	Glial Fibrillary Acidic Protein
GRIP	Glutamate receptor-interacting protein 1
GTP	Guanosine triphosphate
hAPP	Mutated amyloid precursor protein
HTT	Huntingtin
JIP	JNK interacting protein 1
JNK	c-Jun N-terminal kinase
KHC	Kinesin Heavy Chain
KIF3	Kinesin Family member 3
KLC	Kinesin Light Chain
LRRK2	Leucine-rich repeat kinase 2
MAP7	Microtubule Associated protein 7
MAPS	Microtubule-associated Proteins
MEA	Microelectrode Array
Miro	Mitochondrial Rho GTPase

MPP+	1-methyl-4-phenylpyridinium
MPTP	1-methyl-4-phenyl-1, 2, 3, 6-tetrahydropyridine
NAP	Nucleossome assembly protein
PAEZ	Pre-axonal Exclusion Zone
PAR-3	Partitioning defective protein 3
PARK2	Parkin protein 2
PARK7	Parkinson disease protein 7
PDMS	Poly(dimethylsiloxane)
PINK7	PTEN-induced kinase 1
PMP22	Peripheral myelin protein 22
PNS	Peripheral Nervous System
PSEN	Presenilin
Rab4	Rab-related protein
RNA	Ribonucleic Acid
ROT	Pesticide rotenone
SNS	Somatic Nervous System
SOD1	Superoxide dismutase 1
SVP	Synaptic Vesicle Precursor
TDP-43	Transactive-region DNA-binding protein
TRAK	Trafficking kinesin protein
TTX	Tetrodotoxin

Chapter 1

Introduction

1) Context

The complex and polarized neuron architecture poses a great challenge to the neuronal electrochemical communication. Equally important, since some axons are on the order of meters long, neurons cannot rely on diffusion to exchange proteins and organelles, essential for proper neuron functioning, between the cell body and the axon terminals. As a result, the maintenance and proper function of neurons is recognized not only by the faithful propagation of action potentials but also by the regulated transport of intracellular products to and from the presynaptic terminals. The transport of such cargos is regulated by specific molecular motors and adaptor proteins with the structural support of the cytoskeleton components. Given the central role of such process in the neuron homeostasis, an impairment of a single molecular mechanism may lead to neuronal pathologies, promoting the neuron disintegration and ultimately, neurodegeneration. Neurological disorders, such as Parkinson, Amyloid Lateral Sclerosis and Alzheimer's disease, exhibit early signs of axonal transport defects during disease development, thus reinforcing the significance of studying and identifying the regulatory mechanisms that are on the basis of proper axonal trafficking.

In addition to function as a supply chain for the adequate distribution of intracellular proteins and organelles within the polarized neuron compartments, the axon is also the responsible to generate and transmit action potentials and, therefore, mediate the proper electrochemical communication within the nervous system. Given the close association between electrical function of neurons and the requirements of certain intracellular components available in specific neuron localizations (i.e. synaptic activity), it is plausible that neuronal activity may have a regulatory role on the axonal transport dynamics. Recent

evidences have been supporting this idea but our knowledge regarding this topic is still in its infancy. To understand such complex association, it is required the use of advanced experimental and technological tools capable to study such fine structures as the axon. Using a combination of a microelectrode arrays (MEAs) and microfluidics, one can i) compartmentalize axons and control their growth on top of microelectrodes, ii) record the axonal spontaneous and/or evoked electrical activity, with high spatiotemporal resolution and high signal-to-noise ratio, and iii) record simultaneously and in real-time data regarding the electrophysiological profile and intracellular cargos trafficking of specific axons.

2) Motivation

The human nervous system development, connectivity, and synaptogenesis rely on the proper function of its structural unit, the neuron. Given that neurons are highly polarized cells with elongated axons, that can extend over a meter away from their soma, their adequate electrochemical function extensively depends on efficient intracellular axonal transport of organelles and proteins between the somatodendritic and axonal compartments. Although the biochemical mechanisms governing the molecular motors-mediated transport are quite well understood, our current knowledge regarding axonal transport regulatory pathways, namely those related with neurons electrical activity, remains particularly limited. Given that an impairment in axonal transport is often related with neuron malfunction and degeneration, it is critical to increase our knowledge about the regulatory mechanisms under proper axonal transport dynamics. Therefore, it is essential to bring forward this research topic to accelerate better diagnosis and the development of therapeutic strategies capable of restoring the axonal function in neurological diseases.

3) Objectives

The main goal of this dissertation is to investigate the regulatory role of neuronal electrical activity on the mitochondria axonal transport dynamics – one of the most important neuronal organelles for the maintenance of proper neuronal function and connections. More concisely, to unravel which kinetic parameters are affected by changes in neuronal activity, if different action potential rates modulate axonal transport dynamics and if the developmental state affects the modulation of neuronal activity. To address these questions, it will be used a platform combining microElectrode arrays and microFluidics (μEF platform) to simultaneously: i) modulate and record axonal electrical activity of dorsal root ganglion (DRGs) neurons, and ii) live-image mitochondria axonal trafficking in periods of spontaneous and evoked neuronal activity.

4) Document Outline

This document is structured in 5 chapters that will provide an introductory state-of-the-art overview to the topic and will describe the research work proposed for this dissertation. Chapter 2 provides a literature review on: 1) a brief introduction to the physiological and anatomic al properties of neuronal cells; 2) a detailed description of the machinery and mechanisms underlying axonal transport dynamics in a context of neuronal homeostasis; 3) it addresses how impairment of axonal transport contribute to the development of widely known neurodegenerative diseases; 4) the currently known regulatory mechanisms of axonal trafficking dynamics; 5) provides a brief review of the emergent evidences that suggest a regulatory role of neuronal electrical on the transport of different neuronal cargoes; 6) addresses modern techniques of electrophysiology in the neuronal context, with a special attention for axonal signalling, promoted by a system composed by MEAs and microfluidics; 7) presents in detail the regulatory role of neuronal activity on mitochondria its transport mechanisms. In the following Chapter 3 it describes our methodology to change neuronal activity so that effects on mitochondria axonal transport can be observed and further analysed. It starts by in 1), 2) and 3) the preparation of the neuronal culture and labelling of mitochondria; and moves on to 4) the electrophysiological characterization of this type of culture, then in 5) and 6) it approaches the stimulation and inhibition techniques and simultaneous live-imaging of mitochondria dynamic; in 7) there is the data validation; in 8) the description of how electrophysiological data was analysed and 9) the mitochondrial trajectories; 10) presents the statistical analysis and 11) an algorithm to accelerate the mitochondrial trajectories analysis and export relevant features. The results of the experiments are presented in Chapter 4 where 1) provides the neurons electrophysiological activity characterization throughout maturation and 2) we analyse the effects of increasing and decreasing neuronal activity and its regulatory role on mitochondria transport. At the end of the dissertation, in Chapter 5 we discuss the results found in this study and compare with the literature and conclude our findings.

Chapter 2

Literature Review

1) Brief introduction to neuronal physiology and anatomy

The nervous system is the major control system of the body homeostasis, i.e. it controls the relative constancy of the internal environment of the human body and other organisms. To achieve that, the nervous system works by constantly monitoring, through its receptors, any disturbance within the internal and external environment, processing the information received, and sending appropriate outputs to the effectors, muscles and glands [1].

The nervous system can be structurally divided in two major parts, the central nervous system (CNS) and the peripheral nervous system (PNS), which is further subdivided into the somatic nervous system (SNS) and the autonomic nervous system (ANS). The CNS includes the brain, spinal cord and retina [2], whereas PNS is composed by peripheral nerves and ganglia, small enlargements along peripheral nerves that enclose cell bodies. The SNS is composed by sensory and motor neurons and controls all voluntary muscular systems within the body and the process of reflex arcs. Sensory neurons or afferents have their cell bodies clustered in sensory ganglia and long axons projecting to their sensory targets. Their main function is to relay changes in the internal and external environment to the CNS. Motor neurons or efferents have their cell bodies in the CNS and long axons that can go up to meters to reach the target muscles they innervate. Their main function is to send to the effectors the outputs from CNS. The ANS is further organized in the sympathetic and parasympathetic divisions and controls the involuntary processes of the body, such as functions of the internal organs, blood vessels, smooth and cardiac muscles. The sympathetic neurons are activated and produce responses under stress conditions, the known body's “fight or flight” response. In turn, the return to rest

condition after moments of stress is mediated by the parasympathetic neurons, which promote the body's "rest and digest" response [3].

Neurons are the functional unit of the nervous system, which main function rely on the coordination of complex body processes: they receive electrochemical input signals, integrate these incoming signals, and transmit the output signals to their targets. Such neuronal functions are directly linked to the unique and polarized neuron anatomy: cell body, dendrites, axon, and axonal terminals (**Figure 1**). Each of these specialized neuronal regions plays different roles in the overall neuron function.

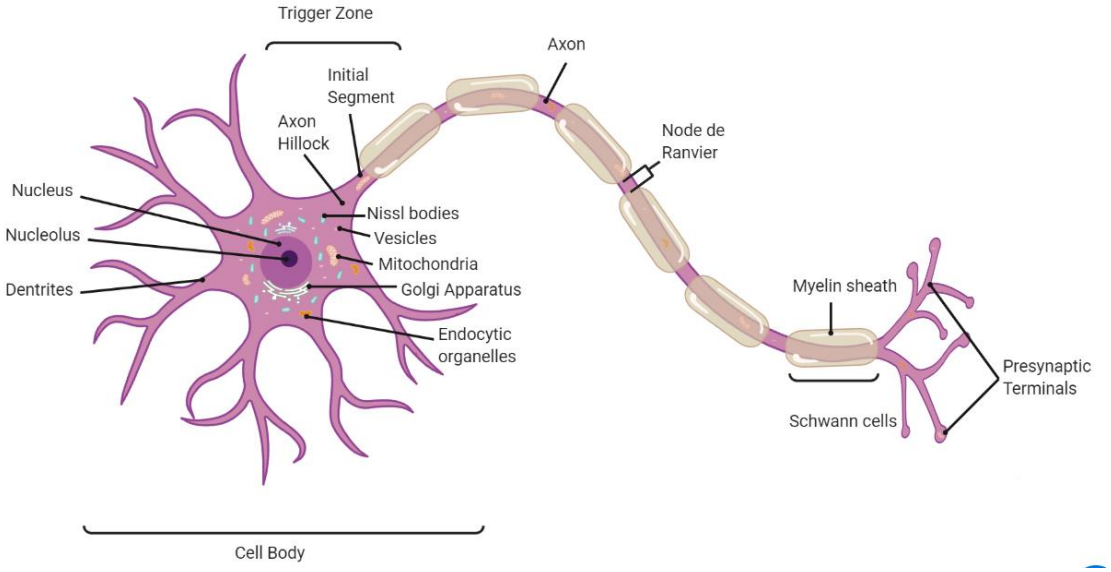

Figure 1- Representation of a multipolar neuron and its main anatomic compartments (dendrites, cell body, axon, and axon terminals) and organelles. Image created using BioRender.com

The neuron cell body withholds the nucleus and all organelles required to regulate cellular activity. The organelles surrounding the nucleus include the rough endoplasmic reticulum, Golgi apparatus, lysosomes, mitochondria, among others. From the cell body, an extensive cytoskeleton, composed of neurofilaments and microtubules, extends outwards into the dendrites and axon. These structures are crucial to cytoplasm organization and to mediate the transport of organelles between the cell body, dendrites and axon.

Dendrites are short branching processes that come from the cell body with the main role of receiving incoming information and transferring it to an integrating region within the neuron. They substantially contribute to increase the surface area of a neuron, allowing it to receive signals from multiple other neurons. Many of them have small extensions called dendritic spines, which expand even more the dendrite's surface area. Dendritic spines vary from thin spikes to mushroom-shaped knobs and may change their size and shape in response to input from neighbouring cells – these changes are important for learning and memory, among other brain functions [4, 5].

The axon is a longer branching process that arises from a specialized region of the cell body called axon hillock that narrows into the axon initial segment (AIS). Axons often split in many branches and end in bulbous swelling regions called presynaptic terminals, which store secretory vesicles containing neurotransmitters (neuronal signal molecules) [1]. Some axons are wrapped by interrupted layers of myelin, formed by Schwann cells or oligodendrocytes, in PNS or CNS neurons respectively. These myelin sheaths act as insulators, reducing the current leak through the membrane and increasing axon capacitance. Therefore, myelinated axons are characterized by increased electrical impulse conduction velocities. The main function of the axon is to generate and propagate the action potentials that trigger synaptic communication with target cells, and also to mediate the transport of multiple biomolecules and organelles between the cell body and the axon terminals. The AIS has a particular elevated concentration of voltage-gated ion channels as well as a number of cell-adhesion molecules anchored by an assembly of ankyrin G and βIV-spectrin that influence both: i) the generation and shaping of action potentials, and ii) the regulation of intracellular trafficking between the cell body and the axonal compartment [6].

Neurons can be generally classified using morphological, physiological and molecular criteria. The morphological classification usually includes the description of shape and branching patterns of dendrites and axons, but sometimes features like soma size and spine density are also used [7]. According to that, neurons can be classified as multipolar, bipolar, unipolar or anaxonic (**Figure 2**). Multipolar neurons have a single long axon that may branch several times and end at enlarged axon terminals, such as spinal motor neurons. Bipolar neurons, like retinal cells, have two processes extending off the central cell body into opposite directions. Unipolar or pseudo-unipolar neurons have one short process – a stem axon [8] - that is further divided into two opposite branches. DRG neurons present this morphology where one axon extends to the spinal cord whereas the other extends to peripheral target tissues/organs such as, skin or muscle [9]. Anaxonic neurons have multiple neurites but no apparent axon.

The physiological classification includes the description of intrinsic firing pattern of the neurons. According to this scheme, neurons can be classified into subtypes such as regular firing, spike-frequency adapting, bursting types, among others [10-12]. Regarding their molecular properties, neurons are classified based on their most common protein and mRNA composition. Neurons can be also categorized in terms of their connectivity properties. However this type of classification is a lot harder to accomplish, hence not frequently used [7].

In addition to anatomical polarity, neurons display also a polarized distribution of some of their intracellular components, which is crucial to maintain their proper function during development, growth, synapse formation and plasticity [13]. . Organelles such as the smooth

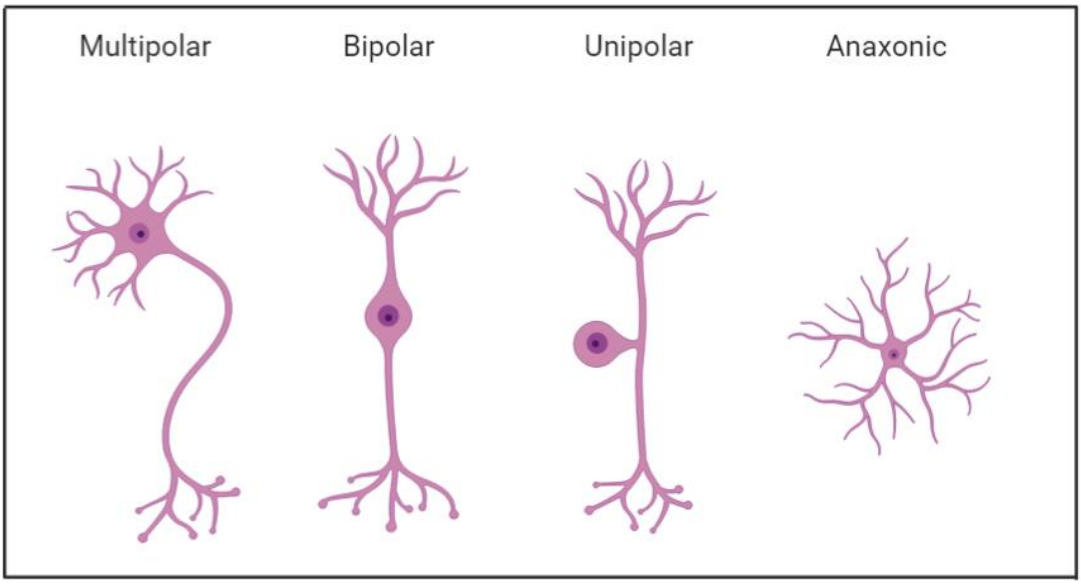

Figure 2 - Different structural types of neurons: multipolar, bipolar, unipolar and anaxonic neurons. Image created using BioRender.com

endoplasmic reticulum, mitochondria, late endosomes, lysosomes, peroxisomes, autophagosomes and dense-core vesicles are distributed in neurons in a non-polarized way [14, 15]. Other organelles, like the classical early endosomes, rough endoplasmic reticulum and the canonical Golgi apparatus are exclusive of the somatodendritic compartment, while synaptic vesicles are mostly found in the axon terminals [14, 16]. Despite the growing number of studies reporting axonal transmembrane protein synthesis and delivery [17], the cell body remains the main contributor for the axonal proteome. As a consequence, such somatodendritic-derived components need to enter in the axon and be transported to the axonal domains where they are required to support the neuronal function demands. Similarly, axon-derived components with cell body as final destination require to be selectively transported to their intended destination. As previously mentioned, the main responsible to regulate the trafficking between the somatodendritic and axonal compartments is the AIS, in particular a proximal region to the AIS recently termed “pre-axonal exclusion zone” (PAEZ) [15]. The PAEZ carries out a polarized sorting of the somatodendritic-specific organelles that rely on the ability of these organelles to interact with specific microtubule motors that drive movement along different microtubule tracks [15]. Thus, long-range organelle axonal movement in neurons is dominated by the action of microtubule-based motors. The next chapter will focus on the description of the axonal transport of intracellular organelles under physiological conditions.

a) Electrophysiology of neurons

Neurons possess the ability to communicate with other neurons or target cells via synapses, where an action potential transmits information from the presynaptic to the postsynaptic neuron. This neuronal junction can propagate signals through electrical, chemical transmission or both simultaneously.

Electrical transmission directly connects two cells through gap junctions increasing the propagation velocities of action potentials, a key advantage in cardiac and smooth muscles. On the other hand, chemical transmission diffuses neurotransmitters from the presynaptic neuron across the cleft towards the postsynaptic neuron, as demonstrated in

Figure 3. An action potential generated in the presynaptic neuron propagates until the synaptic button, which changes the voltage across the membrane potential, inducing calcium influx (voltage-gated channel). The vesicles transporting neurotransmitters dock and release their content (exocytosis) to the small gap. These molecules change the ion concentration which can at this point have an excitatory or inhibitory effect of the other neuron, opposed to electrical synapses which can only excite other cells. Excitatory postsynaptic potentials increase the voltage membrane potential towards firing an action potential, whereas inhibitory maintain the membrane potential below the threshold. At last, the neurotransmitters are removed by glial uptake or enzymatic degradation [18].

Hodgkin and Huxley were able to mathematically explain how an action potential is generated, relating the conductance of voltage-gated channels and the changes in the membrane potential [19, 20]. Action potentials are all or nothing events and result from strong perturbations in membrane voltage potential which lead to the opening of (voltage-gated) sodium (Na^+) channels. The inward flow of Na^+ ions positively charge the intracellular space and cause the membrane to depolarize. At +40 mV the Na^+ conductance inactivates and the now opened potassium channels become the dominating conductance. The combination of these two mechanisms (inactivation of Na^+ channels, and opening of K^+ channels), lead to membrane repolarization (as K^+ ions flow out of the cell following its gradient concentration, thus decreasing the membrane potential). However, K^+ channels are transiently more permeable, undershooting the membrane potential. This hyperpolarization closes K^+ voltage-dependent conductance. The membrane potential is slowly restored to its resting state. During the period during which Na^+ channels change from inactivated to closed state, called refractory period, action potentials are hampered, which prevents back propagation and results in a limited frequency of firing per axon [18].

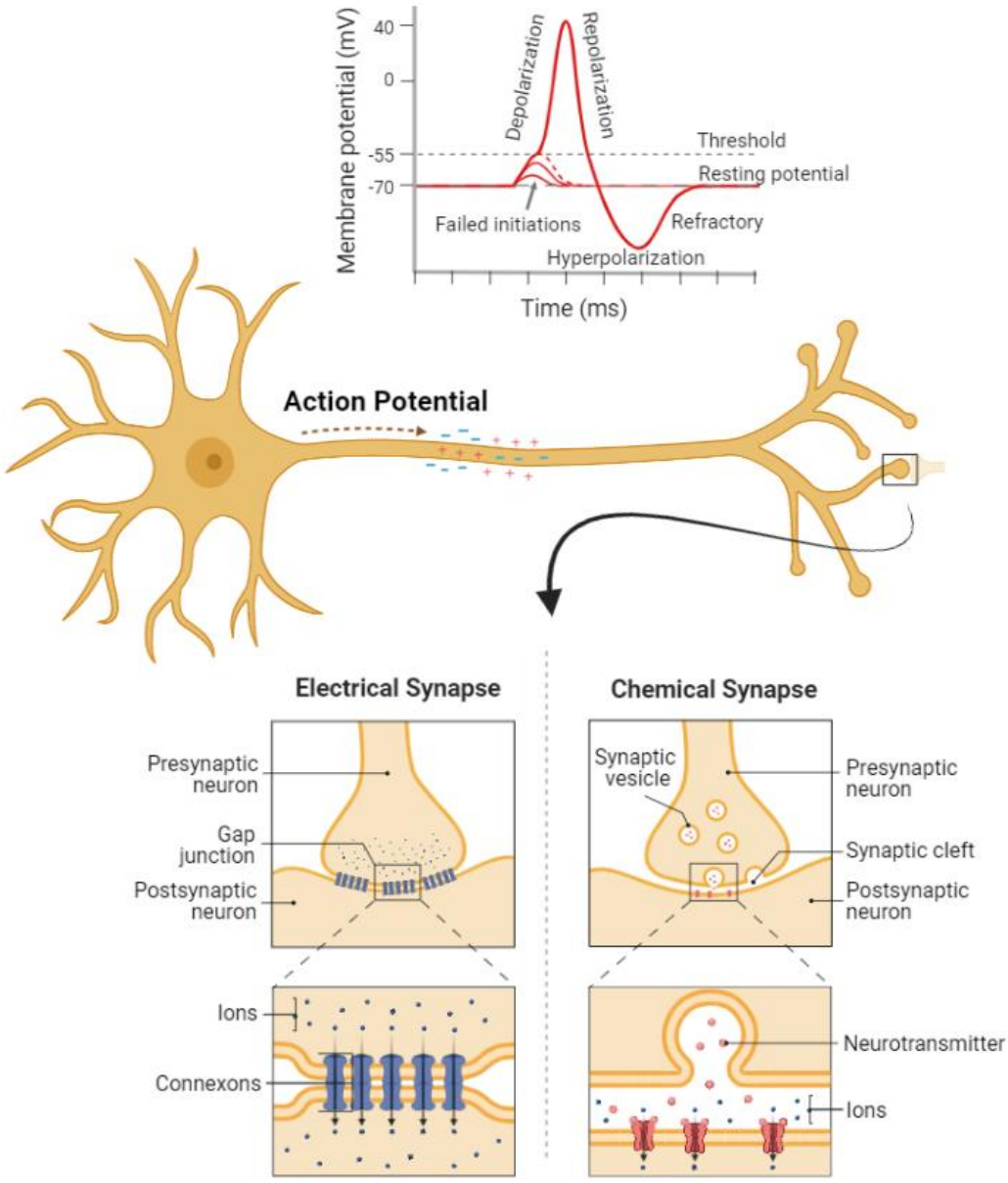

Figure 3 - Types of synapses. After generation on the AIS, the action potential propagates along the axon and is transmitted across synapses in the form of ions flow (electrical synapses) or in the form of neurotransmitters (chemical synapses). Image created using BioRender.com

2) Axonal Transport in Homeostasis

The axon is the longest part of a neuron and, mainly in the PNS, it can extend several meters long. One of its main functions is to allow that all the molecular components synthesized on the soma can travel along it to the more distal region of the neuron, where neuronal connections are established. Similarly, aged proteins and organelles are expected to travel back along the axon to the soma for degradation and recycling. In other words, axonal transport concedes a spatial-temporal distribution of intracellular molecules and organelles that best fit neuronal function requirements. Indeed, this cargoes trade-off enables the neuron growth and maturation, establishment of its polarity, axon stabilization, axon regeneration, alongside the axonal plasticity [21]. Therefore, this regulated movement of intracellular cargoes requires a complex, dynamic and well organized axoplasm capable of integrating the physical cargoes transportation with the maintenance of the physiological conditions for neurons functioning.

The axonal cytoplasm contains a dynamic network of protein polymers known as the cytoskeleton. These protein polymers interact with each other and with other subcellular components in a way that allow them to function as a "rail" for the intracellular components, such as organelles and other proteins. However, these intracellular components, to be transported and delivered to their appropriate destination, are required to attach and detach from the cytoskeleton. This is accomplished by molecular motor proteins: kinesins, dyneins or myosins and their correspondent adaptor proteins. This chapter will briefly describe the complex and dynamic interaction between all these axoplasm elements that enable the proper functioning of the intracellular axonal transport.

a) Structural Components of axonal transport

The cytoskeleton is a dynamic framework composed by a transiently cross-linked polymers network (**Figure 4**). In axons, the cytoskeleton is composed of microtubules, microfilaments, specifically actin filaments, and neurofilaments or intermediate filaments. Together, they contribute to the morphology and functioning of neurons intracellular transport [22].

Microtubules are very long polymers aligned in a parallel array along the axon length, that usually associate with other proteins, such as microtubule-associated proteins (MAPs) and Tau, to acquire more stability. Microtubules are polar and rigid cylindric polymers composed of tubulin heterodimers (α-tubulin and ß-tubulin). The orientation of these tubulin heterodimers gives a structural polarity to microtubules, with distinct ends that differ in their kinetics of assembly. Microtubules polarity is described with its "minus"-end (α-tubulin ends) exposed to the cell body and its "plus"-end (β-tubulin) facing the distal side of the axon [2].

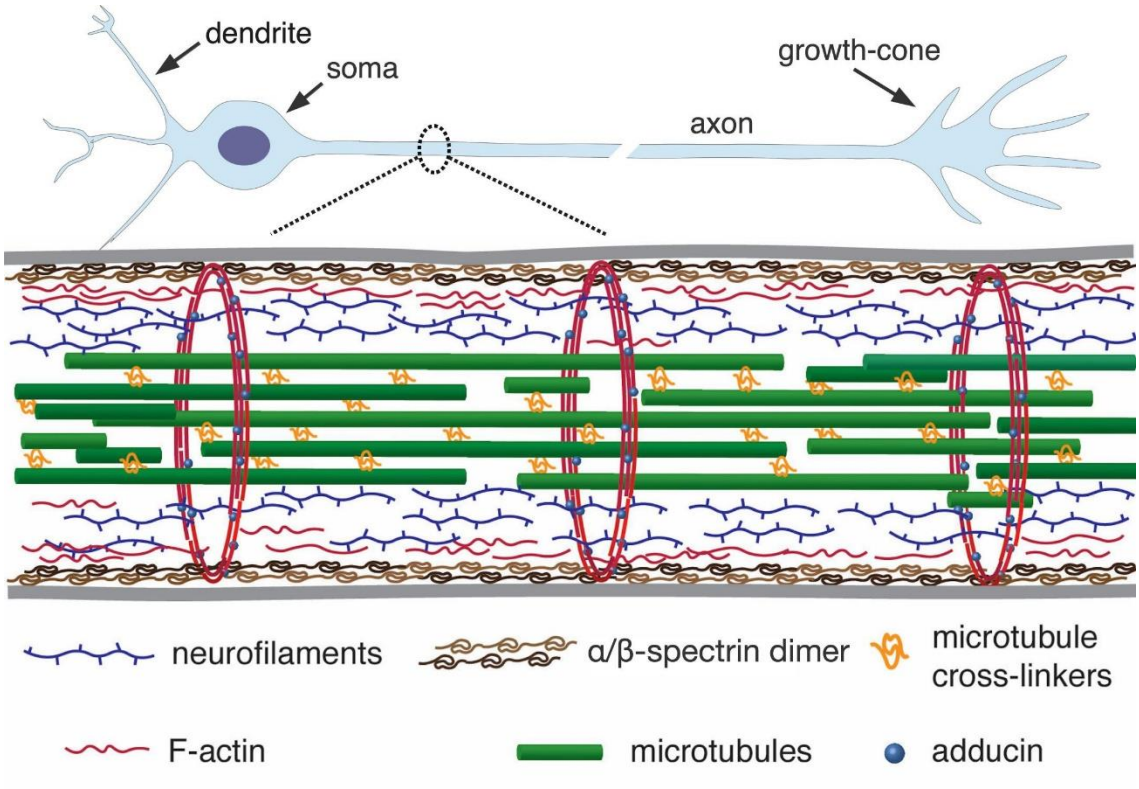

Figure 4 – Schematic representation of the axonal cytoskeleton. Usually, the axonal core has a bundle of microtubules that is surrounded by neurofilaments. The outer part of the axon has periodically spaced rings of F-actin filaments (Adapted from [23])

The centrosome is the microtubule organization centre of the nerve cell, and it is thought to be the sole site of formation of new microtubules in axons. This implies that all new axonal microtubules are transported out into the axons by the mechanisms of anterograde axonal transport. Given their length and organization, microtubules are generally assumed as the tracks for long-range movements in axons. Still, although very long, microtubules do not extend for the entire length of the axon.

Microfilaments are short polymers that are radially and axially oriented within the axon. In the axon, they are mainly present in the AIS, in the vicinity of microtubules and in the growth cones and nerve terminals. Microfilaments are polar and semi-flexible polymers composed by two twisted strands of actin proteins (also known as F-actin). Like microtubules, actin filaments have a defined polarity with a "plus" and "minus" ends that differ in their kinetics of assembly. Based on their short length, actin filaments are considered the tracks for short-range movements (*e.g.* lateral movements in the axon and movements in domains that lack microtubules).

Neurofilaments or intermediate filaments are apolar structures assembled by multiple neuronal intermediate filament proteins, which in contrast to microtubules and microfilaments, do not serve as tracks for the intracellular cargoes movement but provide mechanical support. However, there are some evidences that intermediate filaments may have

a role in vesicular trafficking on the endocytic pathway, as summarized in this review [24]. In the nervous system, the most common intermediate filament is the glial fibrillary acidic protein (GFAP) and vimentin.

Each cytoskeleton component is unique in structure and function. Each of them associates with its own set of binding proteins and perform specialized roles within the axon. During axonal trafficking microtubules and actin filaments function as axonal "rails" and are associated with their specific molecular motor: kinesin and dynein molecular motors associated with microtubules, while myosin motors associated with actin filaments [2].

b) Molecular Motors

The axonal transport of intracellular cargoes is generated by molecular motors: kinesin, dynein and myosin (**Figure 5**). Because of cytoskeleton polarity, the axonal transport of cargoes by molecular motor proteins is unidirectional. For instance, kinesin moves towards the plus-end of microtubules, mediating the anterograde axonal transport. Dynein moves into the opposite direction, mediating the retrograde cargoes transport to the soma. Each molecular motor has intrinsic kinetic properties that influence, at least in part, the velocity of cargo movement along the axon. Thus, cargoes movements may occur via fast or slow axonal transport (some examples in Table 1). Fast axonal transport is characterized by velocities within 0.6 – 5.0 μm/s [13], while slow axonal transport is in the range of velocities between 0.20 – 10 mm/day [25], The slow axonal transport velocities are mainly a result of prolonged pauses between movements [26]. Additionally, complex transport dynamics are regulated by motor activators, adaptors and scaffolds. Examples include dynactin, c-Jun N-terminal kinase (JNK) - interacting protein 1 (JIP1) and Hook1 [27].

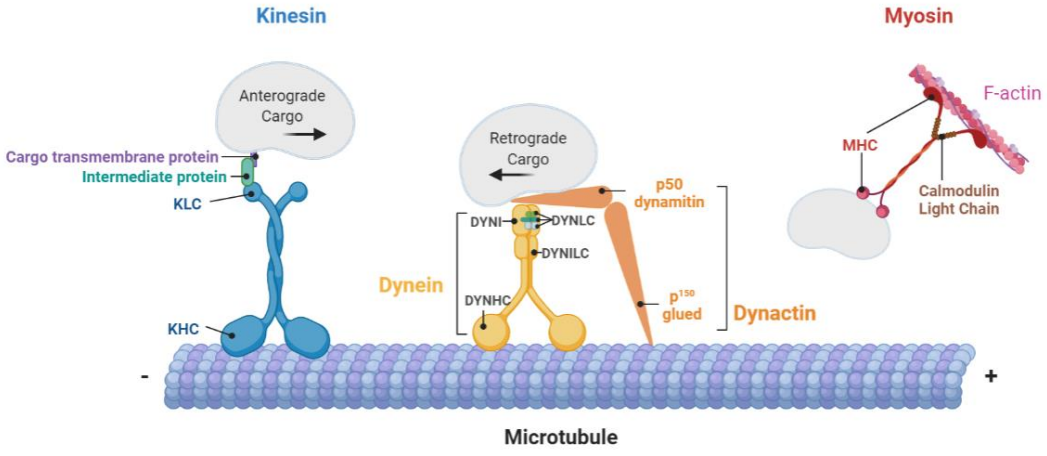

Figure 5 - Molecular motors in neurons: kinesin and dynein associate with microtubules while myosin associates with microfilament F-actin. KLC: kinesin light chain; KHC: Kinesin heavy chain, DYNI: Dynein intermediary chain, DYNHC: Dynein heavy chain, DYNLC: Dynein light chain, DYNILC: Dynein Intermediary light chain, MHC: Myosin heavy chain

i) Kinesin

Kinesin molecular motor drives the anterograde transport of intracellular neuronal cargoes. Anterograde transport enables axonal growth and elongation with newly synthesized proteins and the formation synaptic vesicle precursors (SVPs) in the soma, allowing the establishment and stabilization of neuronal connections, thus maintaining pre-synaptic activity [21, 22]. The discovery of kinesin, took place in the 80s upon the motility evidence in cytoplasm extruded from giant axon the squid [28]. Kinesins motors move vesicles, organelles, proteins and RNA particles at 0.5 – 1.0 μm/s. There are over 40 kinesin genes in the human genome, most of them expressed in the brain, but only 3 kinesin families contribute to the axonal transport dynamics, namely family kinesin-1, kinesin-2 and kinesin-3 [22].

Kinesin is a heterotetramer composed of a dimer tail, alpha-helical stalk, a neck linker and a dimer globular motor. The globular domain consists of two kinesin heavy chains (KHC), whereas the tail contains two kinesin light chains (KLC) (**Figure 5**). To initiate transport, kinesin firstly attaches to the microtubule through tubulin acetylation then, through the action of adaptor proteins, cargoes bind to kinesin and, at last, the globular motor enables its movement via hydrolysis of the ATP of the front head.

Members of the kinesin-1 family drive the transport of a wide range of cargos including vesicles, organelles, proteins, and RNA particles. Kinesin-2 family members contribute to the motility of N-cadherin, ß-catenin and fodrin-positive plasma membrane precursors. Other molecular motors, such as members of the kinesin-3 family are thought to be super processive following cargo-mediated dimerization and drive synaptic vesicle precursors and dense core vesicles [22].

Several studies have been supporting the evidence that the knockouts of kinesins and its protein adaptors promote neurodegeneration, emphasizing their role in neuron homeostasis maintenance. For instance, it was demonstrated that kinesin KIF3, in hippocampal neurons, mediates the transport of the polarity protein PAR-3 to the tip of growing axons and, consequently, the separation of this complex impairs the establishment of neuronal polarity [29]. Others showed that the lysosomal kinesin adaptor Arl8 aids in the delivery of critical components to the presynaptic sites. When overexpressed, it facilitates the presynaptic function, but when absent it leads to deficiencies in the neurotransmission [30].

ii) Dynein

Dynein molecular motor drives the retrograde transport of intracellular neuronal cargoes. Retrograde transport promotes the movement of endosomal recycling vesicles and autophagosomes to the soma, and therefore, the degradation of neuronal components (Table 1).

Dynein 1 is a multisubunit complex that contains two heavy chains (DYNCH), two intermediate chains (DYNCI), four light intermediate chains and several light chains (DYNCL) [31] (**Figure 5**). Similarly to kinesin, dynein heavy chains allow the protein binding to the microtubules and its movement along the axon, whereas the tail allows binding to other dynein subunits. Cargoes attachment to dynein is mediated by another multiprotein complex, particularly the dynactin, that is connected to the dynein tail [31]. Most dynein functions in the cell require the dynein activator dynactin [32]. Dynactin is composed of two subunits, the large dynactin subunit 1 (DCTN1), commonly known as p150 glued, and two other subunits, the p50 dynamitin and the p22/p24 [33].

Dynein are fast motors driving organelles at 0.5 – 1.0 μm/s with back and side steps, that with the aid of activators or team effort, provides a retrograde unidirectional transport more flexible than kinesin, although weaker [22].

iii) Myosin

Myosin Va has been largely studied amongst others, due to its regulatory role of dense core vesicles, neurofilaments and mitochondria [34]. It is composed of two head motor domains, two alpha-helical segments and two glomerular tails (**Figure 5**). The head motors have the ability to bind to actin filaments, ATP and the neurofilaments light chain, whereas the tail domain binds to cargoes and interacts directly with KHC. Myosin Va appears to balance the directionality of axonal transport, meaning that it tends to move organelles in the retrograde direction, counterbalancing the accumulation at the distal side. It is also though that by interacting with actin filaments, the organelles will dissociate from the microtubules at a controlled pace, contributing for the regulation of the delivery rate at the distal side of the axon [35].

Myosins often interact with actin filaments during short-range mobility, such as myosin I during local transport from the core of the axon to the plasma membrane [35], thus sorting and tethering organelles. Additionally, this molecular motor helps both initiation and termination of microtubule-based transport along with cargo transport in low density regions of microtubules or high actin density [27].

c) Bidirectional Transport

Even tough axonal transport presents only two types of movements, anterograde or retrograde, another modality presents themselves as bidirectional. Some organelles during their transport along the microtubules exhibit reversals in direction, culminating in a change of net direction. Examples of that include mitochondria and lysosomes, as seen in **Table 1**. The main reason for reversals in direction during a run remains unclear but may be a result of simultaneous association of both kinesin and dynein motors to the cargo together with different

instantaneous affinity to the cytoskeleton tracks. For instance, specific adaptor cargoes can induce opposite movements [31]. When JNK – interacting protein 1 (JIP1) binds to KLC, the transport occurs in direction to axons [36], whereas when glutamate receptor-interacting protein 1 (GRIP) connects to KHC, it leads cargo trafficking towards dendrites [37]. The regulation of this mechanism is more detailed in 4).

Table 1 - Types of axonal transport for distinct neuron organelles. Adapted from [10, 38]

Type of transport	Velocity of transport	Membrane-bound organelles						Cytoskeleton proteins				RNA
		Mitochondria	Golgi-derived vesicles	Neurosecretory granules	Endosomal recycling vesicles	Lysosomes	Autophagosomes	Neurofilaments	Tau	Tubulin	Actin	
Anterograde	Fast		*	*								
	Slow							*	*	*	*	
Retrograde	Fast				*							
	Slow						*					
Bidirectional	Fast	*										*
	Slow					*						

3) Pathologies associated with defects on axonal transport

As detailed in the previous chapter, axonal transport is critical for maintenance of axonal integrity and neuronal function. Through anterograde kinesin-mediated transport axon is supplied with proteins synthesized in the cell body, and by retrograde dynein-based transport, endosomal signaling organelles are delivered to the cell body. Therefore, any disruption in the proper functioning of axonal transport implicates a dysfunction in the neuronal function, by accumulation of cargoes at a specific location within the neuron [31].

A number of studies have been establishing a major role of axonal transport defects in the pathogenesis of several neurodegenerative diseases, such as Alzheimer disease, Parkinson disease, Huntington disease and Charcot-Marie-Tooth 2, among others [39]. Axonal transport defects may be caused by damages in the i) transport machinery (molecular motors and/or adaptor proteins), ii) integrity of the cytoskeleton, and iii) energy supply chain [26]. However, whether these impairments are a cause, a contributor or simply a consequence of neuronal degeneration remains unclear. Thus, understanding the relationship between axonal transport defects and neurodegeneration is of major interest for the neurodegenerative diseases research field.

a) Defects in transport machinery

Alzheimer's disease presents two mutated genes which contribute to the impairment of axonal transport, namely mutations in the amyloid precursor protein (APP) and int the presenilin (PSEN) 1 and 2 genes [26, 31, 40]. A study using a mutant hAPP mice demonstrated an impaired retrograde transport of axonal autophagosomes, as a consequence of an interaction between amyloid-β oligomers and the dynein motor. This interaction impairs dynein recruitment and an immobilization of these organelles in distal axons, which contributes to autophagic stress in axons displayed in this pathology [41]. Moreover, the hyperphosphorylation of tau, which remains a hallmark in this disease, was shown to interfere with the kinesin binding to microtubules [42]. Other mutations in specific genes have been also associated with other neurological diseases. For instance, alterations in the huntingtin (HTT) gene has been shown to be involved with changes in the bidirectional trafficking of vesicles in the Huntington disease [43]. White et. al. demonstrated that the decline of HTT leads to a deficiency in the dynein and kinesin-1 motors recruitment during transport of Rab4-containing vesicles, thus leading to an accumulation in axons and synapses [44]. Additionally, in the ALS it was also verified that mutations in the superperoxide dismutase (SOD1) gene modify the phosphorylation of molecular motors or cargoes (*e.g.* neurofilaments), whereas mutations in the alsin (ALS2) gene is linked to alterations in the vesicle trafficking by inhibiting retrograde transport [25, 31]. Other studies revealed that mutant TDP-43 (transactive-region DNA-binding protein) mice display *in vivo*

defects in endosomal retrograde transport, in which the mean endosomal speeds decreased and the period of pauses were longer [45].

b) Damages in cytoskeleton integrity

Tau is a neuronal MAP that stabilizes axonal microtubules [46]. In addition, tau modulates the molecular motor motility to direct intracellular transport by regulating the forces exerted by kinesin and dynein. Therefore, it has been suggested that a dysregulation of tau might contribute to neurodegeneration by disrupting the balance of plus- and minus-end directed transport [47]. Another microtubule stabilizer, epothilone D (EpoD) is suggested to improve learning and memory functions on transgenic mice with Alzheimer's disease, which increases key synaptic protein levels and improves the axonal transport of mitochondria [40]. In Parkinson's disease, the mutation on the Leucine-rich repeat kinase 2 (LRRK2) gene promotes filament-like structures that decorate deacetylated microtubule, which disrupts mitochondrial anterograde and retrograde motility by decreasing their velocity and increase their pause durations [48]. Moreover, in mice models of the Charcot-Marie-Tooth 1 (CMT1A) disease that involves duplication or point mutations in the peripheral myelin protein 22 (PMP22) gene, it was observed the loss of cytoskeleton components [49]. Furthermore, in amyotrophic lateral sclerosis disease models, more precisely SOD1 transgenic mice, it was shown direct evidence for axonal defects, namely in the anterograde movement of the cytoskeleton components, including the slowing down of neurofilaments [25, 50].

c) Dysfunctions in energy supply chain

Mitochondria are the primary energy supply factory in cells. These organelles are responsible for maintaining Ca^{2+} homeostasis, stress responses and cell death pathways. Being a fuel supply for the cell metabolism, their transport and distribution along the axon require to be highly regulated to assure proper neuronal function. Familial forms of Parkinsonism present genes associated with proteins involved in the maintenance of mitochondria, such as PARK2, PINK1 and PARK7. It was recently demonstrated that the loss of PINK1 and Parkin leads to mitochondrial degeneration, and that Parkin suppresses mitochondrial transport when activated by PINK1 [51]. On the other hand, it was previously revealed that mitochondria transport may be impaired by neurotoxins, such as 1-methyl-4-phenyl-1,2,3,6-tetrahydropyridine precursor (MPTP) of 1-methyl-4-phenylpyridinium (MPP^+) or the pesticide rotenone (ROT). MPTP/MPP+ induced Parkinson disease models showed an increase speed in mitochondria retrograde transport and decreased anterograde transport [52, 53], whereas the pesticide showed an increase mitochondria retrograde transport [54]. There is a convergent idea that mitochondria dysfunction triggers events leading to pathological hallmarks in

Parkinson. *Esteves et al*. used a peptide called NAP (davunetide) to improve microtubule network assembly and stabilization by increasing α-tubulin acetylation, thus improving mitochondria motility. This way it was possible to recover cell homeostasis in primary cortical neurons [55]. These findings provide themselves as a therapeutic approach for parkinsonism aiming for the improvement of mitochondrial trafficking.

As briefly reviewed, a number of studies from the last two decades have demonstrated that any impairment in axonal transport has an impact on neurodegenerative diseases, although many of the underlying mechanisms are not fully understood. Therefore, it is crucial to deepen our knowledge in the topic, which may contribute to the development of novel therapeutic approaches regarding the improvement of axonal transport deficits.

4) Regulation of Axonal Transport

Being axonal transport a key process for the proper neuronal function, it is crucial to understand its regulatory mechanisms to target defective events that may cause its disruption.

Little is known about the regulatory mechanisms of axonal transport, but important breakthroughs are being achieved by live-cell and *in vivo* imaging approaches [22, 56]. These emerging studies have been demonstrating that axonal transport regulation occurs at multiple levels, including i) coordination of cargo-binding to motors mediated by cargo-specific adaptors, ii) modulation of cytoskeleton tracks, and iii) balance between opposing motors.

a) Regulation of axonal transport initiation

Many motor proteins exist in an enzymatically and mechanically inactive form when they are free, *i.e*. not bounded to cargo [57, 58]. This inhibited state contributes to avoid the useless expenditure of energy. Adaptor proteins assist in the activation of motors by allowing cargoes recognition by the motors. Several studies have identified some of the specific motor-cargo-adaptor combinations, such as syntabulin that allows mitochondria linking to kinesin-1 or Hook1 that activates the dynein-dependent retrograde motility of signaling endosomes [59-61]. Many efforts have been made to scrutinize the regulatory pathway that manage these motor-cargo associations. After cargo binding, motors change their conformation and attach to microtubule tracks. Kinesin motor-microtubule binding is mediated through strong electrostatic interactions and is stabilized upon ADP/ATP nucleotide exchange in the motor domain [62]. But motor subunits, accessory proteins, and (MAPs) can also modulate the motor-microtubule interaction and transport initiation. As an example, MAP7 promotes kinesin-1 binding to microtubules while Tau, an axonal MAP, acts by inhibiting this process [63, 64]. In what regards retrograde transport, dynactin binding to dynein motor promotes its binding to microtubules, through its glycine-rich (CAP-Gly) domain, by the reorientation of the dynein dimer to a more optimal binding conformation [65, 66].

Transport initiation mechanisms contribute to allow the entry of kinesin-bounded cargoes into the axon as well as to aid in the escape of dynein-bounded cargoes from the distal axon, but also to mediate the restarting motor-cargo motility after transient pausing and/or cargo detachment from microtubules.

b) Regulation of the sustained active axonal transport

After initiated, transport along axons is sustained by the continuous motor activity, which is dependent on the intrinsic biophysical properties of the motor and allow the proper cargo distribution to its appropriate destination. *In vitro*, kinesin-1 motor motility can cover around 1 μm distance (step size of 8 nm) prior to microtubule detachment. While monomeric

kinesin-3 is inactive in motility, dimeric kinesin-3 has a superprocessive motion with an average run length of approximately 10 μm, which is around 10-fold longer than that of kinesin-1 [67, 68]. In contrast, dynein motor step varies between 8 to 32 nm, resulting in run lengths of 5 to 10 μm along a single microtubule [69, 70]. It has been verified that function of motor proteins (*i.e.* force production or microtubule binding rates) can be differently affected by the cooperation of homo- or heteromeric assemblies to drive organelle transport [71-75]. For instance, late endosomes/lysosomes are transported by 1 to 4 active kinesin motors and by 1 to 5 dynein motors [76]. Some organelles have simultaneously dynein and kinesin motors attached, which are responsible for bidirectional transport and for frequent pauses and reversals during transport. Several studies demonstrated that the coordination between the activity of these opposing motors is regulated by scaffolding proteins, such as JIP1 and TRAKs 1 and 2 [77-80]. For instance, the connector of kinase to AP-1 (CKA) is a scaffolding protein that associates with dynein and modulates its activity, facilitating the axonal transport of autophagosome and dense core vesicles in neurons [81]. Similarly, Vezatin has been shown to regulate retrograde transport of a subset of endosomes, including signalling endosomes containing activated bone morphogenetic protein (BMP) receptors, probably by regulating dynein-dynactin-dependent movements [82].

c) Regulation of axonal transport termination

Ultimately, the active cargo transport resumes at the appropriate cargo destination, which differs according to the type of organelle in question. The events that mediate cargo delivery are diverse, but all seem to have a common denominator, which is motor proteins instability. For instance, the presynaptic delivery of synaptic vesicle precursors seems to be mediated by the high local density of GTP-rich microtubules plus-ends and the intrinsic low affinity of kinesin-3 for these regions [67]. On the other hand, the presynaptic delivery of mitochondria is caused by a change in the conformation of the accessory protein Miro (in response to local influx of calcium) that detaches and inhibits kinesin-mediated transport [83, 84].

5) Role of neuronal activity in the regulation of axonal transport

In addition to the spatial requisite for cargo distribution within the different neuronal compartments, cargo transportation and delivery is also temporally related with various neuronal function stimuli, such as synaptic activity. However, little is known about whether or how neuronal activity exert a regulatory role in the axonal transport dynamics of neuron intracellular cargoes.

Evidence of activity-dependent axonal transport regulation is limited but has been reported for mitochondria, dense core vesicles and vesicles of the Endosomal Sorting Complex Required for Transport (ESCRT) pathway. For instance, Zhang *et al*. studied the regulation of mitochondria motility at nodes of Ranvier (regions of high ion pumps and mitochondria densities) during continuous frog myelinated PNS axons stimulation by bipolar electrodes over 2 min at 200Hz [85]. They showed that the number of motile mitochondria was reduced during stimulation and concluded that calcium elevation and activation of sodium pumps during action potentials acts synergistically to retard mitochondrial motility. These authors suggest that this may be a mechanism to recruit mitochondria to a node of Ranvier to match metabolic needs. Similar findings were reported by Ohno *et al*. for small myelinated CNS Purkinje cell axons [86]. By using tetrodotoxin (TTX), which blocks voltage-dependent Na^+ channels and eliminates axonal action potentials, or by using bicuculline (BCC), which blocks $GABA_A$ receptors and increases electrical activity, these authors showed that neuronal activity modulates mitochondria motility in nodes of Ranvier. In summary, increased axonal electrical activity decreased mitochondrial transport in nodal/paranodal axoplasm while decreased axonal electrical activity had the opposite effect. The stability and transportation of axonal mitochondria in cultured mouse hippocampal neurons during electrical stimulation was further explored by Obashi and Okabe [87]. Using an electrical field stimulation at 40Hz for 10 s applied every 3 min over 50 min, by two parallel platinum wires, these authors demonstrated that mitochondria dynamics differ between developmental stages and are regulated by neuronal activity. As a matter of fact, they reported that mitochondria transition from stationary to mobile seems to decrease with neuronal maturation (2 weeks to 3 weeks). Finally, Sajic *et al*. investigated the *in vivo* mitochondria trafficking in adult mice's saphenous nerve axons, under resting and electrically active periods (75 min of electrical field stimulation ranging between 1Hz and 50Hz for myelinated axons and capsaicin stimulation for unmyelinated axons) [88]. They concluded that low frequency activity induced by electrical stimulation significantly increases anterograde and retrograde mitochondrial traffic in comparison with silent axons. Higher frequency activity within a physiological range (50Hz) dramatically further increased anterograde, but not retrograde, mitochondrial trafficking. Similarly, topical application of capsaicin to skin innervated by the saphenous nerve increased mitochondrial trafficking in treated axons.

Regarding activity-dependent transport of dense core vesicles, it was demonstrated that vesicular axonal trafficking of semaphoring 3A is reversibly arrested with neuronal depolarization and accelerated when action potentials are blocked with tetradoxin (TTX) [89]. Interestingly, these activity-dependent effects were not evidenced in the dendritic transport of these vesicles. In contrast, vesicles of the ESCRT pathway exhibited increased anterograde and bidirectional motility in response to neuronal firing [90].

Altogether, these studies offer some noticeable divergent conclusions regarding activity-dependent cargoes motility but highlights a possible strong regulatory role of neuronal activity on the axonal trafficking dynamics of key neuronal cargoes. Though we understand aspects of the major players of axonal transport and their physiological functions, details of the spatial and temporal regulation of neuron cargoes transport under physio- or pathological scenarios remains mostly unknown. Thus, dissecting the molecular mechanisms of axonal transport and its activity regulation during development and maturation of the nervous system is key to understand nervous system biology and hopefully to accelerate the discovery of underlying mechanisms of neurodegenerative diseases.

6) Models in neuroscience research to study activity-dependent axonal transport

a) Electrophysiological recordings in neuroscience research

The faithful propagation of action potentials along axons is a key neurophysiological property upon which neural communication depends. Understanding this electrical communication is fundamental to comprehend neuronal functions. In this context, electrophysiology remains the standard methodology in neuroscience research, since it allows the monitoring and modulation of neuron electrical activity, both at the single level as well as at the network level (involving a large number of interacting cells). Although it is the axon that performs the main electrical operation in neurons, early electrophysiological studies were mainly limited to recordings from the soma and dendritic spines [91, 92]. Indeed, collecting electrophysiological data from axons has been challenging owing to its thin, long and tangling nature [93]. As a result, we know much more about dendrites, somas and synapses than we know about axons.

The conventional electrophysiology technique is the patch-clamp. Patch-clamp recordings provide the highest resolution for electrophysiological data from single neuron to single channel. It has the ability to monitor the intrinsic, synaptic and biophysical properties of ion-channels. This technique consists of the use of a glass pipette filled with an electrolyte solution, which is tightly sealed onto the surface of the neuron and isolates a "patch" of its membrane (**Figure 6**). In this way, it is possible to establish a high resistance seal between the neuronal membrane and the opening of the pipette. Therefore, currents flowing through the channels within this patch flow into the pipette and can be recorded by an electrode. Patch-clamp technique has many recording configurations, namely cell-attached, outside-out, inside-out and whole-cell (**Figure 6**), being each one more appropriated to specific research aims. In general, with these configurations, this technique allows to record electrical potentials and currents from small cell patches or from the entire cell. Even though patch-clamp is the most commonly used method in electrophysiology, it is a low throughput technique that has limited spatial and temporal resolution (*i.e.* by damaging cell membrane allows only short-term studies), is labor intensive, and difficult to be used in accessing smaller neuronal compartments (*i.e.* axons) [94, 95]. Indeed, besides the difficulty to patch axons, patch-clamp methods are not the most appropriate to track the action potentials propagation at more than two sites or even across an axonal arbor [96]. An alternative to study axons includes the use of imaging tools (*e.g.* calcium imaging) and optogenetics [97, 98]. However, these methods are still limited in signal-to-noise ratio as well as in temporal resolution [99]. Giving these limitations, and with the increased interest in exploring the electrophysiological properties of the axon, the extracellular recordings using microelectrode arrays (MEAs) became very popular in the recent years [100], not to mention its usability in understanding neuronal networks.

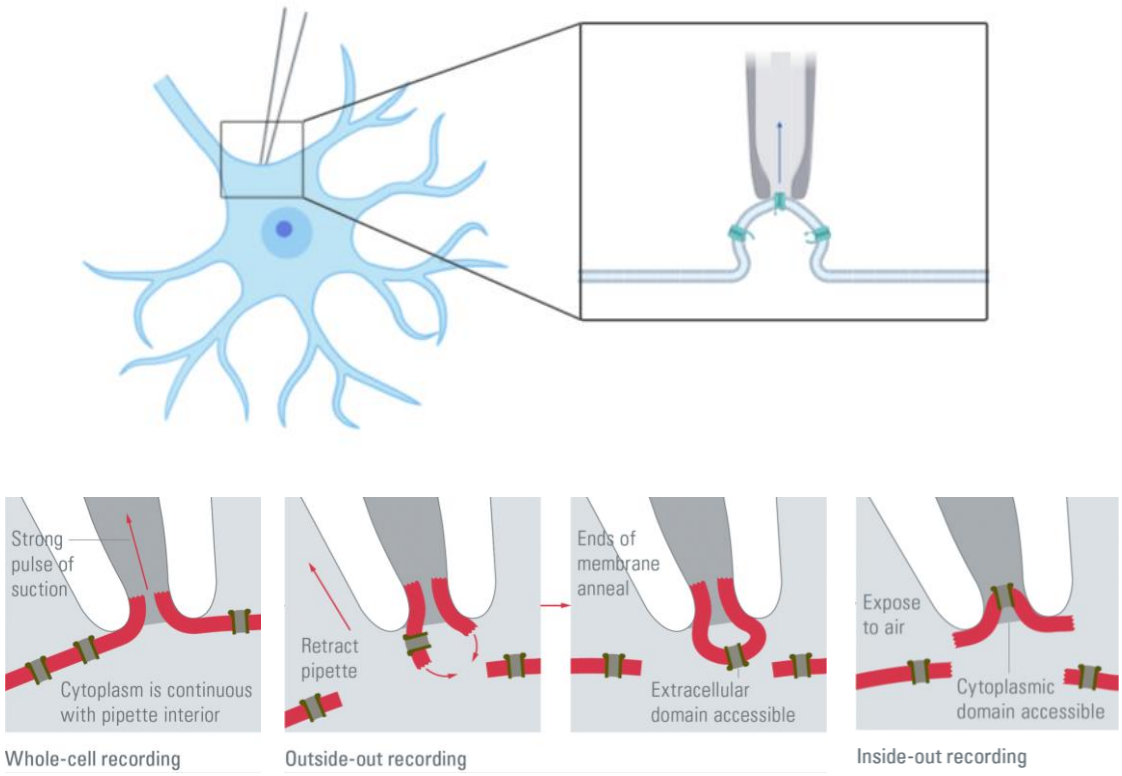

Figure 6 – The four recording methods for patch-clamp: cell-attachment performing a mild suction and tight contact between pipette and membrane (Image created in Biorender.com) (on top); **Whole-cell**: the cell membrane is ruptured and the pipette gains access to the cytoplasm (left); **Outside-out**: the pipette is retracted resulting in two small pieces of membrane that reconnect and form a small vesicular structure (center); **Inside-out:** the pipette is retracted and the patch is separated from the rest of the membrane and exposed to air (right) (Adapted from [101]).

MEAs use in neuroscience research emerged mainly due to its appropriate spatial and temporal resolutions that allow to access extracellular electrical activity at the single cell or network level (at multiple sites). Since it is non-invasive, it can be used to manipulate and/or record electrophysiological data in long-term studies. This state-of-the-art technology is based on a substrate-integrated microelectrode array with the capacity to, in a well-controlled *in vitro* setting, record and/or stimulate neuronal cultures/tissue slices, at the millisecond time scale (**Figure 7**). Overall, their use contributes to the interpretation of neuronal communication, information processing and encoding, and action potentials propagation [102].

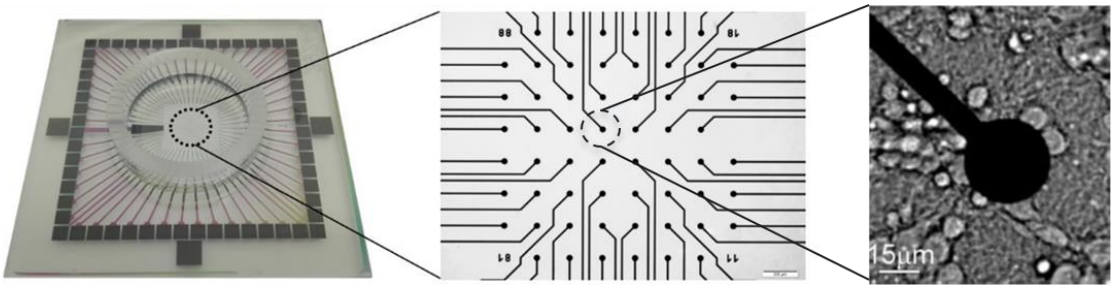

Figure 7 - Standard planar microelectrode array and an example of a neuronal culture (MEA, 30 µm electrode diameter)

The analysis of axonal electrical activity using conventional MEAs is challenging to accomplish, mainly due the small size of axons, whose action potentials induce small changes (magnitude) in the extracellular potential recordings and, thus, difficult their discrimination [103, 104]. Moreover, in conventional cultures under MEAs it is virtually impossible to align axons with microelectrodes and, therefore, the source-target action potential information is almost inaccessible. In addition, the presence of glial cells in culture often interfere with axonal recordings as well [105]. However, these limitations can easily be overcome through the combination of MEAs with microfluidics devices (μEF platform – previously described by the host group) [106, 107].

b) Microfluidic devices in neuroscience research

Microfluidic devices consist of compartmentalized cell culture chambers composed of two or more isolated cell seeding compartments, functionally interconnected by microchannels. Many microfluidic platforms used for biological research are composed of poly(dimethylsiloxane) (PDMS), a low-cost flexible elastomer, with optical transparency, high gas permeability, biocompatibility, and thermal stability [108, 109]. One major advantage of microfluidic-based cell cultures is the ability to precisely define the cell microenvironment and control cell growth within different compartments. This way it enables the study of biochemical and physical properties of neurons or neuron-surface interactions. When applied to neuroscience research, microfluidic devices provide the possibility to separate cell bodies from axons and axon terminals in distinct compartments (**Figure 8**) and manipulate them. Neuronal compartmentalization allows the guided growth of axons within microchannels and, therefore, the assessment of axonal growth and regeneration [110], synapses formation [111] , axonal behavior [112] and axonal transport [109, 113, 114], among others.

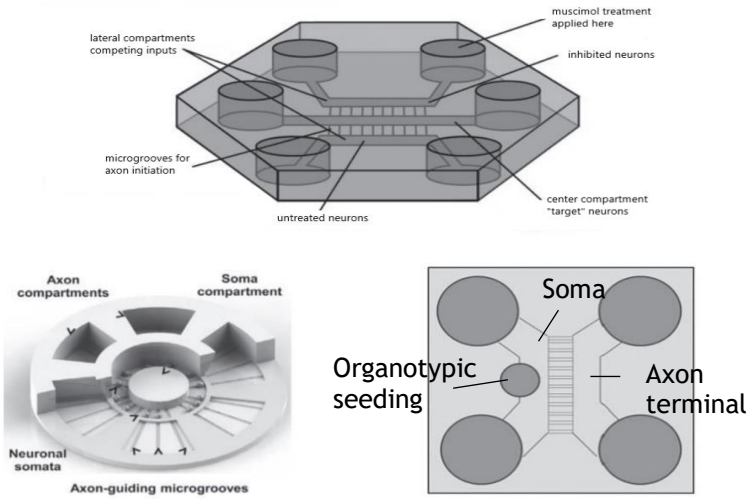

Figure 8 - Distinct types of microfluidics devices used in neuroscience research. (Adapted from [108])

c) μEF platforms

Extracellular recordings usually have a lower amplitude when compared to intracellular recordings, therefore the strength of that signal drops as the distance from the cell - electrodes increases, emphasizing a key aspect required for proper recordings, which is neuron-electrode coupling. By using μEF platforms, one can align microchannels above multiple microelectrodes and, therefore, control the growth of axons within microchannels and on top of microelectrodes. This configuration creates an electrically isolated microenvironment within the microchannel, that amplify axonal signals and significantly increases the signal-to-noise ratio. As a consequence, propagating axonal signals can be easily detected and measured [115, 116]. Moreover, the presence of multiple sensing microelectrodes along a microchannel is fundamental for detection and characterization of axonal signal propagation.

A further point is that these platforms offer a high-throughput axonal analysis, during the course of several weeks, that are fundamental to comprehend key biological questions in neuroscience, such as axonal transport dynamics as well as axonal electrical activity. Indeed, the ability to simultaneously combine microscopy techniques with electrophysiological data recording within μEFs, renders these platforms the ideal model to investigate the hypothesis that neuronal activity regulates the axonal trafficking dynamics of neuronal cargos.

7) Role of the neuronal activity in the regulation of mitochondria transport

The previous chapters of this dissertation have established a background regarding the axonal transport of cargoes in neurons, their intrinsic electrophysiological features and the up-to-date techniques used to evaluate these properties. This chapter focuses on mitochondria, a key neuronal cargo for proper neuron function, and will review what is known regarding its neuronal activity-dependent axonal transport, since it is stated that mitochondria anchor its motility during periods of increased neuronal activity.

As mentioned before neuronal organelles are driven through the axon by kinesin, when moving anterogradely, and by dynein, when moving retrogradely, whereas myosin provides short range motility or aids cargoes in low density microtubule areas. Organelles, such as mitochondria, play a fundamental role in these post-mitotic cells, since they are required to provide energy to all parts of the neuron which is a challenge due to their unique morphology. Importantly, peripheral neurons, such as DRG neurons, can extend their processes up to a meter long, posing even substantial challenges for the regulation of proper mitochondria axonal transport. Mitochondria are primarily produced in the soma and are required to travel as far away as the distal part of the axon. The proper distribution of mitochondria along the axon enables axonal growth, Ca^{2+} homeostasis maintenance, energy supply to the distal part of the axon, synapses and fulfill local requirements. During synapses, neurotransmitters are released in the post synaptic terminals generating a Ca^{2+} influx. To restore the membrane potential, ATP will be hydrolyzed to place the ions back to the extracellular space [117]. Zhu *et al*. recently highlighted the importance of energy in the human brain, stating that a single resting cortical neuron consumes around 4.7 billion ATPs per second [118]. On the other hand, action potentials also require energy, since the sodium/potassium pump enables the membrane potential to restore the balance to its negative state, through active transport. Therefore, it seems evident that mitochondria's distribution relates to localized energy needs and may be also dependent on neuronal activity levels.

a) Mitochondrial axonal transport

Mitochondria dynamics involves motility, anchoring, fusion and fission processes [119]. These organelles can only replicate themselves from fusion and fission, however their distribution depends on their motility and anchoring mechanisms, since only 30% are in fact motile. To understand how mitochondria moves along the axon to target the neurons demands, one must understand how mitochondria transport machinery is assembled and how it is regulated, which is not yet fully understood.

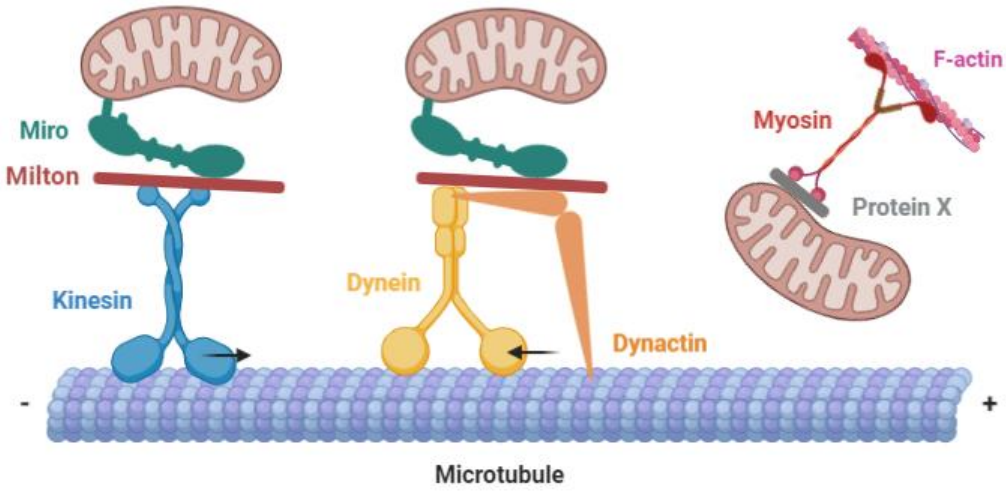

Figure 9 - Representation of mitochondrial transport machinery; The anterograde microtubule-mediated transport using molecular motor kinesin, miro and milton. The dynactin/dynein mediated retrograde transport including miro and milton; Mitochondrial transport along actin filaments using a myosin motor and a potential motor adaptor, Protein X (grey).

Mitochondria transport machinery is based on a motor protein that binds to the microtubules or actin filaments, and the adaptor proteins that binds simultaneously to the mitochondria membrane and motor protein (**Figure 9**). Mitochondria anterograde transport uses kinesin-1 motor protein (KIF5), the adaptor protein Miro (or RhoT1 and RhoT2) attached to the outer membrane of the organelle and the adaptor protein Milton (or TRAK1 and TRAK2) which makes the bridge between Miro and kinesin. Alternatively, another adaptor that drives mitochondria movement in the anterograde direction is syntabulin, which contributes to activity-dependent presynaptic assembly [60, 61]. The retrograde transport uses the dynein/dynactin complex.

Mitochondria axonal transport is characterized to be bidirectional. The cargoes bidirectionality was first explained by the model "tug-of-war", which suggest that both kinesin and dynein motors are simultaneously bound to cargoes membrane and dispute for the binding to the microtubules. Even though this model explained the behaviour of some cargoes, other studies denied it, thus founding that scaffolding proteins would regulate this transport [27]. Taking mitochondrial axonal transport as an example, Milton remains the adaptor that links two proteins and upholds this regulation of directionality, whereas Miro activates mitochondria transport, dynamics (fusion and fission) and Ca^{2+} homeostasis. This organelle changes its direction and additionally, exhibits other behaviours during their time in transit, such as dynamic pauses [120], stationary periods and reversals [121]. Therefore, it is crucial to understand how mitochondria are regulated.

Stationary periods comprise the majority of mitochondrial motility. How mitochondria are maintained stationary in specific neuronal locations is still poorly understood. Different possible mechanisms are emerging to explain stationary pools of mitochondria. It has been suggested that actin cytoskeleton removes mitochondria from the microtubule using myosins to transiently oppose their movement and anchor their movement. Myosin V anchors mitochondria from its anterograde and retrograde runs , whereas myosin VI only stops from retrograde movements [122]. Additionally, PINK1 recruits Parkin in response to low mitochondria membrane potentials and initiates mitochondria clearance [51]. Prior to the autophagic process, PINK1 phosphorylates Miro in a way that detaches kinesin from mitochondria, thus stopping its movement [123].

Another anchoring mechanism that has been proposed is the docking of mitochondria to the microtubules involving syntaphilin. Syntaphilin docks axonal mitochondria to the microtubules through its microtubule-binding domain. Its action is dependent on both, kinesin and dynein – studies show that kinesin heavy chain, KIF5 binds to syntaphilin, whereas dynein light chain, LC8 acts as a stabilizer of the docking interaction [124, 125]. In the absence of this protein mitochondria mobile fraction is increased [126]. Kang *et al*. proposed that syntaphilin controls mitochondria docking at nonsynaptic sites or in the proximity of synapses thus, facilitating the access to ATP at specific and high demand sites [126]. Furthermore, despite explaining the stationary mitochondria in the axons, syntaphilin is absent from dendrites which suggest that this is not the only anchoring mechanism for mitochondria.

b) Mitochondrial neuronal activity-dependent regulation

Previous studies showed that neuronal activity arrests mitochondrial motility, highlighting their activity-dependent motility regulation and the importance to unravel this process. Many studies point to the fact Ca^{2+} influx during synapses attaches to the two EF-hand motifs of Miro, enabling a reversible mechanism in which it can interrupt its movement, although it does not disrupt miro/milton/kinesin complex [80]. Miro knockout showed an impaired anterograde but also retrograde movement by Ca^{2+} regulation, supporting the dynein interaction with the complex [80]. However, the interactions between both molecular motors and their coordination in the presence of Ca^{2+} remains elusive. Macaskill *et al*. proposed a conformational change of the complex towards its dissociation. The rise in the calcium levels evoked by glutamate would uncouple the kinesin from mitochondria surface at the miro-KIF5 bound [127]. However, in environments with high levels of Ca^{2+} these proteins remain coprecipitated [128]. An alternative suggests that kinesin when activated interacts with the microtubule and when inactivated binds to Ca^{2+}, anchoring its movement [128]. A few years later, a new model emerged called “Engine-Switch and Brake” which explains some inconsistencies shown above regarding how Ca^{2+} regulates the arrest of mitochondria. Among

different anchoring mechanism, they identified syntaphilin has one of them and determined with biochemical and stimulation assays that KIF5-syntaphilin interaction was crucial to the activity-dependent anchoring of axonal mitochondria. As a response to the stimulation, Ca^{2+} molecules would induce mitochondria to recruit syntaphilin to arrest its motion. Therefore, this model suggests that when Ca^{2+} levels are increased, syntaphilin will dock mitochondria and switch the link of KIF5 from miro to itself, inhibiting motor ATPase activity. [124] (**Figure 10**). To sum up, several evidences have been suggesting that synaptic activity causes calcium influx which, in consequences, decreases mitochondrial motility by anchoring mechanisms.

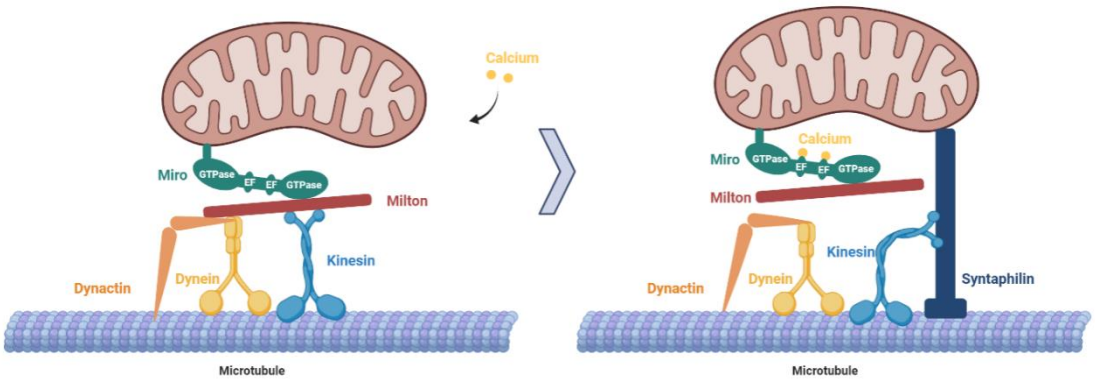

Figure 10 - Proposed "Engine-Switch and Brake" model. When intracellular calcium initiates the process and connects to the EF hands in the Miro protein (engine). Then, kinesin motor will detach from Milton and attach to the syntaphilin protein (switch). Syntaphilin locks the mitochondria directly to the microtubule preventing its movement (brake). Image created in Biorender.com

Mitochondrial axonal transport impairment has been related with neurodegenerative diseases, which raises the question of how this transport evolves in different maturation stages [117] . Studies have reported a mitochondrial motility decline in different animals models in an age-related dependence, such as *C.elegans [129], Drosophila [130]* and cortical axons *in vitro* and *in vivo* [131]. Using cortical neurons from E18 mice, Zhou's group managed to compare the expression of mitochondria complex proteins throughout their development and noticed changes only in the syntaphilin expression. The increase in its expression was detected after 9 days *in vitro* (div) reaching its peak at 22 div, whereas in early embryonic stages (before 3 div) it was undetectable. The study also evaluated mitochondrial axonal transport parameters, where they observed that mitochondrial motility progressively decreases during maturation from 7 to 18 div. With the additional information that the deletion of syntaphilin increases mitochondrial transport, an association was established between the increase in the syntaphilin expression and decrease of mitochondria motility. This data supports the engine-switch and brake model in which syntaphilin has a role to anchor mitochondria [132].

Considering these previous studies, there is still a room for investigating the relationship between neuronal activity and mitochondrial trafficking dynamics and, how this relationship evolves throughout neuronal development. A study of such dimension requires a high spatial-temporal resolution of neuron's electrophysiological properties and cargoes trafficking analysis for extended periods of time.

Chapter 3

Materials and Methods

1) Preparation of microelectrode/microfluidic devices

PDMS microfluidic devices were prepared by mixing in a 1:10 ratio the silicone elastomer (Sylgard 184 elastomer, Dow Corning) and its curing agent. The mixed solution was degassed in a vacuum desiccator for air removal, casted in the SU-8 master mold, and cured at 70°C for 3h. Once removed from the mold, the PDMS was cut in square devices and four wells of 6 mm in diameter were punched using a steel biopsy punch to give access to the cell seeding chambers. An additional well of 3 mm in diameter was made at the center of the cell seeding compartment (somal side), in order to allow the seeding of the DRG explant near the entry of microchannels. This way, the microfluidic devices consist of two cell seeding compartments (somal and distal) interconnected by 16 microchannels with 700 µm length x 10 µm width x 10 µm height dimensions, with interspacing that matches the microelectrodes interspacing in the MEAs used. Before the µEF platform assembly, PDMS devices were cleaned from dust using a vinyl tape 471 (3M), sterilized with 70% ethanol and air-dried inside the laminar flow hood.

MEAs (Multi Channel Systems) used in this work consist of 252 titanium nitride recording microelectrodes organized in a square matrix of 16 x 16, and 4 internal reference electrodes. Each recording electrode is 30 µm in diameter and interspaced by 200 µm (center-to-center spacing). µEF platforms were prepared as previously described [107]. In brief, MEAs were air plasma-treated for 2 min to increase surface hydrophilicity. Using a stereomicroscope, microchannels of the microfluidic device were carefully aligned with the microelectrode grid to include 5 microelectrodes per microchannel (**Figure 11**). On the previous day of the cell seeding, the culture surface of the µEF platform was once again plasma-treated, this time for a better adhesion of the coatings. The µEF platform was coated with 0.01 µg/mL of Poly-D-lysine (PDL, 150-300 kDa, Sigma-Aldrich) for 1h at 37°C to increase cell adhesion. After three

washing steps with sterile water, the µEF culture surface was additionally incubated overnight at 37°C with 0.005 µg/mL of Laminin (Sigma-Aldrich) diluted in DMEM/F12 (Corning).

2) DRG explants isolation and culture on µEF platform

Experimental procedures involving animals were carried out following current Portuguese laws on Animal Care (DL 113/2013) and the European Union Directive (2010/63/EU) on the protection of animals used for experimental and other scientific purposes. The experimental protocol (reference 0421/000/000/2017) was approved by the ethics committee of the Portuguese official authority on animal welfare and experimentation (Direção-Geral de Alimentação e Veterinária). All possible efforts were made to minimize the number of animals and their suffering.

Primary DRG explants were isolated from Wistar rat embryos (E18). In brief, after removal from the embryonic sac, embryos were decapitated. A surgical incision was made at the medial plan of the column and the spinal cord was removed to allow the access to the DRG in situ. DRG explants were extracted and maintained in Hank's Balanced Salt Solution (HBSS) until use. Previous to DRG seeding, laminin solution was removed from the µEF platform and replaced with DMEM/F12 supplemented with 2% (v/v) of B27 supplement (Gibco, ThermoFisher Scientific), 4% (v/v) of 1 mM 5-fluoro-2'-deoxyuridine/Uridine (FDU-U, Sigma-Aldrich), 1% (v/v) Penicillin/Streptomycin (Biowest), 1% (v/v) of fungizone (Capricorn Scientific) and 50 ng/mL of nerve growth factor (NGF, Sigma-Aldrich). At this point, a single DRG explant was seeded in the respective compartment of a µEF platform, as seen in **Figure 11**. DRG cultures were preserved for 14 days *in vitro* in a humidified incubator at 37°C with 5% of CO_2 with medium changes every 2 to 3 days.

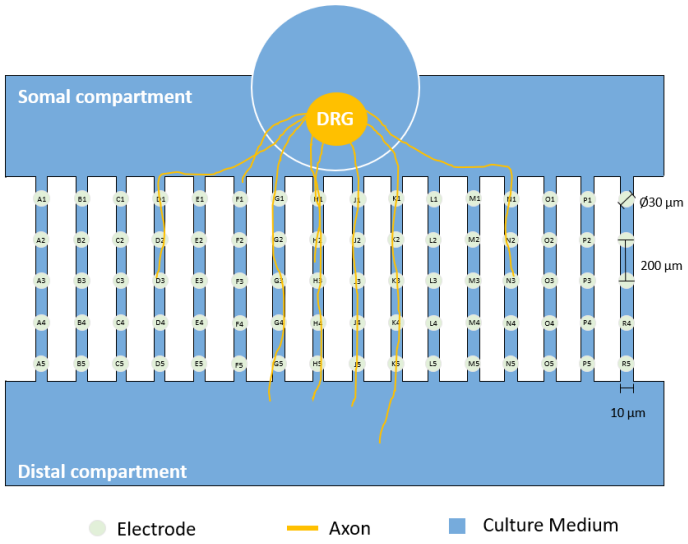

Figure 11 - Schematic representation of a DRG explant culture on a µEF platform. The DRG explant is seeded in a dedicated well close to the entry of microchannels. Microchannels direct axonal growth on top of microelectrodes. Each microchannel includes 5 recording electrodes interspaced by 200 µm.

3) Mitochondria labelling

Mitochondria of DRG neurons cultured on µEF platforms were labeled at 3 days *in vitro* (the day prior to the first live imaging session). For labeling of mitochondria, DRG explant cultures were incubated with 200 nM MitoTracker Orange CMTMRos (Molecular Probes, Thermo Fisher Scientific) diluted in DMEM/F12 for 30 min, at 37°C. The volume in the somal compartment were twice the volume in the distal compartment to allow diffusion of the dye solution throughout the microchannel. Afterward, DRG explants were washed once with medium and returned to normal culture conditions with the supplemented culture medium.

4) Recording and analysis of DRG neurons electrophysiological spontaneous activity

To characterize the development of spontaneous firing activity of DRG neurons *in vitro*, the extracellular axonal potentials were recorded at 4, 7, 10, 12 and 14 div using the *in vitro* MEA2100 System (Multi Channel Systems). During the recordings, the DRG cultures were maintained under a 5% CO_2 atmosphere and the temperature was maintained at 37°C using a TCO_2 temperature controller (Multi Channel Systems).

Neurons were allowed to adjust to the recording environment for at least 5 min before recordings. All the recordings were acquired with a sampling rate of 10kHz during 30 min. The electrical signals were filtered using a butterworth high pass filter with 200Hz cut-off, followed by a ± 5 standard deviation (SD) of the signal noise threshold and 5 ms of dead time in spike detection, as seen in **Figure 12**.

For the measurement of the mean firing rate (MFR) it was only included in the analysis those microchannels of a µEF where at least one axon grew and where an AP propagation throughout the 5 electrodes was observed. The propagation of an AP throughout the microchannel was confirmed through a Raster Plot, using Matlab. The MFR detected in each microchannel was calculated using the median of the data recorded by the 3 inner electrodes of each microchannel, the ones that provide a superior signal-to-noise ratio. Only those electrodes displaying MFR values above 0.01Hz were considered active and included in the analysis. An average of 30 microchannels in each div were analyzed.

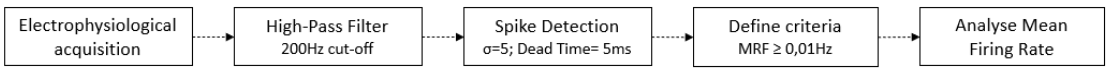

Figure 12 - Workflow for the characterization of the DRG neurons electrophysiological spontaneous activity on each day *in vitro*.

5) Simultaneous recording of DRG stimulus-evoked activity and live-imaging of mitochondria axonal transport

Mitotracker-labelled DRG cultures were used to concomitantly record the DRG neurons activity and live-image axonal mitochondria transport for a total period of 6 minutes: 2 min of spontaneous activity (baseline), followed by 2 min of stimulus-evoked activity, and 2 min of spontaneous activity (recovery period). These experiments were performed by coupling the MEA2100 System with an inverted widefield microscope stage (Axiovert 200M, Zeiss or Eclipse Ti2-E, Nikon). During the experiment, cultures were maintained at 37°C and constantly supplied with a 5% CO_2 atmosphere. As described before, previous to recordings, DRG cultures were allowed to stabilize within the experimental conditions for at least 5 min. It is to be noted that in all experiment's axons were stimulated every two days for two weeks.

a) Recording of DRG stimulus-evoked activity

The DRG neuron's electrophysiological activity was recorded with a sampling rate of 10kHz. Only microchannels with axons and displaying propagating action potentials were considered for electrophysiology/imaging acquisition and further analysis. One of the five microelectrodes enclosed in the microchannel (generally the second inner electrode from the top) was selected to electrically stimulate the axon. During the stimulus-evoked activity period, axons were stimulated in 10Hz or 20Hz frequency for 2 min, with a biphasic stimulus (-500/500 mV amplitude and 200 μs per phase).

b) Live-imaging of mitochondria axonal transport

Live-imaging of axonal mitochondria was performed using a sCMOS camera Prime 95B, 22mm (Teledyne Photometrics, UK), mounted on a Nikon Eclipse Ti2-E inverted microscope (Nikon, Japan), with a Nikon PI Apo 40X/1.15NA objective. Image acquisition was performed by Micromanager (V1.4) with a 200 ms of exposure. The images were acquired during 6 min at 5 frames/s in post-sequence mode (to avoid acquisition delays), using a tetramethylrhodamine (TRITC) filter. A region of interest (ROI) was defined between 2 electrodes (200 μm segment), including an axon region distal to the stimulation electrode.

In order to synchronize the imaging acquisition with the electrophysiological recording and stimulation, as seen in **Figure 13**, it was used a trigger via a transistor-transistor logic (TTL) signal. In this way, one is capable of consistently correlating the mitochondria kinematic features and the electrophysiological properties of a specific axonal segment.

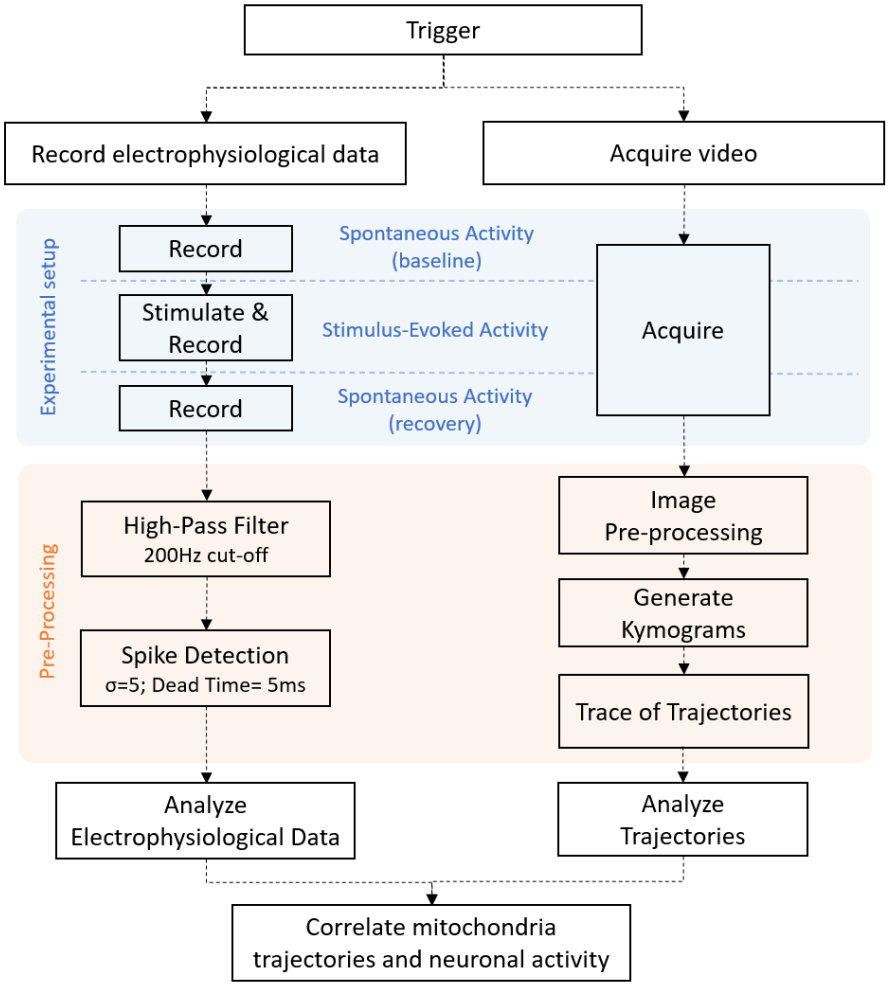

Figure 13 - Workflow followed for the simultaneous recording of the electrophysiological activity and the live-imaging of axonal mitochondria transport and the correspondent data analysis procedure.

6) Axonal activity inhibition and live-imaging of mitochondria axonal transport

Neuronal activity was selectively blocked by incubation with tetrodotoxin (TTX), a potent fast voltage-gated sodium channel blocker. Previous to recording experiments, TTX was diluted in culture medium at a final concentration of 1 µM.

Mitotracker-labelled neurons activity was recorded simultaneously with the live-imaging (as previously described) for three distinct periods: 2 min of spontaneous activity (baseline; before TTX addition), 2 min during TTX incubation, followed by 2 min of spontaneous activity (recovery period; 1h30 after TTX washing out of the culture), (**Figure 14**).

For the TTX-induced activity inhibition, the somal compartment medium was replaced with culture medium containing TTX. Recording/ imaging was performed after 5 min of stabilization in these conditions. Afterwards, TTX was removed from cultures, and these were washed 3 times with supplemented medium. Neurons were allowed to recover their basal spontaneous activity for 1h30m before the recording/imaging of the recovery period.

Figure 14 - Graphical description of the protocol used for TTX-induced neuronal activity inhibition. Blue boxes represent the timepoints of imaging and electrophysiological acquisition.

7) Data Validation

Given that DRG neuron's extracellular action potentials have a higher duration than other neurons types commonly studied in the host lab, it was crucial to perform some tests in the spike detection algorithm before the calculation of the MFR, in order to correctly extract the firing activity of these neurons, namely during the stimulus-evoked period. Different parameters were evaluated, such as the standard deviation from the noise and the dead time, the period in which the algorithm does not detect a change above or beneath the threshold after a given spike. Standard deviations between 5 and 6, and concurrent dead times between from 3 and 4 ms were tested. Using these parameters, the filtered signals were compared to raster plot graphs (graphs that represent a number of events in a time scale), in order to validate the best conditions for the analysis. The best performing parameters were the use of a standard deviation of 6 and a dead time of 4 ms (in studies of 10Hz stimulation frequency) as seen in the **Figure 15**. Additionally, a standard deviation of 5 and 5 ms of dead time also provided good results. Since already acquired data was obtained with this last set and could not be altered, we continued with these parameters.

At the time of the 20Hz stimulation analysis we verified the spike detection algorithm since the stimulation artefacts were doubling their voltage (absolute values) and took longer to cease. Therefore, a new combination of parameters was evaluated with ranges between 5 and 6 of standard deviation and 3 to 9 of dead time. The best set of parameters that captured elicited spikes was with standard deviation of 6 and 8ms of dead time as seen in **Figure 16**. It demonstrates a single event per artefact and real spike.

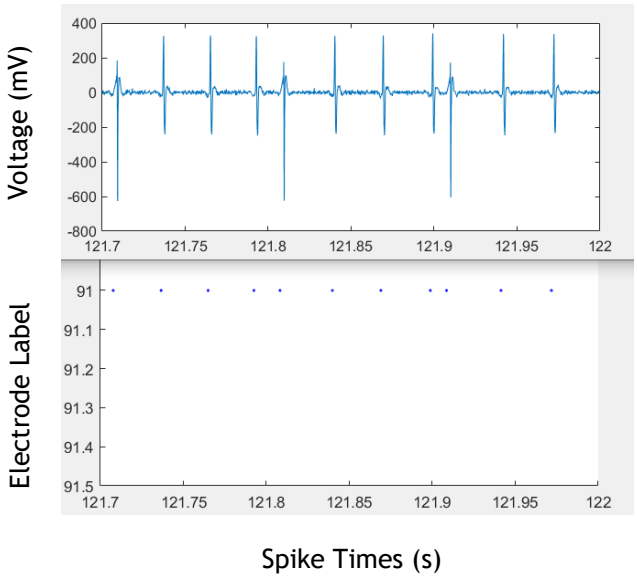

Figure 15 - Comparison of filtered signals and matching raster plot (SD=6, dead time=4). Signals that reach -600mV are stimulation artefacts

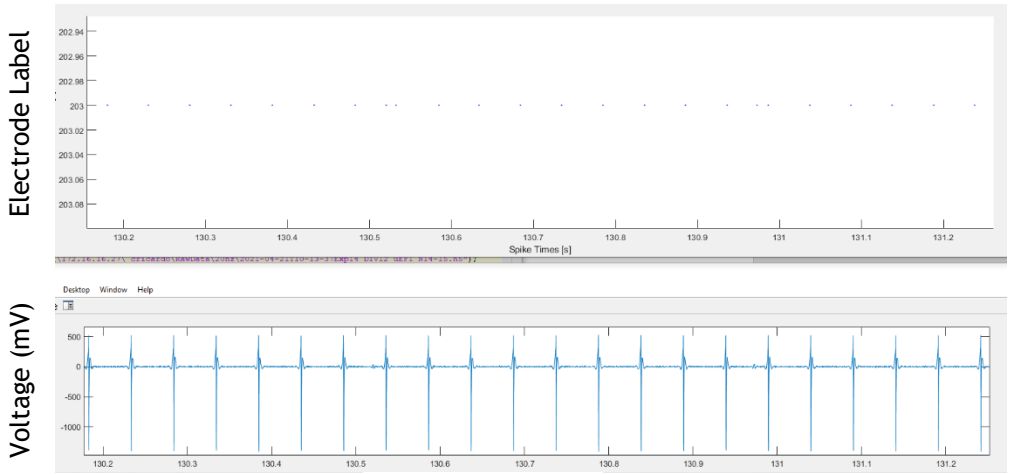

Figure 16 - Comparison of filtered signals and matching raster plot (SD=6, dead time=8). Signals that reach -1500mV are stimulation artefacts

8) Analysis of the stimulus-evoked activity data

The electrical signals were filtered using a Butterworth high pass filter with 200 Hz cut-off, followed by a ± 5 standard deviation (SD) of the signal noise threshold and 5 ms of dead time in spike detection. Given that the signal-to-noise ratio (SNR) values of each electrode inside the microchannel vary according to its location in relation to the outer part of the channel, the central electrode was the one selected for the analysis due to its better SNR

values. In addition, the central electrode is the nearest to the stimulation electrode, thus the distance between them is maintained throughout the analysis.

During the stimulation period, the system used enables a blanking period during each stimulus delivery. However, such electronic systems exhibit an artefact in the neighboring electrodes for each stimulus delivered. To avoid the contabilization of this artefact as a false action potential, during the 2 min stimulation period the corresponding stimulus frequency was subtracted to the mean firing rate of the central electrode, thus removing the artefacts.

9) Analysis of the axonal mitochondria trajectories

For the tracking and analysis of axonal mitochondria, the acquired time-lapse image series were firstly corrected from eventual drifts in the field of view (may result from some instability on the recording system installed on the microscope). This was achieved by using a video registration algorithm written in Python programming language developed by a former member of the host group. In brief, acquired image series were stabilized in the same coordinate system through a Point Feature Matching approach, which detects feature points in the reference and input frames, estimates the motion between them, and tries to align the global field of view. Stabilized time-lapse image series were then preprocessed with a median filter (3 x 3 kernel) in each frame to remove the noise and increase the contrast between labelled mitochondria and background. The background was subtracted to each frame, so that only the noise levels would decrease. Kymograph analysis was used to capture mitochondria dynamics and plot mitochondria trajectories over time. Kymographs were generated using the open-source KymoResliceWide ImageJ plugin. In brief, a polyline (with thickness adjusted to the axon diameter) was drawn on top of the axon. Kymographs were then computed with the maximum across the line and the path of the axonal mitochondria over time series plotted. In the kymograph, paths of stationary mitochondria appear as horizontal lines, whereas paths of motile mitochondria show slopes (**Figure 17**). Each mitochondria trajectory was then traced, and the position/time data extracted using the open-source Simple Neurite Tracer ImageJ plugin. Only motile mitochondria that showed a trajectory over the three periods of the experimental analysis (baseline, stimulation and recovery periods) were considered for analysis were taken into account. The coordinates of each mitochondria trajectory were exported to a swc file and subsequently analyzed in the Axonal Transport Kinetic program, a custom-made program written in MATLAB. With Axonal Transport Kinetic program one can extract and analyze detailed mitochondria kinematic parameters and thus, characterize mitochondria dynamics (**Figure 17**). One important input for this program to extract these metrics is the definition of a motile versus stationary mitochondria. Therefore, mitochondria were considered stationary if their mean velocity during 15 frames is below 0.05 μm/s. Higher mean velocity values characterize motile mitochondria. Using the parameters described in **Figure 18**, mitochondria dynamics

were analyzed for each experimental period and compared between them in order to determine the effect of the increased neuronal activity on mitochondria dynamics.

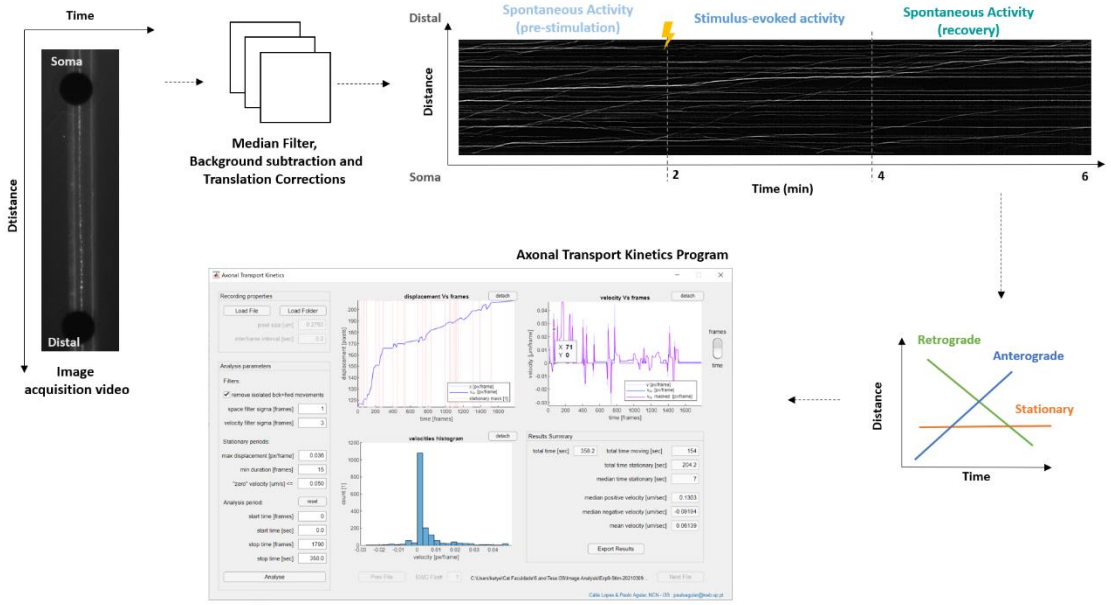

Figure 17 - Workflow of the mitochondria axonal transport dynamics analysis. The acquired time-lapse image series is primarily stabilized and separated in frames, so that it can be pre-processed for background removal. Kymographs with the mitochondria trajectories coordinates are then generated. Each trajectory file obtained is loaded into the Axonal Transport Kinetics Program, which extracts the metrics related to each mitochondrion dynamic.

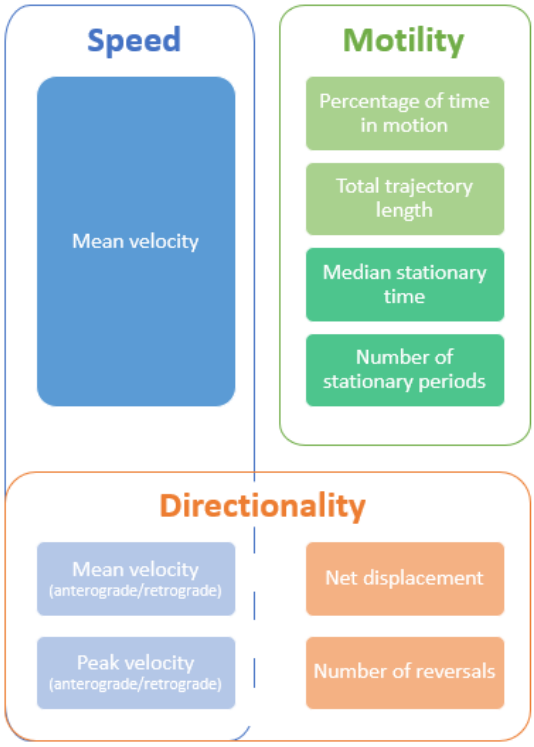

Figure 18 - Mitochondria axonal transport parameters analyzed grouped into three major categories.

10) Statistical analysis

All data was tested for normal distribution using the D'Agostino & Pearson test, which didn't show a normal distribution. Therefore, all the statistical tests were non-parametric. For significance evaluation, a two-tailed Mann-Whitney *U* test was performed to compare two different groups. To evaluate more than two groups, a Kruskal-Wallis test was performed. Wilcoxon signed-rank test was used to compare the sample medians in the fold change analysis. Measurements are presented as medians and interquartile range. Otherwise, it is stated in the legend's figure. Significant values are denoted as * $0.01 < p < 0.05$ (significant), ** $0.001 < p < 0.01$ (very significant), *** $p < 0.001$ (extremely significant), ns $p < 0.05$ (not significant).

11) Algorithm developed to analyze mitochondrial trajectories

The Axonal Transport Kinetics program exports a single excel sheet for each period of analysis (baseline, stimulus and recovery), with the summary of multiple metrics (example in **Figure 19**). Joining all this data is very time consuming and prone to human error. Therefore, it was developed an algorithm in Matlab, to gather and organize all the metrics extracted in a fast and error-free way. The algorithm chronologically organizes all mitochondria trajectories of a single microchannel by period of analysis and extracts metrics regarding directionality, for example, number of cargos for the whole protocol only in an anterograde movement (**Figure 20**). Additionally, it organizes the general metrics on another sheet by period, facilitating the further calculations for each axon segment (**Figure 21**).

frame [1]	time [s]	vel [um/s]		v mean [ur	-0,02247	v- [um/s]	v- mean [u	-0,13709	v+ [um/s]	v+ mean [	0,132365
1200	240			v median [	0	-0,1138	v- median	-0,139	0,011894	v+ median	0,149192
1201	240,2			v std [um/s	0,06682	-0,1365	v- std [um/	0,065337	0,047914	v+ std [um	0,061564
1202	240,4					-0,15604	v- peak [ur	-0,26054	0,082331	v+ peak [u	0,198681
1203	240,6			total recor	119,4	-0,17128			0,114213		
1204	240,8			total trajec	4,928713	-0,18206			0,142261		
1205	241			net displac	-3,80126	-0,18907			0,165223		
1206	241,2			total time i	25,8	-0,19342			0,182326		
1207	241,4	0		% time in r	21,60804	-0,19633			0,193413		
1208	241,6	0		total time :	93,6	-0,19895			0,198681		
1209	241,8	0		% time stal	78,39196	-0,2022			0,198216		
1210	242	0				-0,20681			0,191615		
1211	242,2	0		number of	3	-0,21319			0,177943		
1212	242,4	0		median sta	30,6	-0,2213			0,156122		
1213	242,6	0		number of	2	-0,23067			0,125615		
1214	242,8	0				-0,24041			0,087129		
1215	243	0				-0,24938			0,042952		
1216	243,2	0				-0,25641					
1217	243,4	0				-0,26045					
1218	243,6	0				-0,26054					
1219	243,8	0				-0,2558					
1220	244	0				-0,24557					
1221	244,2	0				-0,22957					
1222	244,4	0				-0,20833					
1223	244,6	0				-0,18336					
1224	244,8	0				-0,15699					
1225	245	0				-0,13187					
1226	245,2	0				-0,11024					
1227	245,4	0				-0,09338					
1228	245,6	0				-0,08151					
1229	245,8	0				-0,07393					
1230	246	0				-0,06956					
1231	246,2	0				-0,06728					

Figure 19 - Example of the data extracted from the Axonal Transport Kinetics program for a specific period of analysis (here data related with the 'recovery period' for a specific mitochondrion trajectory).

microchannel	kymo	mito#	pre_A	stim_A	pos_A	pre_R	stim_R	pos_R
F12-13	KymoT	000	0,21	0,26	0,14	0,09	0	0,13
F12-13	KymoT	001	0,26	0,06	0,1	0,05	0,07	0
F12-13	KymoT	002	0	0	0	0,38	0,48	0
F12-13	KymoT	003	0,19	0,14	0,11	0,15	0,18	0
F12-13	KymoT	004	0,51	0,29	0,16	0	0	0
F12-13	KymoT	005	0,15	0,32	0,33	0,57	0,3	0,11

total_1	total_2	total_3	pre_1	pre_2	pre_3	stim_1	stim_2	stim_3	pos_1	pos_2	pos_3
#cargoes	6		#cargc	6		#cargc	6		#cargoes	6	
#anterograde	1	16.6667	#anter	1	16.666	#anter	2	33.333	#anterograde	3	50
#retrograde	1	16.6667	#retroç	1	16.666	#retroç	1	16.666	#retrograde	0	0
#bidirectional	4	66.6667	#bidire	4	66.666	#bidire	3	50	#bidirectional	2	33.3333
#stationary			#statio	0	0	#statio	0	0	#stationary	1	16.6667

Figure 20 – Data summary of all mitochondria trajectories detected in a specific axon segment (single microchannel). This example shows data regarding 6 independent mitochondria trajectories tracked along the axonal segment F12-13. Bottom table displays the summary of mitochondria population distribution in terms of directionality

Geral Statistics	pre_1	pre_2	pre_3	pre_4	pre_5	pre_6	stim_1	stim_2	stim_3	stim_4	stim_5	stim_6	pos_1	pos_2	pos_3	pos_4	pos_5
nr_mito	0	1	2	3	4	5	0	1	2	3	4	5	0	1	2	3	4
v mean [um/s]	-0,16	-0,15	0,33	0,06	-0,48	0,3	-0,05	0	0,07	0,05	-0,25	0,14	-0,02	-0,01	0	0	-0,01
v median [um/s]	-0,15	-0,14	0,25	0,03	-0,5	0,14	0	0	0	0	-0,24	0,05	0	0	0	0	0
v std [um/s]	0,15	0,16	0,24	0,12	0,27	0,36	0,13	0,03	0,19	0,14	0,17	0,26	0,07	0,03	0	0,01	0,03
total recording time [s]	120,4	119,8	119,6	119,4	119,6	120	120,2	120,2	120,2	120,2	120,2	120,2	119,4	119,6	119,2	119,6	119
total trajectory length [um]	23,07	19,64	39,39	14,04	57,53	43,73	7,42	2,63	9,56	13,92	30,22	22	4,93	1,92	0,27	1,09	1,44
net displacement [um]	-19,62	-18,6	39,39	6,73	-57,53	37,86	-6,97	-1,57	9,55	5,78	-29,89	18,73	-3,8	-1,38	-0,27	0	-1,44
total time in motion [s]	104,6	74,4	102,4	73	113,2	77,4	23,6	19,2	19	67,2	104,2	65,2	25,8	8,4	0,4	2,2	5,4
% time in motion	86,88	62,1	85,62	61,14	94,65	64,5	19,63	15,97	15,81	55,91	86,69	54,24	21,61	7,02	0,34	1,84	4,54
total time stationary [s]	15,8	45,4	17,2	46,4	6,4	42,6	96,6	101	101,2	53	16	55	93,6	111,2	118,8	117,4	113,6
% time stationary	13,12	37,9	14,38	38,86	5,35	35,5	80,37	84,03	84,19	44,09	13,31	45,76	78,39	92,98	99,66	98,16	95,46
number of stationary periods	2	4	1	6	1	4	4	2	1	3	1	3	3	2	1	2	1
median stationary time [s]	7,9	12	17,2	4,4	6,4	10,4	8,6	50,5	101,2	17,6	16	22,2	30,6	55,6	118,8	58,7	113,6
number of vel. reversals	9	2	0	11	0	8	0	1	0	8	0	3	2	0	0	0	0
peak velocity [um/s] - antero	0,57	0,5	0	0,42	1,05	0,31	0,62	0,07	0	0,32	0,65	0,46	0,26	0,11	0	0,13	0,18
peak velocity [um/s] - retro	0,3	0,07	0,76	0,31	0	0,99	0	0,09	0,65	0,38	0	1,19	0,2	0	0	0	0

Figure 21 - Data summary of all metrics extracted from all mitochondria trajectories detected in a specific axon segment (single microchannel. This example shows data regarding 6 independent mitochondria trajectories during the 3 periods of analysis ('pre' stands for baseline period; 'stim' stands for stimulus evoked activity period, 'pos' stands for the recovery period)

Chapter 4

Results

1) Characterization of DRG neurons spontaneous activity across early developmental stages

To date, very few studies have provided information about the spontaneous electrophysiological properties of DRG neurons across early developmental stages *in vitro*. Here, using μEF platforms, we have described how DRG neurons change their spontaneous electrical activity as they mature *in vitro* (analysis at 4, 7, 10, 12 and 14 div). As detailed in the previous section, DRG explants cultured in μEF platforms grow their axons throughout microchannels with time. Given the increased signal-to-noise ratio offered by microchannels, we have characterized the electrophysiological profile of these cultures by assessing the MFR of axons growing inside microchannels. Each μEF includes 16 microchannels, each one enclosing 5 microelectrodes. Only those microchannels that enclosed at least an axon that exhibited electrical activity in 5 consecutive microelectrodes were considered for the analysis (total of 26 to 33 microchannels per div). This electrical activity checking was made through the analysis of the heat maps (**Figure 22C**) and confirmed by a raster plot (**Figure 22D**). Our results showed an increase in the median values of the MFR from 4 to 14 div (from 0.65Hz to 1.12Hz), although without statistical significance between divs (**Figure 22E**). Given the increased variability of the data distribution throughout the analyzed timepoints, the mean MFR values increased between 4 and 10 div and subsequently decreased in the following 12 and 14 div (**Figure 22E**). The MFR evolution of two independent microchannels are highlighted in Figure 18E. One can observe an increase in the MFR between 4 and 7 div, followed by a stabilization starting in 10 div.

Furthermore, a frequency distribution of the DRG neurons MFR across developmental stages showed that increased maturation stages were more likely to show higher MFR values

(**Figure 22F**). For instance, at 14 div DRG neurons presented the lowest percentage (~40%) in MFR values between 0 and 1.5Hz (lowest range), (**Figure 22F**).

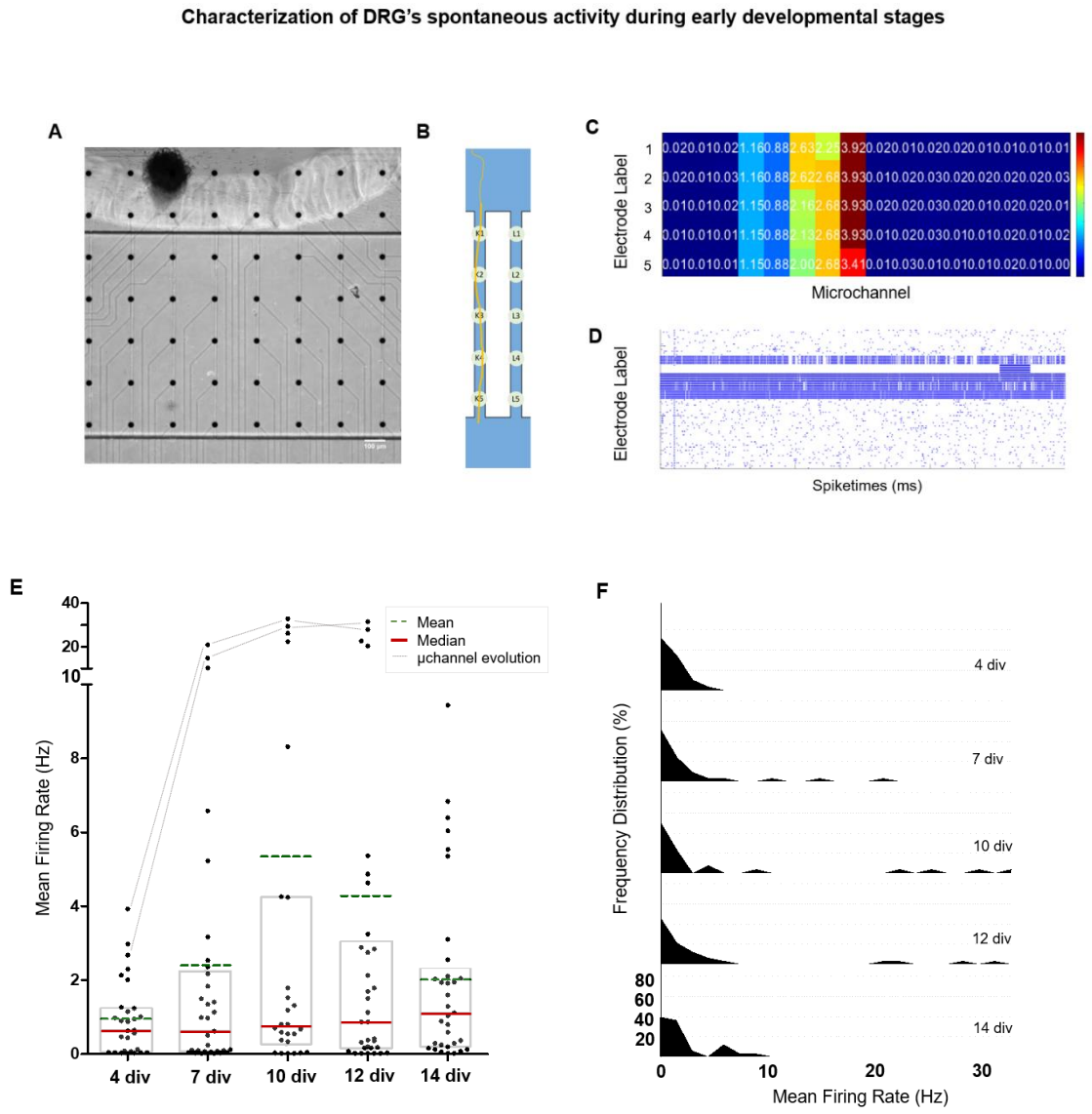

Figure 22 - Characterization of dorsal root ganglion (DRG) neurons spontaneous activity across early developmental stages (4 to 14 div). A) Representative image of DRG explant cultured in a µEF for 10 div. Scale bar 100 µm; **B)** Graphical representation of an axon growing on top of the 5 microelectrodes (numerically ordered) enclosed in a microchannel (K and L); **C)** Sub-section of the activity/heat map of the microelectrodes enclosed in microchannels of a µEF platform at 4 div. The color-coded values represents the mean firing rate (MFR) of the axons present in those microchannels; **D)** Raster Plot of 30 minutes of activity of the axons highlighted in the previous activity map; **E)** Spontaneous MFR of DRG neurons across development *in vitro* (total of 26 to 33 microchannels per div). Grey lines represent the MFR evolution of 2 independent microchannels. Dark green dash lines and full red lines represent the mean and median, accordingly; **F)** Frequency distribution of the MFR across developmental stages *in vitro*.

2) Characterization of mitochondria transport dynamics across early developmental stages

This type of longitudinal study over the course of several days *in vitro* allowed a follow-up of mitochondria dynamics. Most studies usually evaluate the axonal transport during one stage of maturation, which hampers the comprehension of any mechanism that influences their time in transit. During the neurons development the energy needs may vary like any other organism. Therefore, by analysing solely the baseline period of mitochondria transport dynamics over the course of their development, we can evaluate how mitochondria axonal transport evolves throughout time (**Figure 23**). It is to be noted that these results were taken separately from the 10Hz and 20Hz stimulation experiments. We started with the 10Hz stimulation experiment and then provide the results for the 20Hz stimulation experiment.

Mitochondria decreased around 20% of their time in motion from 10 to 12 div (**Figure 23A**), which was corroborated by the decline in the trajectory length from 4 to 12 div and 10 to 12 div (**Figure 23B**). Additionally, the number of stationary periods was consistently higher at each successive day *in vitro*, with a significant increase, which doubled from 4 to 14 div (3 to 6 stationary periods) (**Figure 23C**). However, the time that mitochondria remained in pause decreased by nearly half, from 13.2 s to 6.4 s (4 to 14 div) (**Figure 23D**). Interestingly, at 7 div the mitochondria stationary time decreased by ~50% compared to 4 div and at 10 div it rose by the same amount (**Figure 23D**). In a similar way, the number of reversals follows that same pattern at 7 div compared to the adjacent divs (**Figure 23E**). At last, the mean velocity of axonal mitochondria decreases throughout neuronal development (from 4 to 14 div) (**Figure 23F**). No statistical differences were observed in the net displacement analysis (data not shown).

These findings suggest that after 10 div mitochondria spend less time in motion, hence taking shorter trajectories. These organelles stop more often during transport but remain less time stationary.

In comparison, the 20Hz stimulation study we also analysed the baseline periods in various axonal transport parameters and found that no changes were observed over time, apart from net displacement (Figure **24**). Metrics such as time in motion, total trajectory length, number of stationary periods, median stationary time, number of reversals and mean velocity (data not shown) didn't provide with any trend or statistical significance (**Figure 24A/B/C/D/E**). However, the net displacement seems to increase in the retrograde direction throughout maturation (**Figure 24F**). In the 10Hz experience we observed a clear trend in the follow-up of the maturation in culture, which lacks in the 20Hz stimulation experiment. This finding leads to a possibility that as the stimulation levels increase the mitochondria axonal transport tends to remain in the same levels as at early developmental stages.

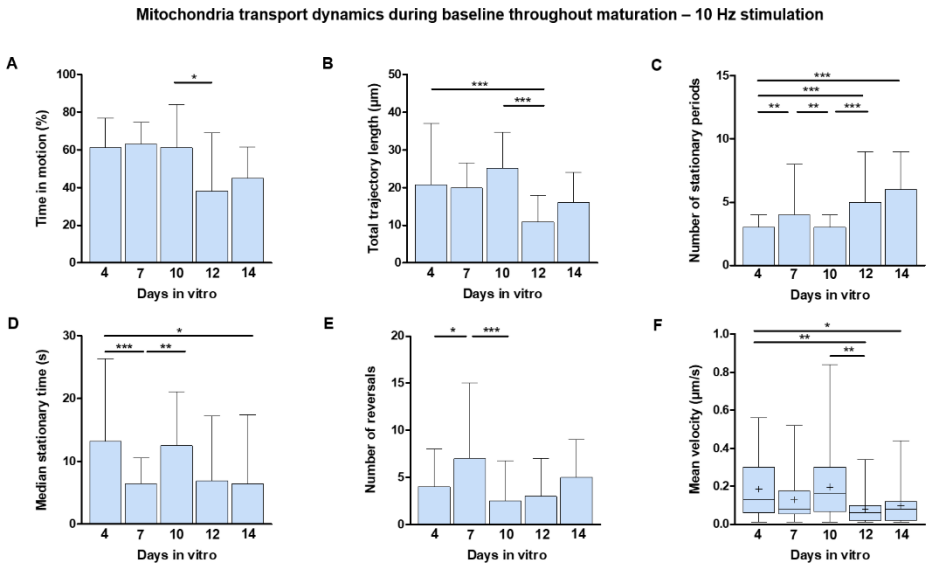

Figure 23 – Mitochondria transport dynamics during baseline throughout maturation. A: Percentage of mitochondrial time in motion at 4, 7, 10, 12 and 14 div; **B:** Total trajectory length of mitochondria at 4, 7, 10, 12 and 14 div; **C:** Quantification of the number of stationary periods at 4, 7, 10, 12 and 14 div; **D:** Median mitochondria stationary time at 4, 7, 10, 12 and 14 div; **E:** Number of mitochondria reversals during time in transit at 4, 7, 10, 12 and 14 div; **F:** Mitochondrial mean velocity regardless of directionality at 4, 7, 10, 12 and 14 div. Statistical significance with Kruskal-Wallis test.

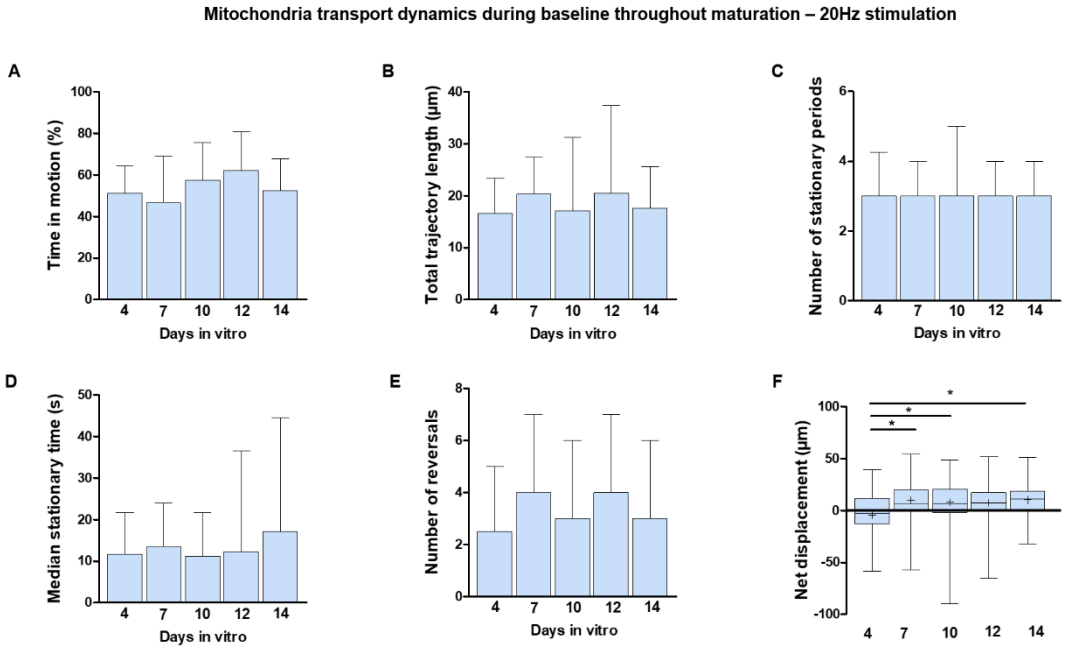

Figure 24 - Mitochondria transport dynamics during baseline throughout maturation. A: Percentage of mitochondrial time in motion at 4, 7, 10, 12 and 14 div; **B:** Total trajectory length of mitochondria at 4, 7, 10, 12 and 14 div; **C:** Quantification of the number of stationary periods at 4, 7, 10, 12 and 14 div**; D:** Median mitochondria stationary time at 4, 7, 10, 12 and 14 div; **E:** Number of mitochondria reversals during time in transit at 4, 7, 10, 12 and 14 div; **F:** Mitochondrial net displacement at 4, 7, 10, 12 and 14 div. Statistical significance with Kruskal-Wallis test.

3) The effects of altering neuronal activity across DRG's early developmental stages

In this section we will describe the results of increasing and decreasing DRG's neuronal activity. We increased the neuronal activity by electrical stimulating at a frequency of 10Hz and 20Hz and observed the effects on the mitochondria dynamics. On another experiment, we reduced the neuronal activity by using a blocker of the voltage-dependent Na^+ channels (TTX). Therefore, to each different form of changing neuronal activity, we divided the results into two subsections: first we describe the effects at the electrophysiological level and secondly, the effects on the mitochondria dynamics by live-imaging tracking.

a) 10Hz electrical stimulation

i) Electrophysiological analysis of 10Hz stimulus-evoked activity

We acquired electrophysiological axonal features with microelectrode arrays enabling a long-term high temporal resolution. The analysis of stimulus-evoked activity was performed across maturation in culture. In brief, it was established a 6 min protocol comprising a baseline period of spontaneous electrical activity, followed by a 10Hz stimulation period and then a recovery period of DRG neurons spontaneous activity (2 min each, **Figure 25A**). During the stimulation period, electrophysiological systems such as microelectrode arrays capture an artefact produced by the stimuli, demonstrated by the yellow lines in **Figure 25A**. The signals shown in between correspond to an evoked action potential (**Figure 25A ii**). Using this protocol, we would be able to analyse the effects of the stimulation on neurons activity and whether they recover their baseline activity after stimuli cessation (**Figure 25C**).

The 10Hz stimulation protocol was able to successfully increase the MFR of DRG neurons at 4, 7 and 10 div. Although later on the maturation, this stimulation protocol did not produce any significant effect on the MFR of these neurons. Additionally, when comparing the stimulation with the recovery period, we found that at 4, 7, 10 div ($p<0,001$) and 14 div ($0,01<p<0,05$) the MFR decreased at values similar to the baseline period. Remarkably, no statistical differences were found at 12 div.

The variability of data distribution was high between 4 and 10 divs. Therefore, to avoid the effects of this high variability in the data distribution and better understand the effects of the stimulation in each microchannel, we performed a fold change analysis. Our results show that the 10Hz stimulation protocol increased the MFR of DRG neurons in all days *in vitro* (4 div -19.16; 7 div – 16.20; 10 div – 5.35; 14 div - 3.1 fold-change), except for 12 div (1.1 fold-change) in which the baseline firing rate level was maintained (**Figure 25C i**). Additionally, with the course of the developmental stages the increase in the MFR progressively decreased. As

mentioned before, the MFR decreased from the stimulation period to the recovery period (**Figure 25C ii**), returning to their baseline levels (**Figure 25C iii**). Although early days *in vitro* maintain a median below 0.1 (4 div – 0.01; 7 div – 0.07; 10 div – 0.04), later ones seem to be more prepared to maintain some level of activity, since median doubled to 0.2 (12 div – 0.22; 14 div – 0.18) (**Figure 25C ii**). When exploring in detail the fold change between the baseline and recovery period, we observed that the MFR in the recovery period remains the same as the baseline at 4, 7, 10 and 12 div (4 div - 0,39; 7 div – 1; 10 div – 0,95; 12 div – 0,67), whereas it decreases on the last day *in vitro* (14 div - 0,67).

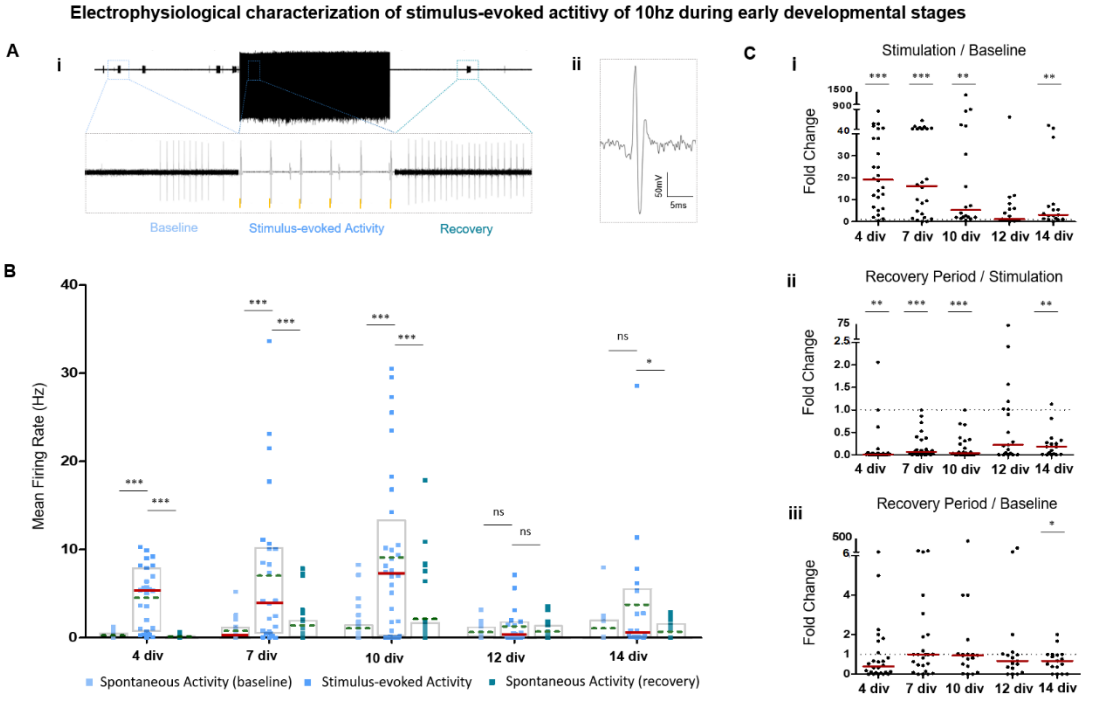

Figure 25 - Electrophysiological characterization of DRG neurons under baseline, 10 Hz stimulus-evoked activity and recovery periods across early developmental stages. A) i. Example of an electrophysiological recording for the whole protocol of 6 min (baseline - stimulus - recovery; each period is 2 min long), at 7 div; The yellow line represents stimulus; **ii.** Representative action potential of the DRG neurons during the spontaneous activity period (baseline); **B)** Mean Firing Rate of DRG neurons during spontaneous activity (baseline), 10 Hz stimulus-evoked activity and spontaneous activity (recovery phase) in all divs tested (18<N<32, microchannels); Green dash lines and full red line represents the mean and median, accordingly; Statistical analysis was performed with Kruskal-Wallis test, *** $p < 0.001$, * $p < 0.05$. **C)** Fold change of the mean firing rate during the **(i)** stimulation period (normalized to baseline), **(ii)** recovery period (normalized to stimulation), and **(iii)** recovery period (normalized to baseline). The dotted line at 1 represents the value for which each condition was normalized.

Besides this direct type of analysis, we correlated the MFR across maturation and different periods using a Spearman's rank correlation, which assesses monotonous relationships. If the values of both variables increase (i.) or if one variable increases and the other decreases (ii.), then a perfect coefficient is achieved (1 for situation i. and -1 for situation ii.). For analytical purposes we considered values above 0.7 as a strong correlation coefficient. **Figure 26** shows before and after graphs in each period of analysis and their correlation coefficients, which facilitates de visualization of different behaviours in the

electrophysiological scope. Correlating the baseline and the recovery period, we observe that in 4, 7 and 14 div the MFR stimulation period increased at the same time as the baseline, maintaining the same behaviour within the population, whereas 10 and 12 div the coefficients are lower, meaning that axons exhibited two types of behaviour, since some do not preserve the order relation (**Figure 26A**). Axons with higher MRF during the baseline period increased their values, whereas others decreased their MFR in the recovery period. Comparing the stimulation with the recovery, we see that the coefficients are higher at 7, 10 and 14 div than the rest, meaning that MFR levels decreased at the same pace: higher levels of activity decreased as the lower levels also decreased and maintained the same ranking order. These coefficients combined with the before and after graphs, suggest that at some level the neurons were able to maintain some activity that was previously evoked by the stimulation.

The spider plot graph resumes all three correlations throughout the maturation (**Figure 26B**). At 4 div the stimulation doesn't maintain the excitability in the recovery period; at 7 div DRG neurons that fired during the stimulation period seem to be able to sustain some electrical activity during the recovery, whereas at 10 div this capacity seems to increase; at 12 div there is no strong correlation between the periods; at 14 div the stimulation protocol evokes neuronal activity, however in the recovery period the firing rate retakes the baseline levels.

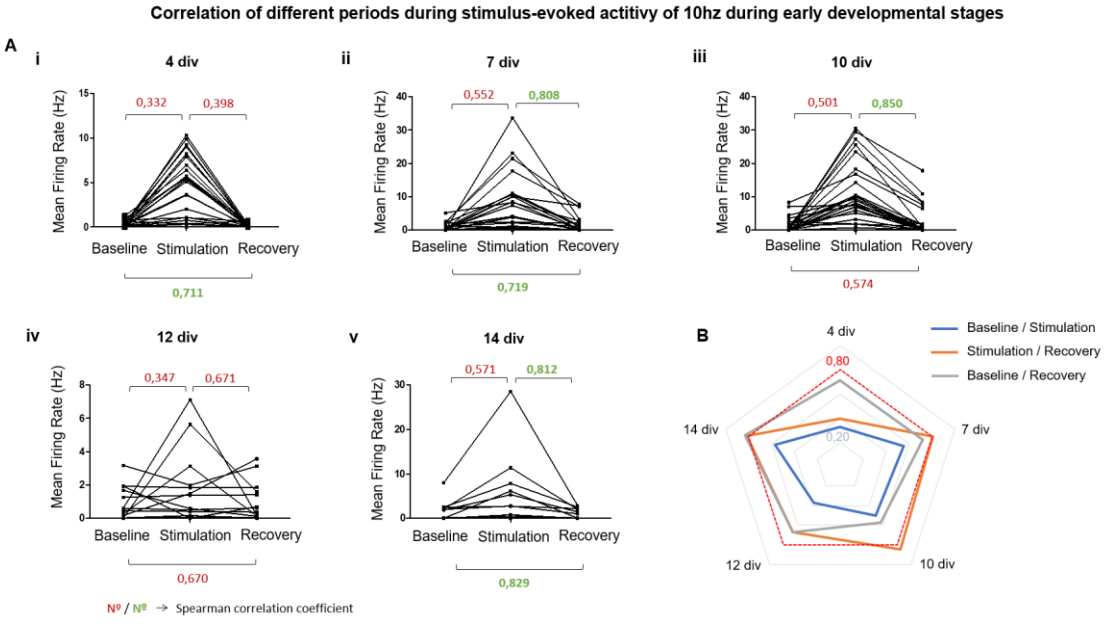

Figure 26 - Spearman correlation between treatment conditions during early developmental stages; A) Before and after graphs of the MFR for the baseline, stimulation and recovery periods, at **(i)** 4 div, **(ii)** 7 div, **(iii)** 10 div, **(iv)** 12 div, and **(v)** 14 div; Values represent the spearman correlation coefficients; **B)** Spider plot illustrating the evolution of the Spearman correlations across time (scale 0.20).

ii) Mitochondria axonal transport dynamics

To assess the impact of neuronal activity elevation on axonal mitochondria dynamics, mitochondria axonal transport was live-imaged simultaneously with the electrophysiological recording described in the Results' section 2. As for the previous analysis, mitochondria axonal trafficking was tracked during the three consecutive time periods: baseline, stimulation and recovery.

Here, we tracked and analyzed single mitochondria trajectory taking place in all three periods of analysis, which enable the observation of any direct effect of the stimulation on the mitochondria dynamics. To track mitochondria trafficking we have used a kymograph-based analysis. The most common measurement in the axonal transport research field relies on the counting of the stationary vs motile mitochondria and their overall mean velocity. In this study, using a custom-made MATLAB program "Axonal Transport Kinetics", we analysed the mean velocity of mitochondria along with more detailed kinematic parameters (**Figure 17**), so that we can shed light on the mechanisms regulating this transport.

Our results demonstrate a tendency for decreased mitochondria mean velocity values, regardless of its direction, during the stimulation period (statistical significance at 4 and 10 div), (**Figure 27A**). After the stimulation period, the axons were maintained in their basal conditions to recover from an elevated state of neuronal activity. We observed a consistent decrease in the mean velocity of mitochondria throughout their development during this recovery period (**Figure 27A**). According to the results shown in the fold change analysis, we notice that the mean velocity during stimulation was only significantly lower than the baseline period at 4 div (**Figure 27B i**). However, the mean velocity of mitochondria during the recovery was significantly lower than the baseline at 4, 10 and 14 div (**Figure 27B ii**). These results suggest that a 2 min period window is not enough time for mitochondria to recover their basal motility kinetics, hence the stimulation effects are still being reflected in the mitochondria movement.

Mitochondrial movement classifies as bidirectional, meaning they can move anterogradely (towards the distal part of the axon) or retrogradely (towards the soma). To understand if there was a preference in direction during the activity-evoked period, we analysed the mean and peak velocities in each direction. No statistical differences were seen in the mean velocities depending on the directionality (**Figure 27C/D**). However, by analysing the mitochondria peak velocities, we found that at 10 div these organelles present a lower peak velocity in the anterograde direction between the baseline and the recovery period (**Figure 27D)**.

The evaluation of other kinematic parameters of mitochondrial transport, helps to canvass the decrease seen in mean velocities graph. We measured specific dynamical features of these organelles like mitochondrial time in motion, total trajectory length, number of

stationary periods, number of reversals, duration of mitochondrial stationary periods and at last, their net displacement. Our results show that mitochondria spent less time in motion throughout their development during and after stimulation protocol (recovery period) (**Figure 28A**). However, at the late developmental stages, such as 12 and 14 div, mitochondrial time in motion during stimulus-evoked activity was maintained similar to their baseline behavior, whereas early developmental stages presented a higher downward slope. Aligned with that observation that mitochondria spent less time in motion, our results showed that their total trajectory length also decreased throughout their maturation in a similar way (**Figure 28B).** When observing the three periods of analysis we see a significant decrease at 4 and 10 div between the baseline and stimulus-evoked activity, whereas at 12 and 14 div a decrease is noted between the stimulus-evoked activity and recovery periods. These findings suggest that the maturation stage of these neurons can influence how the mitochondrial transport is regulated when axons are being stimulated: at early maturation stages the stimulus-evoked activity may have a greater influence than at later developmental stages.

Mitochondria trafficking is characterized by frequent stops, which led us to investigate several parameters related to pauses. We observed a tendency to decreased stationary periods of mitochondria after and/or during stimulation, where a statistical difference was only achieved at 7 div (**Figure 28C**). The number of reversals presented a predisposition to decrease during early developmental stages (4, 7 and 10 div) whereas values remained similar during later developmental stages (**Figure 28D**). After neuronal stimulation mitochondria increased their time in stationary periods at 4, 7, 10 and 12 div during the recovery period (**Figure 28E**). The mitochondrial net displacement regarding its trajectory showed no statistical differences (**Figure 28F**).

Overall, the increased neuronal activity has proven to have an impact on mitochondria axonal transport dynamical features, which consequently reduces their motility properties.

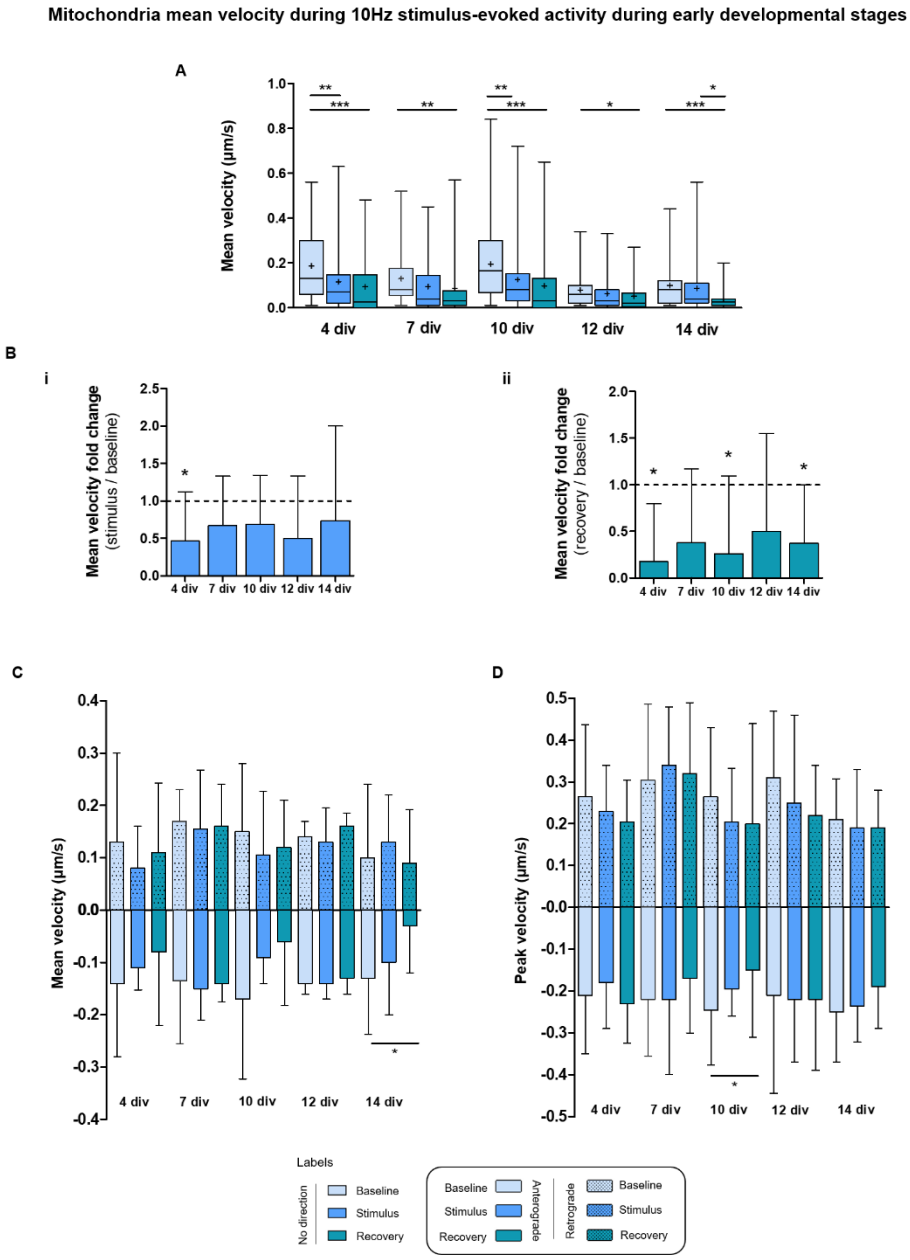

Figure 27 - Effect of the 10 Hz stimulus-evoked activity on mitochondria mean velocity across early developmental stages; A: Mitochondria mean velocity values during baseline (light blue), stimulus-evoked activity (blue), and recovery (green) periods, at 4, 7, 10, 12 and 14 divs. *, **, *** ($p < 0.05$) Mann-Whitney test; **B:** Fold change of mitochondria mean velocities during the stimulation period normalized to their baseline values **(i).** * $p < 0.05$ Wilcoxon signed-rank test, indicates median velocities significantly different than baseline values; fold change of mitochondria mean velocities during the recovery period normalized to their baseline values **(ii).** * $p < 0.05$ Wilcoxon signed-rank test, indicates median velocities significantly different than baseline values; **C:** Mitochondria mean velocity in retrograde (positive axis) and anterograde (negative axis) movements during baseline, stimulus-evoked activity, and recovery periods, at 4, 7, 10, 12 and 14 divs. **D:** Mitochondria peak velocity in retrograde (positive yy axis) and anterograde (negative yy axis) movements during baseline, stimulus-evoked activity, and recovery periods, at 4, 7, 10, 12 and 14 divs. Data presented as median with interquartile range; + indicates mean;

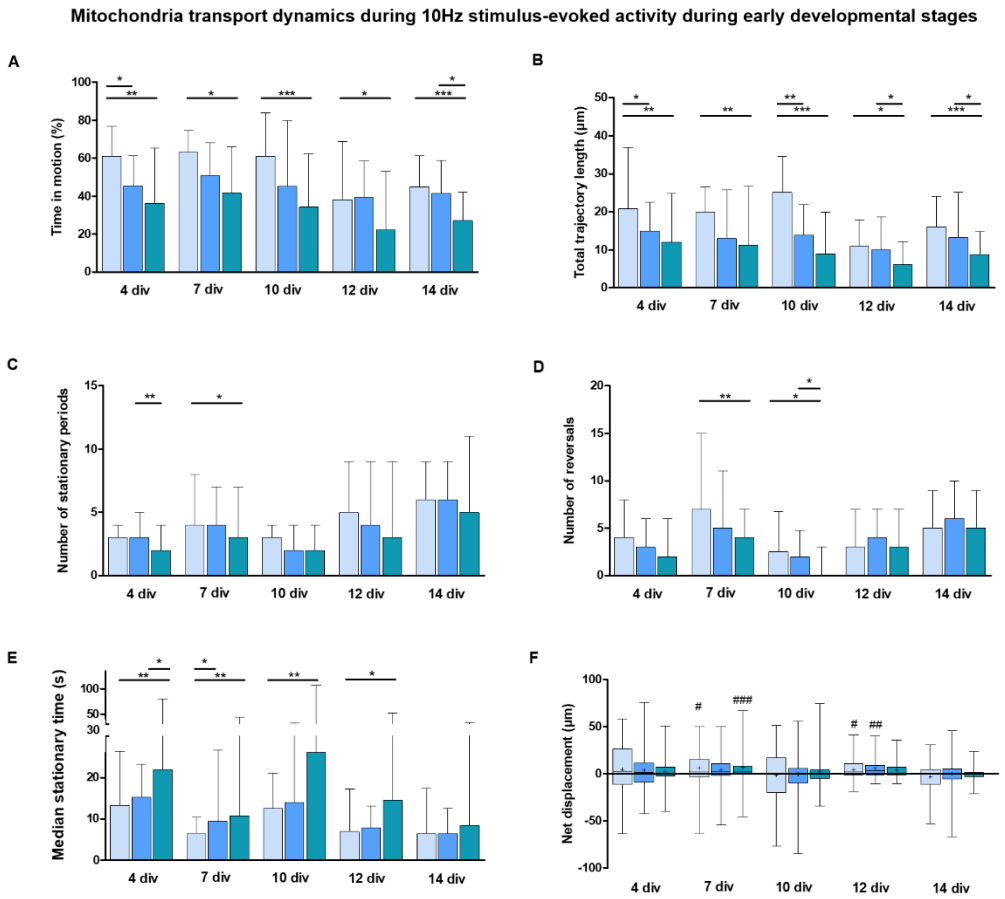

Figure 28 - Effect of the 10 Hz stimulus-evoked activity on mitochondria axonal motility across early developmental stages; A: Percentage of time in motion during baseline, stimulus-evoked activity, and recovery periods, at 4, 7, 10, 12 and 14 divs; **B:** Total trajectory length during baseline, stimulus-evoked activity and recovery periods, at 4, 7, 10, 12 and 14 divs; **C:** Number of stationary periods during baseline, stimulus-evoked activity and recovery periods, at 4, 7, 10, 12 and 14 divs**; D:** Number of reversals in direction . Data presented as median with interquartile range. *, **, *** $p < 0.05$, Mann-Whitney test; **E:** Median stationary time during baseline, stimulus-evoked activity and recovery periods, at 4, 7, 10, 12 and 14 divs; **F:** Whisker-box plot for the mitochondria net displacement during baseline, stimulus-evoked activity and recovery periods, at 4, 7, 10, 12 and 14 divs. Retrograde and anterograde movements displayed in positive and negative yy axes, respectively. + indicates mean; Data presented as median with interquartile range;

iii) Correlation of neuronal activity with mitochondrial transport dynamics

As seen in the electrophysiological analysis, the 10Hz of stimulation protocol leads to an increase in the firing rate of DRG neurons, specially at 4, 7 and 10 div. Accordingly, most of the mitochondria transport dynamics parameters (except median stationary period) also presented a higher downward slope in those same div. Later developmental stages - 12 and 14 div - exhibited slightly lower MFR and there was a tendency to maintain mitochondrial dynamical features. Therefore, we investigated if there was a correlation between neuronal activity and

the most statistically significant mitochondrial parameters, such as mean velocity and total trajectory length.

First, the mean velocity parameter was plotted with all MFR of the diverse maturation stages and conditions showing that in the stimulation period there was a greater density of data points between -0,2 and 0,2 µm/s velocity values with firing rates above 5Hz, whereas lower firing rates were more distributed across the x-axis **(Figure** 29**).** Therefore, we observed a bottleneck of data towards higher firing rates, suggesting that increasing neuronal activity may lead to a decrease in the mean velocity of axonal mitochondria in both directions. To confirm this hypothesis, we calculated the standard deviation of the mitochondria mean velocity with respect of the MFR and encountered that there wasn't a consistent decrease in the variability of data. In fact, the variability only decreased with MFR above 5 Hz. Additionally, since our data showed that mitochondria motility requires more than 2 min to recover, the MFR seen at the same time as the mitochondria velocity might correspond to a delayed effect of the stimulation. With this in mind, the mean velocity of mitochondria during the recovery period might not be true to that level of neuronal activity.

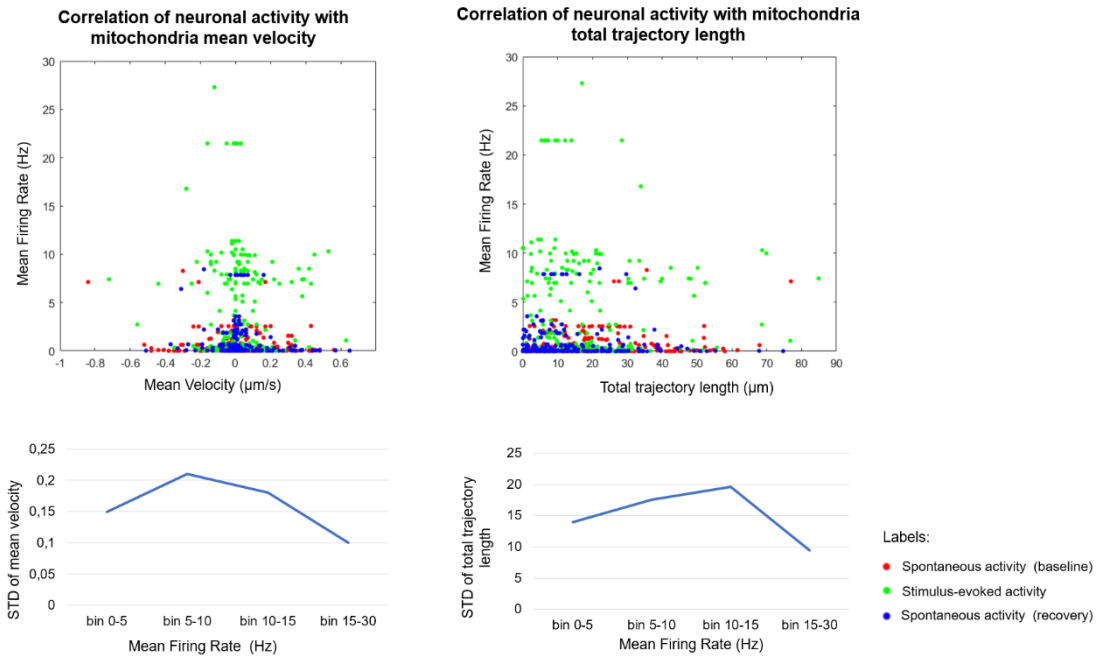

Figure 29 - Correlation of neuronal activity with mitochondrial dynamic features. The mean firing rate versus the mean velocity of mitochondria of all experimental conditions across maturation (baseline, stimulation, and recovery). Correlation of neuronal activity with the total trajectory length of mitochondria of all experimental conditions across maturation (baseline, stimulation, and recovery). Variability study of the data related to mean velocity of mitochondria and total trajectory length using standard deviation and mean firing rate intervals.

When plotting the total trajectory length with the mean firing rate of DRG neurons, there wasn't a visible trend between variables. Therefore, by evaluating the standard deviation of the mitochondrial total trajectory length we demonstrated that it increases the mean firing

rate levels up to 15Hz and afterwards it dramatically decreases, probably due to the few neurons that fire at higher levels of activity (**Figure 29**).

Evaluating the correlation between the different levels of neuronal activity and mitochondrial dynamics, has led to the conclusion that neuronal activity has no influence in the mean velocity and total trajectory length.

b) 20Hz electrical stimulation

i) Electrophysiological analysis of 20Hz stimulus-evoked activity

After the stimulation of neurons at 10Hz, we elevated the neuronal activity with a 20Hz frequency stimulus during the same 6 min protocol – spontaneous activity (baseline), stimulus-evoked activity and again spontaneous activity (recovery), 2 min each. The data analysis between these experiments was slightly different, with higher parameters for spike detections. This way, during the stimulus-evoked activity the artefact could conceal neuronal activity, thus the inferences made in this experience are required to bare that detail in mind.

When comparing the two types of stimulation, our results clearly show a lack of evoked neuronal activity from 4 to 10 div (higher in 10Hz stimulation) and an increase at 12 div (lower in 10Hz stimulation) (**Figure 30A**). However, when looking only at the baseline data before any stimuli was applied, in both experiments the spontaneous activity remains similar. Our results may indicate that by eliciting electrical activity at a frequency of 20Hz at an early stage, the neurons won't be able to withstand such high frequencies. During the recovery period the DRG neurons remained silent with low activity levels. In a general way, with a 20Hz stimulation our data showed less variability when compared to the 10Hz stimulation.

We performed a fold change analysis where we observe a significant increase of the MFR at the time of stimulation at 10, 12 and 14 div, whereas early maturation stages failed to elevate neuronal activity (**Figure 30B i**). Afterwards, in the recovery period, the axons decreased significantly their MRF across all maturation stages except for 10 div (**Figure 30B ii**). At last, the axons seem to maintain the same MFR levels between the baseline and recovery periods at 7, 12 and 14 div, whereas the remaining ones decreased their neuronal activity (Figure 30B **iii**).

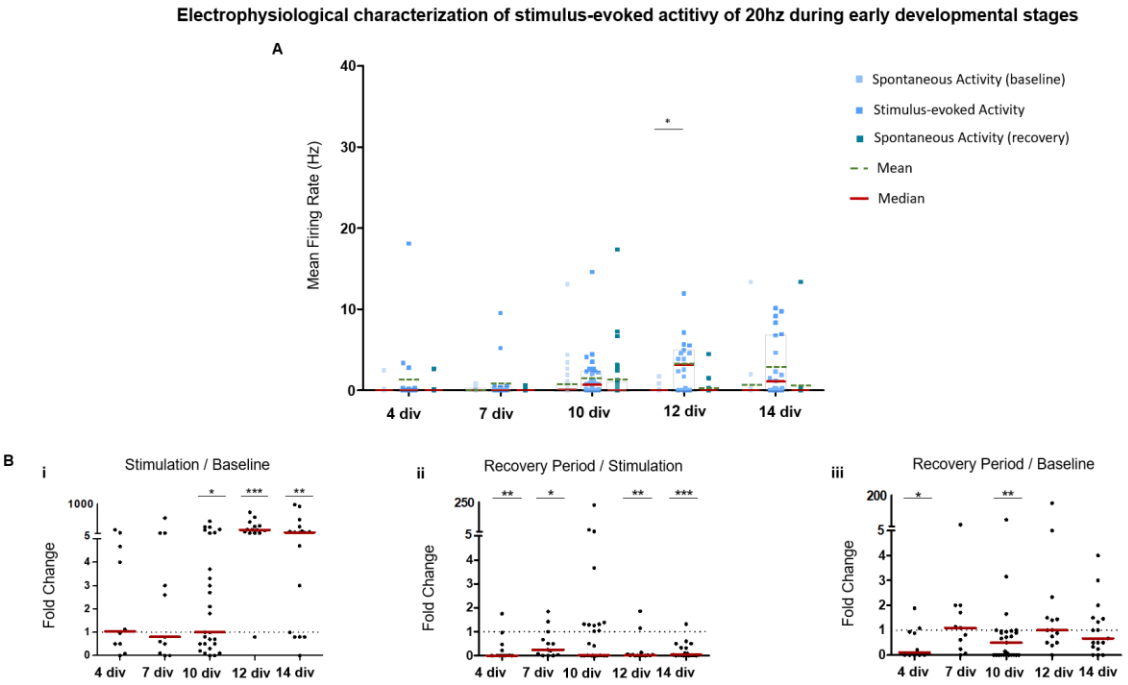

Figure 30 - Electrophysiological characterization of DRG neurons under baseline, 20 Hz stimulus-evoked activity and recovery periods across early developmental stages. A) Mean Firing Rate of DRG neurons during spontaneous activity (baseline), 20 Hz stimulus-evoked activity and spontaneous activity (recovery phase) in all divs tested (17<N<30, microchannels); Green dash lines and full red line represents the mean and median, accordingly; Statistical analysis was performed with Kruskal-Wallis test, *** $p < 0.001$, * $p < 0.05$. **B)** Fold change of the mean firing rate during the **(i)** stimulation period (normalized to baseline), **(ii)** recovery period (normalized to stimulation), and **(iii)** recovery period (normalized to baseline). The dotted line at 1 represents the value for which each condition was normalized.

ii) Mitochondria axonal transport dynamics

Similarly to the last experiment, the electrophysiological stimulation was performed simultaneously with the mitochondrial tracking. During the 20Hz stimulation we evaluated different mitochondrial kinematic parameters for two weeks such as mean velocity, time in motion, total trajectory length, among others. As before, each mitochondria analysed was tracked during the three consecutive periods (baseline, stimulation and recovery) for the whole 6 min protocol.

Looking at the mitochondrial mean velocity we verified that like in the 10Hz experiment, the velocity decreases between the baseline and recovery periods (**Figure 31A**). Additionally, during stimulation the mean velocity also presented a tendency to decrease, with statistical significance at 7 and 10 div. The fold change analysis provides a comparison between the three periods, where we can evaluate if there was a significant increase or decrease in comparison to a designated period (**Figure 31B**). The mitochondria mean velocity decreased significantly in the stimulation period at 7 div and in the recovery period at 7 and 10 div in comparison to the baseline regardless of directionality (**Figure 31B i, ii**). Considering the directionality of these organelles we verified that at 7 div there was a significant decrease in

both anterograde and retrograde direction from the baseline to the recovery periods (**Figure 31C**). However, at 10 div only mitochondria travelling in the retrograde direction decreased their mean velocity during and after stimulation. A similar trend also appears in the peak velocity analysis, where at 7 and 10 div the retrograde peak velocity mitochondria decreased **(Figure 31D).** Interestingly, none of these differences were observed in the 10Hz stimulation experiment.

Mitochondria time in motion appears to decrease from the baseline to the recovery period with statistical significance at 10 and 14 div (**Figure 32A**). Accordingly, their total trajectory length also drops between the baseline and recovery which is demonstrated in all maturation stages, except at 12 div (**Figure 32B**). During the stimulation mitochondria also took shorter paths at 7 and 10 div. One can hypothesize that the decreased time in motion and distance travelled could be explained by the change in the number of stationary periods, their duration or number of reversals. To further address this question, our results show that the number of stationary periods pose a downward trend in all maturation stages between the baseline and recovery periods (statistical significance at 4, 7 and 14 div, **Figure 32C**) as the number of reversals (statistical significance at 7,10 and 14 div, **Figure 32D**). Nonetheless, mitochondria increased by nearly half the duration of their pauses from the baseline to the recovery period (**Figure 32E**). Regarding the net displacement, mitochondria presented a preference towards the retrograde direction in a general way. When comparing the different conditions, the net displacement decreased from the baseline to the recovery period (**Figure 32F**).

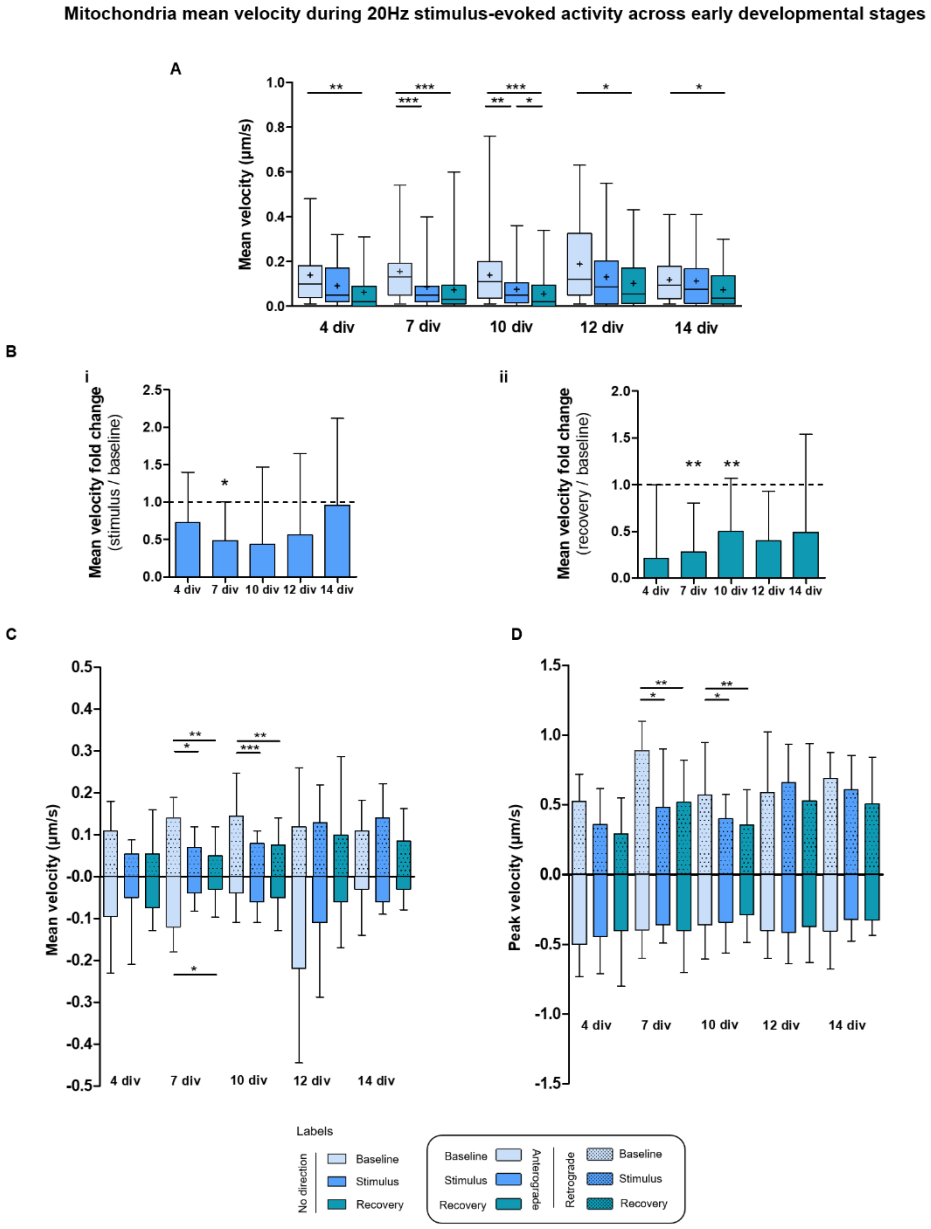

Figure 31 - Effect of the 20 Hz stimulus-evoked activity on mitochondria mean velocity across early developmental stages; A: Mitochondria mean velocity values during baseline (light blue), stimulus-evoked activity (blue), and recovery (green) periods, at 4, 7, 10, 12 and 14 divs. *, **, *** ($p < 0.05$) Mann-Whitney test; **B:** Fold change of mitochondria mean velocities during the stimulation period normalized to their baseline values **(i).** * $p < 0.05$ Wilcoxon signed-rank test, indicates median velocities significantly different than baseline values; fold change of mitochondria mean velocities during the recovery period normalized to their baseline values **(ii).** * $p < 0.05$ Wilcoxon signed-rank test, indicates median velocities significantly different than baseline values; **C**: Mitochondria mean velocity in retrograde (positive axis) and anterograde (negative axis) movements during baseline, stimulus-evoked activity, and recovery periods, at 4, 7, 10, 12 and 14 divs. **D**: Mitochondria peak velocity in retrograde (positive yy axis) and anterograde (negative yy axis) movements during baseline, stimulus-evoked activity, and recovery periods, at 4, 7, 10, 12 and 14 divs. Data presented as median with interquartile range; + indicates mean;

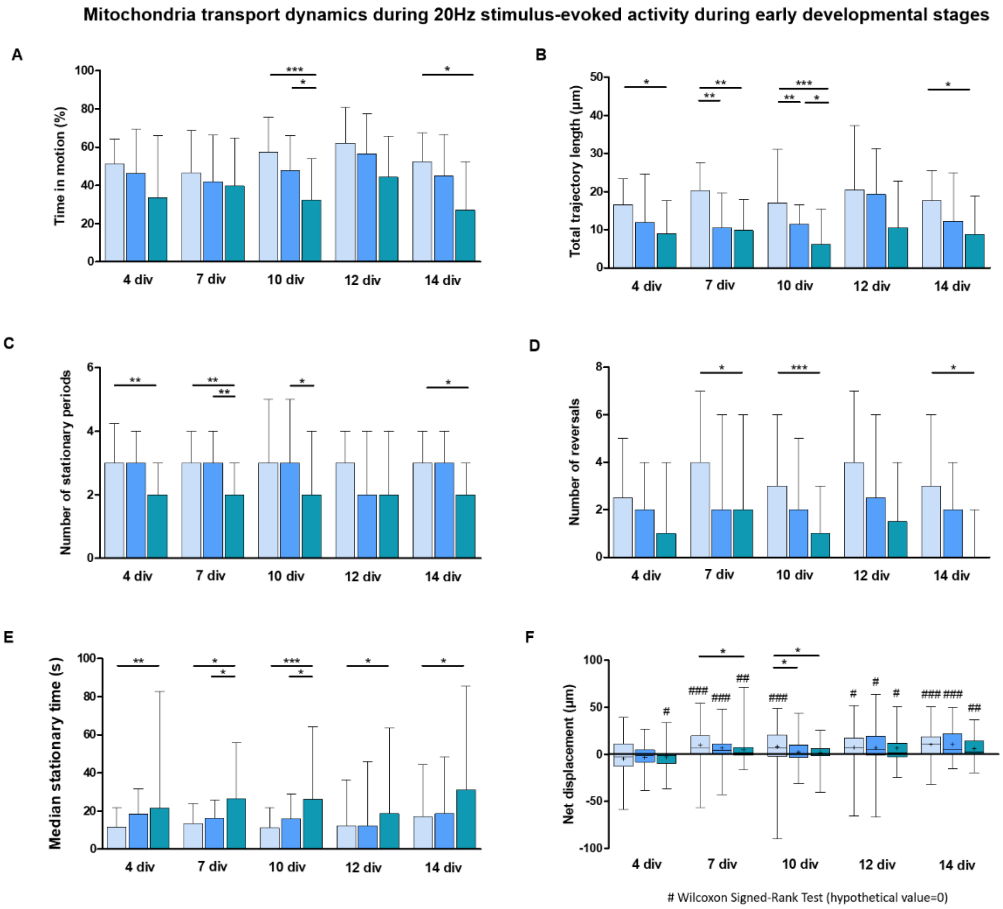

Figure 32 - Effect of the 20 Hz stimulus-evoked activity on mitochondria axonal motility across early developmental stages; A: Percentage of time in motion during baseline, stimulus-evoked activity, and recovery periods, at 4, 7, 10, 12 and 14 divs; **B:** Total trajectory length during baseline, stimulus-evoked activity and recovery periods, at 4, 7, 10, 12 and 14 divs; **C:** Number of stationary periods during baseline, stimulus-evoked activity and recovery periods, at 4, 7, 10, 12 and 14 divs; **D:** Number of reversals in direction. Data presented as median with interquartile range. *, **, *** $p < 0.05$, Mann-Whitney test; **E:** Median stationary time during baseline, stimulus-evoked activity and recovery periods, at 4, 7, 10, 12 and 14 divs; **F:** Whisker-box plot for the mitochondria net displacement during baseline, stimulus-evoked activity and recovery periods, at 4, 7, 10, 12 and 14 divs. Retrograde and anterograde movements displayed in positive and negative yy axes, respectively. #, ##, ### < 0.05 Wilcoxon signed-rank test, indicates net displacement significantly different than 0. + indicates mean;

c) Chemical inhibition induced by TTX

The increase of the neuronal activity of the axons has been described to have a negative effect on the mitochondria motility (which was supported by our data showed previously). To further understand how neuronal activity plays a regulatory role on mitochondria motility we investigated the behaviour of mitochondria dynamics under a scenario of neuronal activity inhibition by using TTX.

i) Electrophysiological analysis of TTX-induced inhibition

We evaluated the potential effects of neuronal activity inhibition using the neurotoxin tetrodotoxin. This sodium channel blocker was incubated at later maturation stages to ensure the presence of axons inside and across the microchannels, but more importantly to obtain higher levels of neuronal activity that could be inhibited. Our results showed a significant difference between the baseline and TTX-induced inhibition across maturation (10 div (*, $p<0,001$), 12 div (*) and 14 div (**, $0,001<p<0,01$), Kruskal-Wallis test), which ensures the proper inhibition of the neuronal activity by TTX (**Figure 33**). At 12 and 14 div some axons managed to recover some of the baseline neuronal activity levels during the recovery period. We successfully inhibited neuronal activity induced by TTX and it is likely that 1h30 was not enough time to recover the basal MFR after washout.

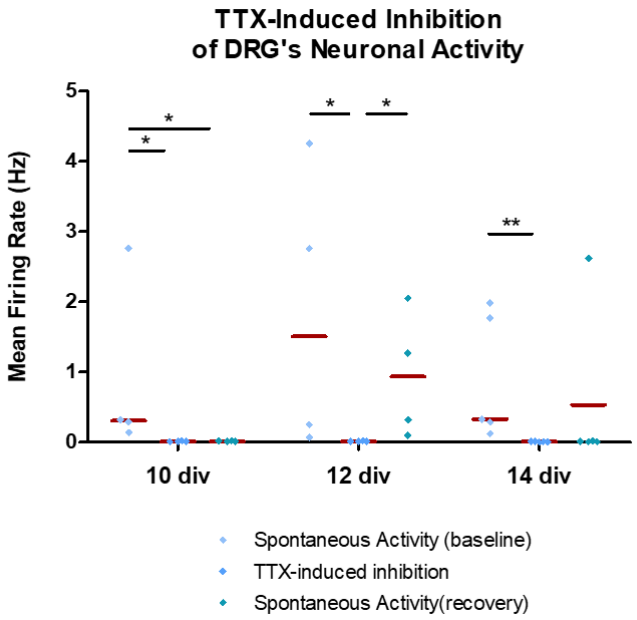

Figure 33 - Mean firing rate of DRG neurons under baseline, TTX-induced inhibition, and recovery periods across early developmental stages ($4<N<5$, microchannels). Statistical significance with the Mann-Whitney test. Red line represents the median.

ii) Mitochondria axonal transport dynamics

Following the results obtained for an increase in the neuronal activity, it was expected that mitochondria motility might increase following an inhibition of the neuronal activity. To test this hypothesis, we analyzed the mean velocity of mitochondria, the number of mitochondria per microchannel that remained motile for each period of acquisition, and at last, the total number of mitochondria that exhibited a motile behavior. In this experiment, since we are using a chemical inhibitor, the protocol to be used required medium changes, long

periods of pause and, thus, some manipulation of the µEF. Therefore, we weren't able to track the same mitochondria throughout the three periods, contrary to the electrical stimulation protocol, hence the metrics analyzed being different from the stimulation.

For a better comprehension of this section, we analyzed the results per div. At 10 div no significant differences in the mean velocity of mitochondria were observed across the three periods of analysis (**Figure 34A**).However the number of motile mitochondria (per microchannel and in total) seems to increase during TTX incubation and recovered the baseline levels in the recovery period (**Figure 34B/C**). At 12 div the mean velocity of mitochondria decreased throughout the three periods (baseline, TTX inhibition and recovery), a trend also present in the number of motile mitochondria per microchannel and total (**Figure 34A/B/C**). At 14 div the mean velocity of mitochondria also tends to decrease throughout the three periods (**Figure 34A**). However, the number of motile mitochondria per microchannel presents no changes in the TTX-induced inhibition, whereas the total number of mitochondria increases (**Figure 34B/C**). During the recovery period, less mitochondria remain motile when compared to the TTX period. To improve the reliability of these results the number of samples would have to be increased, since the results don't seem consistent.

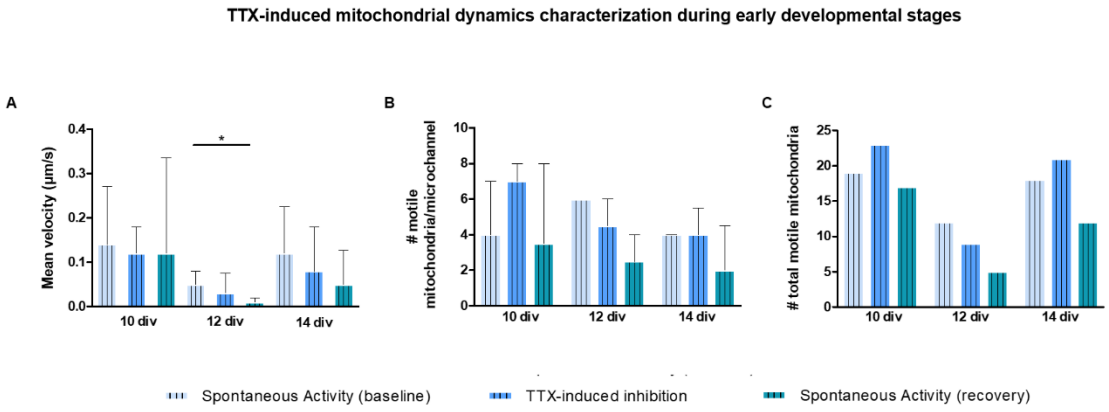

Figure 34 - TTX-induced mitochondrial dynamics characterization during early developmental stages. A: Mean velocity of axonal of mitochondria during spontaneous activity (baseline, light blue), TTX-induced inhibition (blue) and 1h30 after TTX washout during spontaneous activity (recovery, green) across 10, 12 and 14 div (Mann-Whitney test); **B:** Number of motile mitochondria per microchannel during baseline, TTX-induced inhibition and recovery across 10, 12 and 14 div; **C:** Total number of motile mitochondria during baseline, TTX-induced inhibition and recovery across 10, 12 and 14 div. The total number of microchannels is around 4.

Chapter 5

Discussion & Conclusion

The main goal of this dissertation is to investigate the regulatory role of neuronal electrical activity on the mitochondria axonal transport dynamics – one of the most important neuronal organelles for the maintenance of proper neuronal function and connections. To achieve this main goal, DRG explants were cultured on μEF platforms, which allow us to simultaneously: i) modulate and record axonal electrical activity of DRGs neurons, and ii) live-image mitochondria axonal trafficking in periods of spontaneous and evoked neuronal activity.

The electrophysiological characterization of embryonic DRG neurons remains scarce in the literature, varying from patch clamp techniques to the use of multi-well microelectrode arrays with different density populations [133-137]. The first long-term study regarding the characterization of spontaneous and stimulus-evoked activity of adult DRG neurons was performed in 2018, over the course of three weeks [133]. These neurons were cultured in multi-well microelectrode arrays where they observed a raise of the MFR up to 0.99 ± 0.35 Hz at 9 div, value which was preserved until 21 div [133]. However, our results with embryonic DRG explants showed no stabilization of the MFR at this time point - 0.76 Hz at 10 div and 1.12 Hz at 14 div. Therefore, in following studies it would be interesting to increase the time in culture to establish the time at which neuronal activity stabilize. Nevertheless, our electrophysiological characterization was consistent with the literature, Newberry *et al*. reported a MFR of 1.14 ± 0.12 Hz at 14 div [135]. The seeding of DRG explants on μEFs has advantages relative to the multi-well electrodes. The μEF enables the oriented growth of axons within microchannels and a more accurate measurement of the action potentials fired by neurons, by avoiding the dispersion of the signals throughout the medium, thus increasing their signal-to-noise ratio. We highlight the importance to have a long-term characterization of the

MFR of embryonic DRG neuron explants for stimulation studies in different platforms and possibly perform spike sorting to analyse the neuronal activity of a single neuron.

The work developed in this dissertation provided insights regarding the regulation of mitochondria transport though maturation. For that, we analyzed baseline periods along divs and observed changes in mitochondrial dynamical properties. However, we divided the results per stimulation frequency safeguarding any long-term effect on stimulating neurons. We observed that the number of stationary periods increases throughout maturation at the baseline periods from the 10 Hz stimulation experiment, supporting the appearance of syntaphilin at more mature stages of development, the same does not happen in the baseline periods from the 20 Hz stimulation experiment [117, 132, 138]. At the baseline periods from the 10 Hz experiments we observed a decrease of mitochondria time in motion, mean velocity, total trajectory length and median stationary time from 4 to 14 div. These results were consistent with Moutaux *et al.* and *Lewis et al.* where it states that mitochondrial dynamics decreases with network maturation [131, 139]. Oppositely, at the baseline periods from 20 Hz experiments the same kinematic parameters did not change throughout maturation. Only the net displacement was different, in which mitochondria preferably moved retrogradely as neurons mature. However, Moutaux *et al.* did not report any net directional flux changes between 4 to 21 div. Since we analysed only the baseline period of our protocol study for maturation studies, we hypothesize that the long-term stimulation of DRG neurons at higher frequencies might have negative effects on the mitochondria dynamics and inhibit action potentials during maturation. For a better understanding of such differences along maturation, we propose in the future the tracking of mitochondria in an independent experiment (without any stimulation) so that we can reveal with no interferences the normal maturation of these cultures.

Outcomes of modifying DRG's neuronal activity

Frequently, stimulation techniques of neurons are based on chemical treatments, such as KCl and capsaicin, rather than through electrical signals or optogenetics [140-142]. Manipulating the cultures with the addition and removal of drugs by washing methods end up stressing the cells and alter their electrophysiological activity, since they respond to medium changes. With pharmacological intervention the cultures are often overstimulated and do not reproduce the physiological environment. To overcome this issue, electrical stimulation as been used as an alternative by using multi-well devices. However, these systems stimulate both axons and somas which require different stimulation thresholds to induce its activation. Stimulating the soma requires high voltages and induces unreliable responses whereas stimulating the axon initial segment only requires low voltages and produces immediate responses [143]. By compartmentalizing neurons in microchannels we were able to solely

modulate axons and record the response during and after treatment. The use of μEF allows a protocol where once can solely manipulate the axon, and it doesn't require the direct manipulation of the medium and controls the type of stimulus given by setting their amplitude, phase and duration [111].

Most studies are successful in raising neuronal activity by electrical stimulation, however one of the major difficulties in this field is evaluating quantitatively neuronal activity since most systems do not enable the simultaneous recording and stimulation. Usually, the rise of neuronal activity is confirmed by performing calcium imaging, where an increase in the cytosolic calcium concentration relates with an increase in neuronal activity [144]. Our methodology, in addition to confirming the proper elicitation of action potentials it allows its quantification at the time of stimulation.

We increased DRG neurons activity by electrically evoking action potentials at 10 Hz and 20 Hz stimuli. At both stimulation experiments we successfully increased neuronal activity although as the cultures matured *in vitro*, 10 Hz stimulated neurons decreased their excitability, whereas 20 Hz stimulated neurons only expressed excitability after 10 div. After stimulation, 10 Hz stimulated neurons recovered their baseline levels of activity, whereas 20 Hz stimulated neurons at 4 and 10 div decreased their neuronal activity.

Another interesting finding of our work is related to the time required for stimulated neurons to return to their baseline conditions. In terms of firing activity, our results show that during the 2 min period of recovery (after stimulation) neurons return to their baseline firing rate during the 10 Hz stimulation. When evaluating a higher stimulation frequency, the following period decreased their neuronal activity at 4 and 10 div. In addition, the same 2 min period of recovery showed to be insufficient for the stimulus-induced changes in mitochondria dynamics return to their baseline profile. Most of the kinematic parameters analyzed in this work revealed a more pronounced negative effect than those observed during the stimulation period. For instance, our results show that the time in motion of mitochondria decreases during stimulation and, afterwards, it decreases even more in the recovery period suggesting that the 2 min period may be enough to return to basal conditions at the electrical level but not at the molecular level. A recent study using optogenetics revealed a disparity in the timescales of neuronal activity and metabolic flux. They correlated the changes in the calcium influx and local changes in ATP *in vivo*, confirming neuronal activation by calcium imaging. The ATP concentration rises and reaches its peak within 500 ms of neuronal activity increase, however these concentration levels endure for many tens of seconds. The Ca^{2+} signals decayed with a time constant of $\tau = 3s$, whereas ATP had a time constant of $\tau = 43s$ [145]. Given that molecular motors bind and move along the microtubules using ATP, we hypothesize that after neuronal activation kinesin and dynein may be slower in restarting its movement or the anchoring mechanisms of mitochondria take longer to actuate. All together, these findings suggest that the mechanisms responsible for the stimulus-induced changes observed in the mitochondria

axonal transport dynamics are slow, and probably require long periods of time (> 2 min) to restore the initial mitochondria dynamic properties.

To evaluate the effects of neuronal activity on mitochondria dynamics, we analysed several kinematic features. Our results show that by stimulating the neurons the mean velocity decreases (regardless of the direction), so does their trajectory length, time in motion and number of reversals in both stimulation experiments. Obashi *et al*. analysed mitochondria dynamics of hippocampal neurons by stimulating at 40 Hz for 10 s every 3 min (total of 50 min) and reported a decreased mean velocity and increased short-pause frequencies (number of paused mitochondria/number of all passed mitochondria) [87]. Contrary, we observed a decrease in the number of stationary periods. This contrast might be explained by differences in methodologies, since we track a single mitochondrion and observes the direct effect of stimulation, thus analysing only previously moving mitochondria. In terms of mitochondria directionally, an *in vivo*

study reports that by stimulation of the saphenous nerve at 1 Hz both average velocities were preserved, but at 50 Hz stimulation the anterograde velocities doubled to 0.7 μm/s and retrograde remained the same [88]. However, in this study we found no increase in the mitochondria velocities. We report a decrease of the anterograde mean and peak velocity at 10 Hz (mean velocity – 14 div, peak velocity – 10 div). At 20 Hz stimulation, we observed a decrease in both directions regarding mean velocities and only a decrease in the retrograde direction peak velocities.

The time in motion of mitochondria decreases from the baseline to the recovery periods, which was in accordance with the decrease in the total trajectory length. This slope might be explained by an increase in the mitochondria number of stationary periods, such as previously reported in chemical stimulations in Tyrode's solution [87]. However, our results demonstrate that when stimulating they remain the same and remarkably decrease from stimulation to recovery periods. To understand this difference, we analyzed the median stationary time, and verified that the duration of stationary periods increases by almost 50% between the baseline and the recovery. We hypothesize different anchoring mechanisms of mitochondria are responsible between before and after stimulation, since mitochondria exhibit a longer stationary period and the number of reversals also decrease. Another possibility would be that anchoring mechanisms take longer to actuate or molecular motors took longer to restart mitochondria movement. Besides this hypothesis, we need to take into account that we considered as a stationary period mitochondrion that had velocities under 0,05 μm/s for 15 consecutive frames, thus discarding the concept of dynamic pauses – low sustained speed but high transient component velocity, meaning the period where mitochondria present a lower speed before entering a run through the microtubule – which increases a biased towards stationary periods [120]. Mitochondria in dynamic pauses are more likely to start a running phase than stationary ones [120]. This limitation could decrease the stationary periods and

increase the time in motion, thus explaining the differences in our data. Furthermore, the continuous decrease of motility in the recovery period could be explained by the reorganization of mitochondrial complex, thus detaching syntaphilin from KIF5 and mitochondria [124].

The TTX induced inhibition has been used to evaluate the opposite effect of stimulation and verify the possibility of increased mitochondria motility. Hippocampal neurons (14 div) when submitted to TTX stimulation with medium flow on MEAs show a decrease in the MFR to zero in less than 20 s and after adding fresh medium it returns to baseline [146]. However, another study observed that 18% of DRG neurons continued firing after TTX treatment. Such disparity is explained by the presence of TTX-resistant components in DRG cultured neurons. In our study, during TTX treatment DRG neurons completely ceased their activity and no differences were observed at the mitochondria axonal transport level during TTX treatment. To further validate this experiment, a significant number of mitochondria would have to be analysed.

Conclusion and Future work

This dissertation contributed with the first detailed analysis of DRG explant neurons electrical activity in a microfluidics/microelectrode array platform over the course of 2 weeks. The simultaneous live-imaging of mitochondria axonal trajectories enabled the proper knowledge to how much we were increasing neuronal activity by calculating MFR in a more controlled environment. Neuronal activity was successfully increased and showed effects on mitochondria dynamics. Therefore, we provide another confirmation towards this regulatory mechanism with the additional information that they operate in different timescales. However, we found no correlation between the levels of activity risen with mean velocity and total trajectory length, meaning that presence of cytosolic calcium has a role, but it's not regulated by its quantity. Mitochondria increase their time in a stationary period, thus decreasing mean velocity, time in motion and total trajectory length. To elucidate what happens at a molecular level further and different analysis would have to take place.

Neurons can also increase their activity levels by maturation which comprises an asset in studying mitochondria in their lifespan of 2 weeks in culture. Accordingly, we also found that as neurons mature they increase neuronal activity which proved to also regulate mitochondria dynamics. To sum up, the purpose of dissertation was successfully accomplished and increased even further questions towards a better comprehension to which molecular motors anchor mitochondria in stimulus-evoked events. Does stimulus-evoked activity require different anchoring mechanism? How long does it take for mitochondrial to return to their baseline levels? Does long-term stimulation effectively regulate mitochondrial dynamics? These questions remain to be elucidated in future experiments.

References

1. VanPutte, C.L., J.L. Regan, and A.F. Russo, *Seeley's Anatomy & Physiology*. 11th Edition ed.: McGraw-Hill Education.
2. Franze, K. and J. Guck, *The biophysics of neuronal growth*. Reports on Progress in Physics, 2010. **73**(9): p. 094601.
3. Ziemssen, T. and T. Siepmann, *The Investigation of the Cardiovascular and Sudomotor Autonomic Nervous System-A Review*. Front Neurol, 2019. **10**: p. 53.
4. Pchitskaya, E. and I. Bezprozvanny, *Dendritic Spines Shape Analysis-Classification or Clusterization? Perspective*. Frontiers in synaptic neuroscience, 2020. **12**: p. 31-31.
5. Lefebvre, J.L., J.R. Sanes, and J.N. Kay, *Development of Dendritic Form and Function*. Annual Review of Cell and Developmental Biology, 2015. **31**(1): p. 741-777.
6. Leterrier, C., *The Axon Initial Segment: An Updated Viewpoint*. The Journal of Neuroscience, 2018. **38**(9): p. 2135.
7. Zeng, H. and J.R. Sanes, *Neuronal cell-type classification: challenges, opportunities and the path forward*. Nat Rev Neurosci, 2017. **18**(9): p. 530-546.
8. Nascimento, A.I., F.M. Mar, and M.M. Sousa, *The intriguing nature of dorsal root ganglion neurons: Linking structure with polarity and function*. Prog Neurobiol, 2018. **168**: p. 86-103.
9. Esposito, M.F., et al., *Unique Characteristics of the Dorsal Root Ganglion as a Target for Neuromodulation*. Pain Med, 2019. **20**(Suppl 1): p. S23-S30.
10. Emmenegger, V., et al., *Morphological and Functional Characterization of Non-fast-Spiking GABAergic Interneurons in Layer 4 Microcircuitry of Rat Barrel Cortex*. Cereb Cortex, 2018. **28**(4): p. 1439-1457.
11. Hosp, J.A., et al., *Morpho-physiological criteria divide dentate gyrus interneurons into classes*. Hippocampus, 2014. **24**(2): p. 189-203.
12. Hernáth, F., K. Schlett, and A. Szücs, *Alternative classifications of neurons based on physiological properties and synaptic responses, a computational study*. Scientific Reports, 2019. **9**(1): p. 13096.
13. Takano, T., et al., *Neuronal polarization*. Development, 2015. **142**(12): p. 2088-93.
14. Britt, D.J., et al., *Mechanisms of Polarized Organelle Distribution in Neurons*. Front Cell Neurosci, 2016. **10**: p. 88.
15. Farías, G.G., et al., *Sorting of Dendritic and Axonal Vesicles at the Pre-axonal Exclusion Zone*. Cell reports, 2015. **13**(6): p. 1221-1232.
16. Ramírez, O.A. and A. Couve, *The endoplasmic reticulum and protein trafficking in dendrites and axons*. Trends Cell Biol, 2011. **21**(4): p. 219-27.
17. González, C., V.H. Cornejo, and A. Couve, *Golgi bypass for local delivery of axonal proteins, fact or fiction?* Current Opinion in Cell Biology, 2018. **53**: p. 9-14.
18. Purves D, A.G., Fitzpatrick D, et al.,, *Neuroscience*. 6th edition ed.
19. Häusser, M., *The Hodgkin-Huxley theory of the action potential*. Nature Neuroscience, 2000. **3**(11): p. 1165-1165.
20. Hodgkin, A.L. and A.F. Huxley, *Action Potentials Recorded from Inside a Nerve Fibre*. Nature, 1939. **144**(3651): p. 710-711.
21. Guillaud, L., et al., *Anterograde Axonal Transport in Neuronal Homeostasis and Disease*. Frontiers in Molecular Neuroscience, 2020. **13**(179).
22. Maday, S., et al., *Axonal transport: cargo-specific mechanisms of motility and regulation*. Neuron, 2014. **84**(2): p. 292-309.
23. Dubey, S., et al., *The axonal actin-spectrin lattice acts as a tension buffering shock absorber*. bioRxiv, 2019: p. 510560.
24. Margiotta, A. and C. Bucci, *Role of Intermediate Filaments in Vesicular Traffic*. Cells, 2016. **5**(2): p. 20.

25. De Vos, K.J. and M. Hafezparast, *Neurobiology of axonal transport defects in motor neuron diseases: Opportunities for translational research?* Neurobiol Dis, 2017. **105**: p. 283-299.
26. De Vos, K.J., et al., *Role of axonal transport in neurodegenerative diseases.* Annu Rev Neurosci, 2008. **31**: p. 151-73.
27. Nirschl, J.J., A.E. Ghiretti, and E.L.F. Holzbaur, *The impact of cytoskeletal organization on the local regulation of neuronal transport.* Nat Rev Neurosci, 2017. **18**(10): p. 585-597.
28. Endow, S.A., F.J. Kull, and H. Liu, *Kinesins at a glance*. Journal of Cell Science, 2010. **123**(20): p. 3420-3424.
29. Nishimura, T., et al., *Role of the PAR-3-KIF3 complex in the establishment of neuronal polarity.* Nat Cell Biol, 2004. **6**(4): p. 328-34.
30. Vukoja, A., et al., *Presynaptic Biogenesis Requires Axonal Transport of Lysosome-Related Vesicles.* Neuron, 2018. **99**(6): p. 1216-1232.e7.
31. Millecamps, S. and J.P. Julien, *Axonal transport deficits and neurodegenerative diseases.* Nat Rev Neurosci, 2013. **14**(3): p. 161-76.
32. Schroer, T.A., *DYNACTIN.* Annual Review of Cell and Developmental Biology, 2004. **20**(1): p. 759-779.
33. Xiang, X. and R. Qiu, *Cargo-Mediated Activation of Cytoplasmic Dynein in vivo.* Front Cell Dev Biol, 2020. **8**: p. 598952.
34. Arnold, D.B. and G. Gallo, *Structure meets function: actin filaments and myosin motors in the axon.* Journal of Neurochemistry, 2014. **129**(2): p. 213-220.
35. Bridgman, P.C., *Myosin-dependent transport in neurons.* J Neurobiol, 2004. **58**(2): p. 164-74.
36. Verhey, K.J., et al., *Cargo of kinesin identified as JIP scaffolding proteins and associated signaling molecules.* The Journal of cell biology, 2001. **152**(5): p. 959-970.
37. Setou, M., et al., *Glutamate-receptor-interacting protein GRIP1 directly steers kinesin to dendrites.* Nature, 2002. **417**(6884): p. 83-7.
38. Welte, M.A., *Bidirectional Transport along Microtubules.* Current Biology, 2004. **14**(13): p. R525-R537.
39. Liu, X.A., V. Rizzo, and S.V. Puthanveettil, *Pathologies of Axonal Transport in Neurodegenerative Diseases.* Transl Neurosci, 2012. **3**(4): p. 355-372.
40. Guo, B., et al., *Stabilization of microtubules improves cognitive functions and axonal transport of mitochondria in Alzheimer's disease model mice.* Neurobiol Aging, 2020. **96**: p. 223-232.
41. Tammineni, P., et al., *Impaired retrograde transport of axonal autophagosomes contributes to autophagic stress in Alzheimer's disease neurons.* eLife, 2017. **6**: p. e21776.
42. Dubey, M., et al., *Tau inhibits anterograde axonal transport and perturbs stability in growing axonal neurites in part by displacing kinesin cargo: Neurofilaments attenuate tau-mediated neurite instability.* Cell Motility, 2008. **65**(2): p. 89-99.
43. Goldstein, L.S. and U. Das, *Neurodegenerative Diseases and Axonal Transport*. 2018: p. 345-367.
44. White, J.A., et al., *Excess Rab4 rescues synaptic and behavioral dysfunction caused by defective HTT-Rab4 axonal transport in Huntington's disease*. Acta Neuropathologica Communications, 2020. **8**(1): p. 97.
45. Sleigh, J.N., et al., *Mice Carrying ALS Mutant TDP-43, but Not Mutant FUS, Display In Vivo Defects in Axonal Transport of Signaling Endosomes.* Cell Reports, 2020. **30**(11): p. 3655-3662.e2.
46. Kadavath, H., et al., *Tau stabilizes microtubules by binding at the interface between tubulin heterodimers.* Proc Natl Acad Sci U S A, 2015. **112**(24): p. 7501-6.
47. Chaudhary, A.R., et al., *Tau directs intracellular trafficking by regulating the forces exerted by kinesin and dynein teams.* Traffic, 2018. **19**(2): p. 111-121.
48. Godena, V.K., et al., *Increasing microtubule acetylation rescues axonal transport and locomotor deficits caused by LRRK2 Roc-COR domain mutations.* Nat Commun, 2014. **5**: p. 5245.
49. Verhamme, C., et al., *Myelin and axon pathology in a long-term study of PMP22-overexpressing mice.* J Neuropathol Exp Neurol, 2011. **70**(5): p. 386-98.

50. De Vos, K.J., et al., *Familial amyotrophic lateral sclerosis-linked SOD1 mutants perturb fast axonal transport to reduce axonal mitochondria content*. Human Molecular Genetics, 2007. **16**(22): p. 2720-2728.
51. Imai, Y., *PINK1-Parkin signaling in Parkinson's disease: Lessons from Drosophila*. Neuroscience Research, 2020. **159**: p. 40-46.
52. Qi, H., et al., *Ursodeoxycholic acid protects dopaminergic neurons from oxidative stress via regulating mitochondrial function, autophagy, and apoptosis in MPTP/MPP+-induced Parkinson's disease*. Neuroscience Letters, 2021. **741**: p. 135493.
53. Kim-Han, J.S., J.A. Antenor-Dorsey, and K.L. O'Malley, *The parkinsonian mimetic, MPP+, specifically impairs mitochondrial transport in dopamine axons*. J Neurosci, 2011. **31**(19): p. 7212-21.
54. Arnold, B., et al., *Integrating multiple aspects of mitochondrial dynamics in neurons: age-related differences and dynamic changes in a chronic rotenone model*. Neurobiol Dis, 2011. **41**(1): p. 189-200.
55. Esteves, A.R., I. Gozes, and S.M. Cardoso, *The rescue of microtubule-dependent traffic recovers mitochondrial function in Parkinson's disease*. Biochimica et Biophysica Acta (BBA) - Molecular Basis of Disease, 2014. **1842**(1): p. 7-21.
56. Guedes-Dias, P. and E.L.F. Holzbaur, *Axonal transport: Driving synaptic function*. Science, 2019. **366**(6462).
57. Verhey, K.J. and J.W. Hammond, *Traffic control: regulation of kinesin motors*. Nat Rev Mol Cell Biol, 2009. **10**(11): p. 765-77.
58. Sellers, J.R., et al., *Calcium and cargoes as regulators of myosin 5a activity*. Biochem Biophys Res Commun, 2008. **369**(1): p. 176-81.
59. Olenick, M.A., R. Dominguez, and E.L.F. Holzbaur, *Dynein activator Hook1 is required for trafficking of BDNF-signaling endosomes in neurons*. Journal of Cell Biology, 2018. **218**(1): p. 220-233.
60. Cai, Q., C. Gerwin, and Z.H. Sheng, *Syntabulin-mediated anterograde transport of mitochondria along neuronal processes*. J Cell Biol, 2005. **170**(6): p. 959-69.
61. Cai, Q., P.-Y. Pan, and Z.-H. Sheng, *Syntabulin–Kinesin-1 Family Member 5B-Mediated Axonal Transport Contributes to Activity-Dependent Presynaptic Assembly*. The Journal of Neuroscience, 2007. **27**(27): p. 7284.
62. Qin, J., et al., *How Kinesin-1 Utilize the Energy of Nucleotide: The Conformational Changes and Mechanochemical Coupling in the Unidirectional Motion of Kinesin-1*. International journal of molecular sciences, 2020. **21**(18): p. 6977.
63. Monroy, B.Y., et al., *Competition between microtubule-associated proteins directs motor transport*. Nature Communications, 2018. **9**(1): p. 1487.
64. Dixit, R., et al., *Differential regulation of dynein and kinesin motor proteins by tau*. Science, 2008. **319**(5866): p. 1086-9.
65. Urnavicius, L., et al., *The structure of the dynactin complex and its interaction with dynein*. Science, 2015. **347**(6229): p. 1441-1446.
66. Waterman-Storer, C.M., S. Karki, and E.L. Holzbaur, *The p150Glued component of the dynactin complex binds to both microtubules and the actin-related protein centractin (Arp-1)*. Proceedings of the National Academy of Sciences of the United States of America, 1995. **92**(5): p. 1634-1638.
67. Guedes-Dias, P., et al., *Kinesin-3 Responds to Local Microtubule Dynamics to Target Synaptic Cargo Delivery to the Presynapse*. Current Biology, 2019. **29**(2): p. 268-282.e8.
68. Guo, S.-K., et al., *Run length distribution of dimerized kinesin-3 molecular motors: comparison with dimeric kinesin-1*. Scientific Reports, 2019. **9**(1): p. 16973.
69. Urnavicius, L., et al., *Cryo-EM shows how dynactin recruits two dyneins for faster movement*. Nature, 2018. **554**(7691): p. 202-206.
70. Mallik, R., et al., *Cytoplasmic dynein functions as a gear in response to load*. Nature, 2004. **427**(6975): p. 649-52.
71. Hayashi, K., et al., *Non-invasive force measurement reveals the number of active kinesins on a synaptic vesicle precursor in axonal transport regulated by ARL-8*. Physical Chemistry Chemical Physics, 2018. **20**(5): p. 3403-3410.

72. Gutiérrez-Medina, B., et al., *Differential effect of multiple kinesin motors on run length, force and microtubule binding rate*. Biophysical Chemistry, 2018. **242**: p. 28-33.
73. Encalada, S.E., et al., *Stable kinesin and dynein assemblies drive the axonal transport of mammalian prion protein vesicles*. Cell, 2011. **144**(4): p. 551-565.
74. Rai, A.K., et al., *Molecular adaptations allow dynein to generate large collective forces inside cells*. Cell, 2013. **152**(1-2): p. 172-82.
75. Feng, Q., et al., *Motor Reattachment Kinetics Play a Dominant Role in Multimotor-Driven Cargo Transport*. Biophys J, 2018. **114**(2): p. 400-409.
76. Hendricks, A.G., et al., *Motor Coordination via a Tug-of-War Mechanism Drives Bidirectional Vesicle Transport*. Current Biology, 2010. **20**(8): p. 697-702.
77. Fu, M.-m. and E.L.F. Holzbaur, *Integrated regulation of motor-driven organelle transport by scaffolding proteins*. Trends in Cell Biology, 2014. **24**(10): p. 564-574.
78. Fu, M.M. and E.L. Holzbaur, *JIP1 regulates the directionality of APP axonal transport by coordinating kinesin and dynein motors*. J Cell Biol, 2013. **202**(3): p. 495-508.
79. Fu, M.M., J.J. Nirschl, and E.L.F. Holzbaur, *LC3 binding to the scaffolding protein JIP1 regulates processive dynein-driven transport of autophagosomes*. Dev Cell, 2014. **29**(5): p. 577-590.
80. van Spronsen, M., et al., *TRAK/Milton motor-adaptor proteins steer mitochondrial trafficking to axons and dendrites*. Neuron, 2013. **77**(3): p. 485-502.
81. Neisch, A.L., T.P. Neufeld, and T.S. Hays, *A STRIPAK complex mediates axonal transport of autophagosomes and dense core vesicles through PP2A regulation*. Journal of Cell Biology, 2017. **216**(2): p. 441-461.
82. Spinner, M.A., et al., *A Conserved Role for Vezatin Proteins in Cargo-Specific Regulation of Retrograde Axonal Transport*. Genetics, 2020. **216**(2): p. 431-445.
83. López-Doménech, G., et al., *Miro proteins coordinate microtubule- and actin-dependent mitochondrial transport and distribution*. The EMBO Journal, 2018. **37**(3): p. 321-336.
84. Wang, X. and T.L. Schwarz, *The Mechanism of Ca²⁺-Dependent Regulation of Kinesin-Mediated Mitochondrial Motility*. Cell, 2009. **136**(1): p. 163-174.
85. Zhang, C.L., et al., *Activity-Dependent Regulation of Mitochondrial Motility by Calcium and Na/K-ATPase at Nodes of Ranvier of Myelinated Nerves*. The Journal of Neuroscience, 2010. **30**(10): p. 3555.
86. Ohno, N., et al., *Myelination and axonal electrical activity modulate the distribution and motility of mitochondria at CNS nodes of Ranvier*. J Neurosci, 2011. **31**(20): p. 7249-58.
87. Obashi, K. and S. Okabe, *Regulation of mitochondrial dynamics and distribution by synapse position and neuronal activity in the axon*. Eur J Neurosci, 2013. **38**(3): p. 2350-63.
88. Sajic, M., et al., *Impulse conduction increases mitochondrial transport in adult mammalian peripheral nerves in vivo*. PLoS biology, 2013. **11**(12): p. e1001754-e1001754.
89. de Wit, J., et al., *Vesicular Trafficking of Semaphorin 3A is Activity-Dependent and Differs Between Axons and Dendrites*. Traffic, 2006. **7**(8): p. 1060-1077.
90. Birdsall, V., et al., *KIF13A mediates the activity-dependent transport of ESCRT-0 proteins in axons*. bioRxiv, 2020: p. 2020.04.16.044818.
91. Suk, H.-J., E.S. Boyden, and I. van Welie, *Advances in the automation of whole-cell patch clamp technology*. Journal of Neuroscience Methods, 2019. **326**: p. 108357.
92. Lewandowska, M.K., et al., *Recording large extracellular spikes in microchannels along many axonal sites from individual neurons*. PLoS One, 2015. **10**(3): p. e0118514.
93. Debanne, D., et al., *Axon Physiology*. Physiological Reviews, 2011. **91**(2): p. 555-602.
94. Py, C., et al., *From Understanding Cellular Function to Novel Drug Discovery: The Role of Planar Patch-Clamp Array Chip Technology*. Frontiers in Pharmacology, 2011. **2**(51).
95. Wanzenboeck, H.D., P. Scholze, and J.K. Mika, *Imaging and Electrophysiology of Individual Neurites Functionally Isolated in Microchannels*, in *Neurohistology and*

Imaging Techniques, R. Pelc, W. Walz, and J.R. Doucette, Editors. 2020, Springer US: New York, NY. p. 341-377.
96. Bullmann, T., et al., *Large-Scale Mapping of Axonal Arbors Using High-Density Microelectrode Arrays.* Frontiers in Cellular Neuroscience, 2019. **13**(404).
97. Chen, T.W., et al., *Ultrasensitive fluorescent proteins for imaging neuronal activity.* Nature, 2013. **499**(7458): p. 295-300.
98. Hu, C., et al., *Optical excitation and detection of neuronal activity.* Journal of Biophotonics, 2019. **12**(3): p. e201800269.
99. Emmenegger, V., et al., *Technologies to Study Action Potential Propagation With a Focus on HD-MEAs.* Frontiers in Cellular Neuroscience, 2019. **13**(159).
100. Soucy, J.R., et al., *Instrumented Microphysiological Systems for Real-Time Measurement and Manipulation of Cellular Electrochemical Processes.* iScience, 2019. **21**: p. 521-548.
101. Sophie Veitinger, D. *The Patch-Clamp Techinque: An Introduction*. 2011 09 November 2011; Available from: https://www.leica-microsystems.com/science-lab/the-patch-clamp-technique/.
102. Spira, M.E., et al., *Multisite Intracellular Recordings by MEA.* Adv Neurobiol, 2019. **22**: p. 125-153.
103. Obien, M.E.J., et al., *Revealing neuronal function through microelectrode array recordings.* Frontiers in neuroscience, 2015. **8**: p. 423-423.
104. Obien, M.E.J. and U. Frey, *Large-Scale, High-Resolution Microelectrode Arrays for Interrogation of Neurons and Networks.* Advances in neurobiology, 2019. **22**: p. 83-123.
105. Kole, M.H.P. and M.A. Popovic, *Patch-Clamp Recording from Myelinated Central Axons*, in *Advanced Patch-Clamp Analysis for Neuroscientists*, A. Korngreen, Editor. 2016, Springer New York: New York, NY. p. 123-138.
106. Heiney, K., et al., *microSpikeHunter: An advanced computational tool for the analysis of neuronal communication and action potential propagation in microfluidic platforms.* Sci Rep, 2019. **9**(1): p. 5777.
107. Lopes, C.D.F., J.C. Mateus, and P. Aguiar, *Interfacing Microfluidics with Microelectrode Arrays for Studying Neuronal Communication and Axonal Signal Propagation.* J Vis Exp, 2018(142).
108. Neto, E., et al., *Compartmentalized Microfluidic Platforms: The Unrivaled Breakthrough of In Vitro Tools for Neurobiological Research.* J Neurosci, 2016. **36**(46): p. 11573-11584.
109. Danastas, K., A.L. Cunningham, and M. Miranda-Saksena, *The Use of Microfluidic Neuronal Devices to Study the Anterograde Axonal Transport of Herpes Simplex Virus-1*, in *Herpes Simplex Virus : Methods and Protocols*, R.J. Diefenbach and C. Fraefel, Editors. 2020, Springer New York: New York, NY. p. 409-418.
110. M., T.A., et al., *A microfluidic culture platform for CNS axonal injury, regeneration and transport.* Nat. Methods, 2005. **2**: p. 599.
111. Moutaux, E., et al., *An integrated microfluidic/microelectrode array for the study of activity-dependent intracellular dynamics in neuronal networks.* Lab Chip, 2018. **18**(22): p. 3425-3435.
112. Del Rio, J.A. and I. Ferrer, *Potential of Microfluidics and Lab-on-Chip Platforms to Improve Understanding of "prion-like" Protein Assembly and Behavior.* Frontiers in bioengineering and biotechnology, 2020. **8**: p. 570692-570692.
113. Kim, H.J., et al., *Quantitative analysis of axonal transport by using compartmentalized and surface micropatterned culture of neurons.* ACS Chem Neurosci, 2012. **3**(6): p. 433-8.
114. Zhang, K., et al., *Single-Molecule Imaging of NGF Axonal Transport in Microfluidic Devices.* Lab on a chip, 2010. **10**: p. 2566-73.
115. Pan, L., et al., *Large extracellular spikes recordable from axons in microtunnels.* IEEE Trans Neural Syst Rehabil Eng, 2014. **22**(3): p. 453-9.
116. Dworak, B.J. and B.C. Wheeler, *Novel MEA platform with PDMS microtunnels enables the detection of action potential propagation from isolated axons in culture.* Lab on a Chip, 2009. **9**(3): p. 404-410.

117. Cheng, X.T. and Z.H. Sheng, *Developmental regulation of microtubule-based trafficking and anchoring of axonal mitochondria in health and diseases.* Dev Neurobiol, 2021. **81**(3): p. 284-299.
118. Zhu, X.H., et al., *Quantitative imaging of energy expenditure in human brain.* Neuroimage, 2012. **60**(4): p. 2107-17.
119. Misgeld, T. and T.L. Schwarz, *Mitostasis in Neurons: Maintaining Mitochondria in an Extended Cellular Architecture.* Neuron, 2017. **96**(3): p. 651-666.
120. M., C., et al., *A new method for quantifying mitochondrial axonal transport.* Protein Cell, 2016. **7**: p. 804.
121. Sleigh, J.N., et al., *Methodological advances in imaging intravital axonal transport.* F1000Research, 2017. **6**: p. 200-200.
122. Pathak, D., K.J. Sepp, and P.J. Hollenbeck, *Evidence That Myosin Activity Opposes Microtubule-Based Axonal Transport of Mitochondria.* The Journal of Neuroscience, 2010. **30**(26): p. 8984.
123. Wang, X., et al., *PINK1 and Parkin target Miro for phosphorylation and degradation to arrest mitochondrial motility.* Cell, 2011. **147**(4): p. 893-906.
124. Chen, Y. and Z.-H. Sheng, *Kinesin-1-syntaphilin coupling mediates activity-dependent regulation of axonal mitochondrial transport.* Journal of Cell Biology, 2013. **202**(2): p. 351-364.
125. Chen, Y.-M., C. Gerwin, and Z.-H. Sheng, *Dynein Light Chain LC8 Regulates Syntaphilin-Mediated Mitochondrial Docking in Axons.* The Journal of Neuroscience, 2009. **29**(30): p. 9429-9438.
126. Kang, J.S., et al., *Docking of axonal mitochondria by syntaphilin controls their mobility and affects short-term facilitation.* Cell, 2008. **132**(1): p. 137-48.
127. Macaskill, A.F., et al., *Miro1 is a calcium sensor for glutamate receptor-dependent localization of mitochondria at synapses.* Neuron, 2009. **61**(4): p. 541-55.
128. Wang, X. and T.L. Schwarz, *The Mechanism of Ca2+-Dependent Regulation of Kinesin-Mediated Mitochondrial Motility.* Cell, 2009. **136**(1): p. 163-174.
129. Morsci, N.S., et al., *Age-Related Phasic Patterns of Mitochondrial Maintenance in Adult Caenorhabditis elegans Neurons.* J Neurosci, 2016. **36**(4): p. 1373-85.
130. Vagnoni, A. and S.L. Bullock, *A cAMP/PKA/Kinesin-1 Axis Promotes the Axonal Transport of Mitochondria in Aging Drosophila Neurons.* Curr Biol, 2018. **28**(8): p. 1265-1272 e4.
131. Lewis, T.L., Jr., et al., *Progressive Decrease of Mitochondrial Motility during Maturation of Cortical Axons In Vitro and In Vivo.* Curr Biol, 2016. **26**(19): p. 2602-2608.
132. Zhou, B., et al., *Facilitation of axon regeneration by enhancing mitochondrial transport and rescuing energy deficits.* Journal of Cell Biology, 2016. **214**(1): p. 103-119.
133. Black, B.J., et al., *Adult mouse sensory neurons on microelectrode arrays exhibit increased spontaneous and stimulus-evoked activity in the presence of interleukin-6.* J Neurophysiol, 2018. **120**(3): p. 1374-1385.
134. Koopmeiners, A.S., et al., *Effect of electrical field stimulation on dorsal root ganglion neuronal function.* Neuromodulation, 2013. **16**(4): p. 304-11; discussion 310-1.
135. Newberry, K., et al., *Development of a spontaneously active dorsal root ganglia assay using multiwell multielectrode arrays.* Journal of neurophysiology, 2016. **115**(6): p. 3217-3228.
136. Kayano, T., et al., *Chronic NGF treatment induces somatic hyperexcitability in cultured dorsal root ganglion neurons of the rat.* Biomedical research (Tokyo, Japan), 2013. **34**: p. 329-42.
137. Kitamura, N., et al., *Nerve growth factor-induced hyperexcitability of rat sensory neuron in culture.* Biomedical research (Tokyo, Japan), 2005. **26**: p. 123-30.
138. Schwarz, T.L., *Mitochondrial trafficking in neurons.* Cold Spring Harb Perspect Biol, 2013. **5**(6).
139. Moutaux, E., et al., *Neuronal network maturation differently affects secretory vesicles and mitochondria transport in axons.* Sci Rep, 2018. **8**(1): p. 13429.

140. Hart, W.L., et al., *Combined optogenetic and electrical stimulation of auditory neurons increases effective stimulation frequency - An in vitro study.* Journal of Neural Engineering, 2020. **17**(1).
141. Clark, A.J., et al., *Functional imaging in microfluidic chambers reveals sensory neuron sensitivity is differentially regulated between neuronal regions.* Pain, 2018. **159**(7): p. 1413-1425.
142. Blair, N.T. and B.P. Bean, *Role of Tetrodotoxin-Resistant Na⁺ Current Slow Inactivation in Adaptation of Action Potential Firing in Small-Diameter Dorsal Root Ganglion Neurons.* The Journal of Neuroscience, 2003. **23**(32): p. 10338-10350.
143. Radivojevic, M., et al., *Electrical Identification and Selective Microstimulation of Neuronal Compartments Based on Features of Extracellular Action Potentials.* Sci Rep, 2016. **6**: p. 31332.
144. Hayar, A., C. Gu, and E.D. Al-Chaer, *An improved method for patch clamp recording and calcium imaging of neurons in the intact dorsal root ganglion in rats.* J Neurosci Methods, 2008. **173**(1): p. 74-82.
145. Mann, K., et al., *Coupling of activity, metabolism and behaviour across the Drosophila brain.* Nature, 2021. **593**(7858): p. 244-248.
146. Biffi, E., et al., *A microfluidic platform for controlled biochemical stimulation of twin neuronal networks.* Biomicrofluidics, 2012. **6**(2): p. 24106-2410610.